Flow and sediment behaviour around an Xstream groyne

Data-driven and numerical analysis of hydrodynamic and morphodynamic behaviour in a river bend

E.J. Veraart

TU Delft

bam

Flow and sediment behaviour around an Xstream groyne

Data-driven and numerical analysis of hydrodynamic and morphodynamic behaviour in a river bend

by

E.J. Veraart

to obtain the degree of Master of Science

at the Delft University of Technology,

to be defended publicly on Thursday August 7, 2025 at 10:45 AM.

Submitted on 03-08-2025

Student number: 4714768

Thesis committee:

Prof. dr. ir. W.S.J. Uijttewaal,	TU Delft, chair
Dr. ir. E. Mosselman,	TU Delft / Deltares, supervisor
Ir. B. Reedijk,	BAM Infraconsult, supervisor

TU Delft

Preface

This thesis marks the final step in completing my Master's degree in Civil Engineering at Delft University of Technology. From February to August 2025, I conducted this research as a graduate intern at BAM Infraconsult. I am grateful to BAM for providing not only an engaging and relevant research topic but also the necessary tools and resources to carry it out. Therefore, I would like to start by thanking them for all their help.

I would like to express my sincere gratitude to my thesis committee for their continuous guidance and valuable feedback. I especially thank my supervisor, Bas Reedijk, at BAM Infraconsult, for facilitating access to all relevant data and accompanying me during a memorable day of float measurements at the groyne site. I am equally grateful to my professor, Wim Uijttewaal, whose expertise in turbulent flow greatly helped me navigate the more complex physical aspects of this research. Special thanks also go to Erik Mosselman for his thoughtful advice during the critical stages of the project and for kindly offering me a workspace at the Deltares office. Finally, I would like to thank Erik ten Oever for his technical support during the model design phase in ANSYS Fluent. His assistance significantly improved the outcome of the model simulations.

Finally, I want to thank my family and friends for their encouragement throughout my studies and especially during the challenging phases of this research.

E.J. Veraart
Delft, August 2025

Summary

This research investigates the hydrodynamic and morphodynamic behaviour around an innovative river training structure, the Xstream groyne, compared to traditional groynes. Groynes are widely used in river systems to guide flow, maintain navigability, control sediment transport and protect banks from erosion. Traditional groynes are impermeable structures, typically built with mild 1:3 slopes and layered materials (such as a sand core, filter layers, and rock armour). The Xstream groyne, implemented in a pilot study in the IJssel River near Kampen, introduces a different design: it is constructed entirely from interlocking Xstream concrete blocks, resulting in a steeper 1:1 slope and 60% porosity, allowing partial flow through the structure. This makes it flexible in both placement and geometry.

Field observations revealed unusual sedimentation behaviour downstream of the Xstream groyne, particularly the formation of a sediment ridge or "sediment line," which contrasts with the typical scour patterns associated with traditional groynes. This phenomenon is not accounted for in traditional river engineering theory, encouraging the need for investigation.

To understand the underlying physical mechanisms, a combined approach of field observations and numerical modelling was applied. Multibeam bathymetric surveys were used to monitor changes in bed levels, while ADCP measurements and surface float tracking provided insight into the local flow behaviour. The field data showed that the Xstream groyne significantly alters flow patterns compared to nearby traditional groynes. In particular, recirculation zones behind the groyne were found to be weaker and more elongated and horizontal mixing was suppressed.

Morphodynamically, the sediment line appeared shortly after the groyne was extended to its full length. It initially formed as a sharp ridge downstream of the groyne and later broadened and shifted toward the riverbank during higher discharge periods. While the ADCP data showed no strong vortex patterns, morphological evidence and numerical results indicated the persistent influence of a large, slow-rotating eddy near the channel side of the groyne field. This feature appeared to contribute to the development and stability of the sediment line.

A detailed 3D computational fluid dynamics (CFD) model was developed in ANSYS Fluent to further examine the flow and sediment interactions. The model was constructed using high-resolution riverbed data and simulated realistic boundary conditions. Sensitivity analysis showed the importance of mesh refinement and turbulence modelling for accurate simulation of river flow. Among the turbulence models tested, the k–ω SST model was found to be the most suitable, capturing the separation zones, shear layers, and bed shear stress distribution effectively. The model also successfully incorporated groyne permeability using a porous media formulation, though the steep slope was found to have a more dominant influence than the porosity in shaping the flow field.

Hydrodynamic simulations revealed that the Xstream groyne produces a fundamentally different wake structure than a traditional groyne. Instead of creating compact, well-defined vortices, it generates a longer, more diffuse recirculation zone. The deflection of flow around the groyne head remains strong, but the steeper slope restricts flow curvature and concentrates flow closer to the channel centre. The

reduced mixing across the groyne field contributes to the altered flow structure and lower turbulence intensity.

From a morphodynamic perspective, these hydrodynamic changes translated into more distributed erosion and deposition patterns. Traditional groynes tend to induce intense local scour near the head and defined deposition zones downstream. Bed shear stress maps from the numerical model confirmed that the Xstream design generates lower peak stresses within the groyne field, especially in the zone where the sediment line was observed. The sediment line itself appears to form in a low streamwise velocity area where sediment can settle due to the presence of a counter-clockwise eddy inducing groyne field flow upward. This creates an area of low bed shear stress where sediment can deposit.

In conclusion, this study shows that the Xstream groyne significantly alters the flow and sediment regime in its vicinity compared to traditional designs. The steep slope and partial permeability modify flow separation, suppress turbulence and shift erosion and deposition zones. The combination of field evidence and numerical modelling demonstrates that the design. The slope, particularly, is a critical factor in groyne-induced morphodynamics. These insights highlight the importance of considering three-dimensional flow behaviour in the design and evaluation of modern, flexible groyne structures.

Contents

Preface i

Summary ii

1 Introduction 1
- 1.1 General . . . 1
- 1.2 Research problem . . . 2
- 1.3 Research questions . . . 3
- 1.4 Methodology . . . 4

2 Groyne flow and sediment transport characteristics 5
- 2.1 General . . . 5
- 2.2 Hydrodynamic behaviour around groynes . . . 6
  - 2.2.1 Groyne flow zones . . . 6
  - 2.2.2 Relevant flow parameters and turbulence characteristics . . . 7
- 2.3 Morphodynamic behaviour around groynes . . . 9
  - 2.3.1 Scour and deposition . . . 9
  - 2.3.2 Bed shear stress formulations . . . 10
- 2.4 Spiral flow effects . . . 11

3 Site analysis 13
- 3.1 Approach to the site analysis . . . 13
- 3.2 Area overview . . . 14
  - 3.2.1 General information . . . 14
  - 3.2.2 Hydrograph . . . 14
  - 3.2.3 River and groyne geometries . . . 15
  - 3.2.4 Average water height and flow characteristics . . . 16
  - 3.2.5 Radius of curvature & spiral flow . . . 17
  - 3.2.6 Sediment distribution and river slope . . . 18
- 3.3 Bed level measurement analysis . . . 19
  - 3.3.1 Before and during Phase 1 . . . 19
  - 3.3.2 During Phase 2 . . . 20
  - 3.3.3 Summary on the morphodynamic findings . . . 24
- 3.4 Flow velocity analysis . . . 24
  - 3.4.1 ADCP measurements . . . 25
  - 3.4.2 Float tracking tests . . . 31
  - 3.4.3 Summary on hydrodynamic findings: . . . 32

4 Software selection 33
- 4.1 Software criteria . . . 34

4.2 Multi-criteria analysis 36

5 Numerical modelling **39**
5.1 Approach to the numerical modelling 39
5.1.1 Model set-up 39
5.1.2 Sensitivity analysis 45
5.1.3 Model validation 47
5.1.4 Flow field analysis 49
5.1.5 Sediment response analysis 49
5.2 Results of the numerical modelling 50
5.2.1 Model set-up 50
5.2.2 Sensitivity analysis 52
5.2.3 Model validation 56
5.2.4 Flow field analysis 60
5.2.5 Sediment response analysis 64

6 Discussion **69**

7 Conclusion and Recommendations **74**
7.1 Conclusion 74
7.2 Recommendations 76

References **78**

A ADCP figures **80**

B Model simulation designs **81**

C Cross-sections for traditional groyne case **83**

1

Introduction

1.1. General

Groynes are man-made structures commonly applied in rivers to regulate flow and manage sediment transport. These structures are constructed perpendicular to the riverbank and extend into the flow, redirecting water away from sensitive areas and helping shape the riverbed and banks. Groynes have been used for centuries, evolving from simple spur dikes to more engineered structures designed for stability and hydraulic performance. Nowadays, several types of groynes can be distinguished according to their construction and geometry.

The primary function of groynes is river training, which involves controlling the alignment and shape of the river to ensure navigability, manage sediment transport, and prevent flooding (Yossef, 2002). The obstruction of the flow field due to a groyne modifies its velocity and direction. This leads to a stronger flow in the area of the channel that is used for shipping (referred to as the main channel), which causes deepening of the riverbed and prevents sedimentation in this area, which is beneficial to navigational purposes. Another function is the management of sediment deposition and erosion near the river banks. Upstream of the groyne, sediment accumulation is caused by a decrease in flow velocity. Downstream, the increased flow helps maintain the total capacity of the sediment transport. Other positive effects that can be mentioned are stabilising the river banks and reducing the probability of ice jamming.

The most frequently implemented groyne is the traditional groyne. An example of this type of groyne is shown in Figure 1.1a. At the sides and the head of a traditional groyne, the slopes are mild, usually sloping into the river on a gradient of 1 to 3 (1 vertical unit over 3 horizontal units). A mild slope is considered to be beneficial for reducing the amount of erosion behind the groyne head (Yossef, 2002). The traditional groyne consists of different layers to preserve its stability. Consisting of a sand core with multiple filters and armour layers, the groyne is able to withstand turbulent flows during low and high discharges. Due to its construction, the groyne is impermeable to flow, making sure that the main river flow is deflected around its structure.

A new innovative groyne structure, the Xstream (or flexible) groyne, is being tested on its functionality. This new type of groyne is an outcome of the Self-Supporting River System (SSRS, 2025). This pro-

gram focuses on researching possibilities for affordable, reliable, and sustainable management in the system. Unlike traditional groynes, this groyne is built out of Xstream blocks (Xbloc, 2025). These are small blocks with a highly interlocking effect, which is a highly beneficial effect towards the stability of the groyne. The blocks are easily transported and placed in bulk due to their light weight and size. This opens up the opportunity to easily alter the geometry of the groyne.

Experiments on the practicality of the groyne are done near Kampen on the IJssel (Buschman, 2024), where one Xstream groyne is placed between a series of traditional groynes described above. This Xstream groyne is shown in Figure 1.1b. The slope of the groyne is steeper, decreasing the total area that interferes with the flow. The groyne has no sand core or other protective layers, as it is fully constructed with Xstream blocks. The shape of the Xstream blocks creates a porosity of sixty percent, which leads to a certain permeability in the groyne. This permeability may influence the flow patterns in the groyne field near the Xstream groyne.

(a) Overhead view of the traditional groyne (van der Lee, 2025)

(b) Side view of the Xstream (flexible) groyne (van der Lee, 2025)

Figure 1.1: Visual comparison of the traditional and Xstream groynes implemented in the IJssel

1.2. Research problem

The implementation of the Xstream groyne in the IJssel has revealed unusual hydrodynamic and morphodynamic behaviour that is not yet fully understood. Initially, three Xstream groynes were placed as pilots (two in the inner bend and one in the outer bend of the river near Kampen). Eventually, adjustments were made: the inner bend groynes were removed and the outer bend groyne was extended. Depth measurements and surveys of the riverbed around the remaining Xstream groyne showed distinct scour and deposition patterns compared to those typically seen at a traditional groyne. In particular, where a traditional groyne would produce a deep scour pit immediately downstream of its tip, the Xstream groyne instead exhibits a longer erosion zone and a ridge of deposited sediment, essentially forming a sediment line separating the groyne field from the main channel, which can be observed in Figure 1.2.

This phenomenon has not been reported in the literature on either impermeable or permeable groynes and cannot be fully explained by conventional river engineering theories. Existing research has focused primarily on understanding and mitigating scour around groynes, examining the effects of head shape, groyne permeability and spacing. However, no studies have documented the emergence of a sediment ridge similar to that observed near the Xstream groyne. These findings point to a knowledge gap in the understanding of groyne-induced flow and sediment behaviour. As such, this study seeks to determine how the Xstream groyne influences local hydrodynamics and morphodynamics.

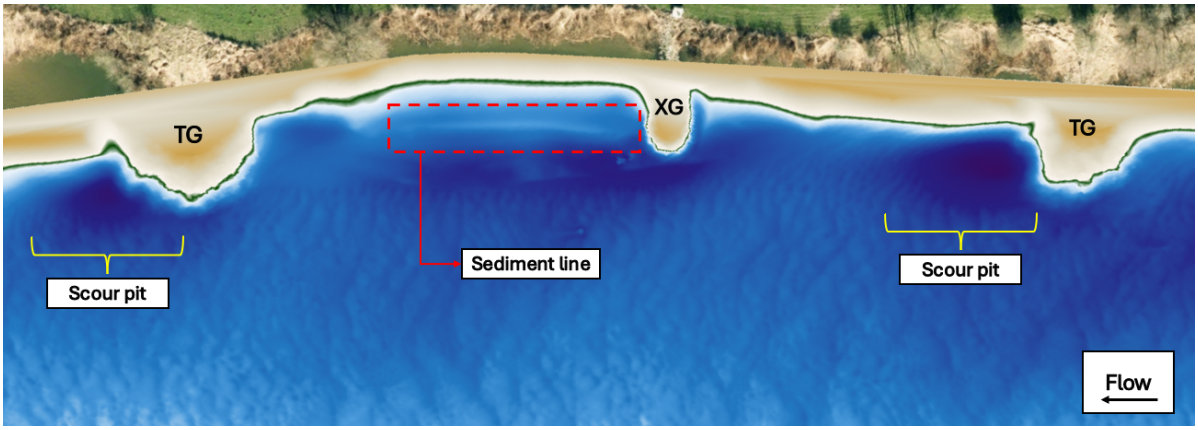

Figure 1.2: Topographic map that indicates the sediment line near the Xstream groyne (XG) and the scour pits in the yellow areas near the traditional groynes (TG)

1.3. Research questions

Based on the research problem and objectives outlined above, the following main research question is stated:

- **What is the influence of an Xstream groyne structure on the hydrodynamics and morphodynamics?**

To answer this main question, four sub-questions are defined. These are structured according to the two core components of the research: the field measurements and the numerical modelling analysis.

Field-based analysis

1. How does the flow structure around the Xstream groyne differ from that of traditional groynes based on field measurements?
2. What morphological changes have occurred around the Xstream groyne compared to traditional groynes based on field measurements?

Numerical modelling analysis

3. To what extent can a numerical model reproduce the flow structures observed around the Xstream groyne?
4. What insights do the model results provide into the hydrodynamic and morphodynamic mechanisms?

The sediment line appeared after the implementation of the Xstream groyne. An explanation for the formation of this line has also been researched through both analyses. For that reason, an additional sub-question is formulated:

5. How do the flow and sediment dynamics contribute to the formation of the sediment line?

1.4. Methodology

To address the research questions, this study combines detailed field measurements with three-dimensional numerical modelling. The research approach involves:

- Establishing a theoretical framework to describe typical hydrodynamic and morphodynamic processes around groynes (Section 2).
- Conducting a field analysis, making use of mainly topographic and velocity measurement data in the Xstream groyne area (Section 3).
- Selecting a suitable modelling software necessary for this research (Chapter 4).
- Developing a numerical model, including the set-up of the model, as well as conducting a sensitivity analysis and validating it. With that, an in-depth analysis of the simulated hydrodynamics and morphodynamics can be performed (Chapter 5).

The results of both the field and modelling analysis are discussed to evaluate their implications, limitations and relevance to the broader understanding of groyne-induced morphodynamics (Chapter 6). Finally, conclusions are drawn and recommendations are made for future research and engineering practice (Chapter 7).

2

Groyne flow and sediment transport characteristics

This chapter theoretically introduces the key hydrodynamic and morphodynamic processes around groynes. It outlines how groynes influence flow structures, turbulence and bed shear stresses. The sections cover typical flow zones, relevant parameters, scour patterns and the effect of spiral flow in river bends.

2.1. General

Groynes are transverse hydraulic structures extending from the riverbank into the channel. These structures are primarily designed for river training and help to regulate flow and protect riverbanks from erosion. As part of broader river training works, they help maintain a stable channel alignment, support navigation, and mitigate flood risks (Yossef, 2002). By altering local flow and sediment dynamics, groynes assist in maintaining the desired cross-sectional shape of the river. River training more generally helps with the control of water levels, managing sediment transport and stabilising the river course. To achieve these goals and preserve dynamic equilibrium in the river system, various hydraulic structures such as groynes, bed fixations, and longitudinal walls are implemented (Przedwojski et al., 1995).

Groyne structures work by locally constricting the channel width, reducing erosion along the banks and promoting sediment scouring in the navigational zone. Moreover, groynes contribute to the formation of sheltered zones, known as groyne fields, where sediment can settle. Effective groyne functioning depends heavily on careful structural design. Groynes are classified based on their permeability, shape, construction material, submergence and orientation angle to the flow (Nandhini et al., 2024). In the Netherlands, traditional groynes are typically composed of a sand core on a fascine mattress, covered with layers of rock, and often reinforced with timber piles near the water surface (Jansen et al., 1994).

While traditional groyne structures have proven effective over time, ongoing research explores innovative alternatives to mitigate drawbacks such as local scour and excessive turbulence. This has led to the development of alternative designs like the Xstream groyne, which is constructed entirely from

X-stream blocks, which are modular concrete elements. This configuration allows for steeper slopes of up to 45 degrees and being slightly permeable.

2.2. Hydrodynamic behaviour around groynes

2.2.1. Groyne flow zones

The presence of groynes in a river system introduces significant alterations to local flow structures. A single groyne obstructs the natural flow, resulting in complex three-dimensional flow interactions, including stagnation zones, flow separation, recirculation, and vortex formation (Zhang & Nakagawa, 2008).

The flow region around a single, emerged groyne can be subdivided into three main zones (Zhang & Nakagawa, 2008),(Nandhini et al., 2024), which are also shown by their numbers in Figure 2.1:

1. **Main flow zone:** Stretching from the groyne head to the opposite side of the channel.
2. **Wake zone:** Area between the groyne head and the riverbank downstream of the groyne. This zone consists of a return flow zone and a reattachment zone.
3. **Mixing zone or mixing layer:** Area between the other two that separates the fast flowing main flow from the recirculating region.

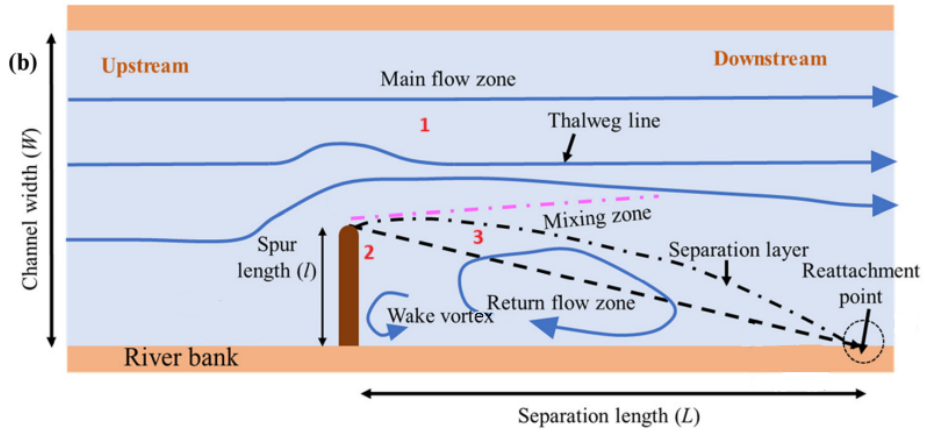

Figure 2.1: Top view of flow zones at a groyne (Nandhini et al., 2024)

The main flow zone describes all flow between the mixing layer and the opposite river bank. Here, the flow is accelerated due to the compression of flow lines. The thalweg line is found in this accelerated area and indicates the zone where the velocities are highest across the channel (Nandhini et al., 2024).

As explained, the wake zone consists of a return flow zone, also known as the recirculation zone, and a reattachment zone. In the recirculation zone, a large recirculating vortex and a smaller lee-wake vortex are typically formed, both shown in Figures 2.1 and 2.2. These vortices are rotating in opposite directions and have different sizes. The lee-wake vortex is located near the groyne, where its centre is located approximately one groyne length from the structure. A second, more significant vortex is observed downstream with its centre approximately six lengths from the structure (Yossef, 2002). These centre-distances are, however, for a single, emerged and rectangular groyne and are highly variable per groyne type. For the case of a series of groyne structures, the size of the recirculation zone and the size of the vortices are determined by the aspect ratio. The aspect ratio refers to the

relative spacing of two groyne structures. In other words, it is the amount of spacing between two groyne structures divided by the length of the groyne structure. For smaller aspect ratios (s/l < 2.0), the recirculation zone contains a single vortex or two transverse vortices, while for larger aspect ratios (s/l > 2.0), a similar recirculation zone is seen as shown in Figure 2.1.

Downstream of the recirculation zone, for a single groyne, the separated flow reattaches to the river-bank. This reattachment zone is usually simplified as a single point. The location of this point is also variable, and when multiple groynes are implemented, the effect of the downstream groyne diminishes the effect of the reattachment point.

The mixing layer is another relevant aspect of the flow near groynes. It is formed due to the large velocity gradients, due to the flow that is pushed around the groyne head. Higher intensities of turbulence are found in this area, which can be mainly described in the form of vortex shedding. Figure 2.2 shows multiple types of these vortices. Starting from the upstream side, the following flow principles are described in the figure. Flow comes from upstream and follows the black arrows. When the flow is obstructed by the groyne, the flow is deviated and directed downward and toward the main channel (indicated by the orange arrows). From there flow in the upper part of the water column follows the groyne head to get around the groyne. In the lower part of the water column, flow is blocked by the groyne and the riverbed, which forces it to go back, creating a vortex shape named the horseshoe vortex (indicated by the red arrows). When these flows go around the groyne head, where it is affected by friction of the groyne slope it is slowed down and reaches the already explained mixing layer and wake zone.

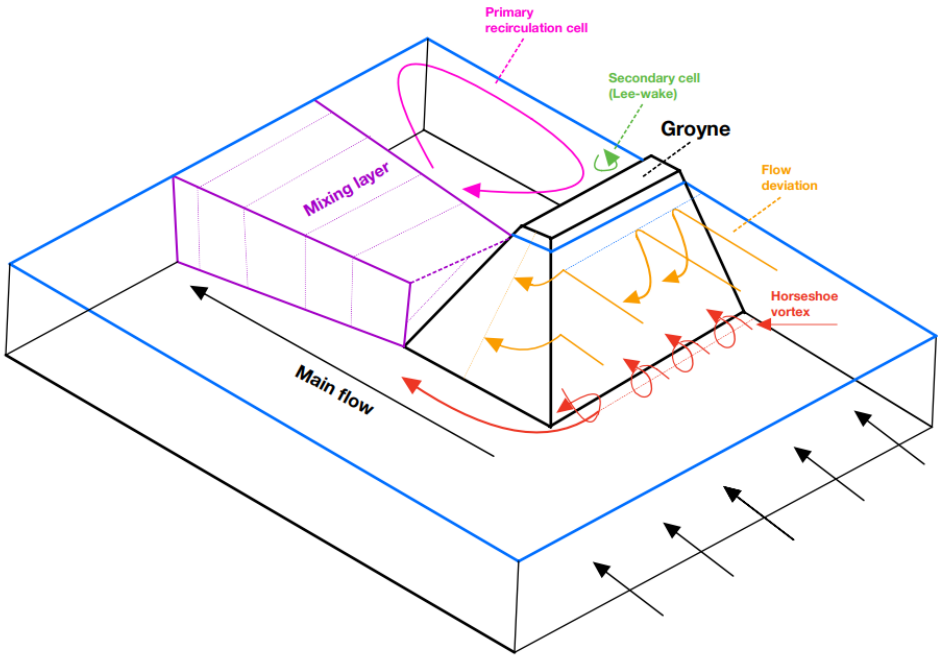

Figure 2.2: Three-dimensional view of typical flow principles at a sloped groyne

2.2.2. Relevant flow parameters and turbulence characteristics

To quantitatively describe the complex hydrodynamics around groynes, several key flow parameters and turbulence quantities are commonly used. These include dimensionless numbers such as the Froude and Reynolds numbers, as well as turbulence-related variables like fluctuating velocity compo-

nents, turbulent kinetic energy (TKE) and turbulent viscosity.

Froude number

The Froude number (Fr) is a fundamental dimensionless parameter that compares inertial forces to gravitational forces in a free-surface flow (Chanson, 2004). It is defined as:

$$Fr = \frac{U}{\sqrt{gh}} \tag{2.1}$$

In this expression, U is the characteristic flow velocity, g is the acceleration due to gravity, and h (for open channel flow) is the flow depth. The Froude number is particularly important in open-channel flow where the free surface has an effect on the flow behaviour.

The Froude number represents the ratio between the inertial forces of the flow and the gravitational forces acting on the free surface. That means the Froude number can be divided into different flow regimes:

- $Fr < 1$: **Subcritical flow** — gravitational effects dominate. The flow is tranquil, and surface disturbances can travel upstream.
- $Fr = 1$: **Critical flow** — inertial and gravitational forces are balanced. This represents a unique and often unstable condition.
- $Fr > 1$: **Supercritical flow** — inertial effects dominate. The flow is rapid, and surface disturbances cannot propagate upstream.

In natural rivers, flow conditions are typically subcritical, meaning that gravitational forces dominate over inertial forces. This allows surface disturbances to propagate both upstream and downstream. However, near hydraulic interventions such as groynes, local changes in velocity and depth can increase the Froude number, mainly due to acceleration of the flow.

Reynolds number

The Reynolds number (Re) is another fundamental dimensionless quantity in fluid mechanics. It characterises the relative importance of inertial forces to viscous forces within a flow and is defined as (Schiereck & Verhagen, 2019):

$$Re = \frac{UL}{\nu} \tag{2.2}$$

Here, U is a characteristic velocity (for rivers usually the depth-averaged flow velocity), L is a characteristic length scale (such as flow depth h and ν is the kinematic viscosity of the fluid. For water at room temperature $\nu \approx 1.0 \times 10^{-6}\,\mathrm{m}^2/\mathrm{s}$.

The Reynolds number represents the ratio between the momentum carried by the flow (inertia) and the resistance due to internal friction (viscosity). That means the Reynolds number can be divided into different classes:

- $Re < 500$: **Laminar flow** — smooth and orderly, with layers of fluid sliding past one another.
- $500 < Re < 2000$: **Transitional flow** — instabilities begin to appear.
- $Re > 2000$: **Turbulent flow** — characterized by chaotic, three-dimensional fluctuations and mixing.

In river and open-channel flows, Reynolds numbers are typically several orders of magnitude higher ($Re \sim 10^4 - 10^6$), indicating fully turbulent flow. In such cases, inertial effects dominate, and turbulence plays a major role in shaping flow patterns, sediment transport, and vortex formation.

Velocity components & turbulence representation:
In turbulent flow, velocity components in each direction can be decomposed into a mean and fluctuating part (Schiereck & Verhagen, 2019):

$$u = \overline{u} + u', \quad v = \overline{v} + v', \quad w = \overline{w} + w' \tag{2.3}$$

where $\overline{u}, \overline{v}, \overline{w}$ represent time-averaged velocities, and u', v', w' are the fluctuations of the velocity over the mean. These fluctuations are responsible for momentum transfer and turbulence generation.

These velocity fluctuations in all directions are the key to give a representation of turbulence. A general description can be given with the turbulent kinetic energy (k), which quantifies the total energy associated with velocity fluctuations and is given by:

$$k = \frac{1}{2}\left(\overline{u'^2} + \overline{v'^2} + \overline{w'^2}\right) \tag{2.4}$$

The turbulent kinetic energy (TKE) is often used as an indicator of turbulence intensity across all directions. However, the fluctuation intensity in a single direction can also be described relative to the mean velocity in that direction. These are expressed using the relative fluctuation ratios:

$$r_u = \frac{\overline{u'^2}}{\overline{u}^2}, \quad r_v = \frac{\overline{v'^2}}{\overline{v}^2}, \quad r_w = \frac{\overline{w'^2}}{\overline{w}^2} \tag{2.5}$$

Eddy viscosity
Eddy viscosity, also known as turbulent viscosity, is a parameter used primarily in numerical modelling to represent the enhanced mixing and momentum transfer caused by turbulence. Unlike molecular viscosity, which is constant for a given fluid, eddy viscosity varies spatially and is not a physical property but a modelling construct. It appears in turbulence models as a way to close the Reynolds-averaged Navier–Stokes (RANS) equations, allowing the effects of unresolved turbulent motions to be approximated. Various turbulence models, such as the k-ε and k-ω models use different approaches to calculate eddy viscosity. In flow visualisations, regions with high eddy viscosity indicate strong turbulence and active momentum exchange.

2.3. Morphodynamic behaviour around groynes

2.3.1. Scour and deposition

Groynes significantly influence riverbed morphology due to the hydrodynamic changes and large turbulence as explained in Section 2.2. The changes in flow velocity, turbulence, and pressure gradients caused by the presence of a groyne result in both erosion (scour) and deposition zones.

Scour around groynes is typically classified into two main categories: constriction scour and local scour (Yossef, 2002). Constriction scour results from the narrowing of the channel by the groyne. Due to the contracting streamlines in the narrowed channel, the flow accelerates and the total bed shear stresses increase (Pizarro et al., 2020). This type of scour can take place over the full width of the groyne head.

Local scour results from the direct effect of the structure on the local flow pattern and with that the generation of the turbulence. This is driven by turbulent features such as the horseshoe vortex at the groyne base, the detached shear layer, and tip-vortex shedding, all of which intensify local bed shear stresses (Nandhini et al., 2024).

Figure 2.3 illustrates the typical development and locations of scour holes and associated flow structures around a single groyne. The maximum scour depth and bed shear stress are strongly correlated and tend to occur in two distinct regions: near the groyne head due to the formation of the shear layer and (if present) upstream due to the formation of a horseshoe vortex (Zhang & Nakagawa, 2008).

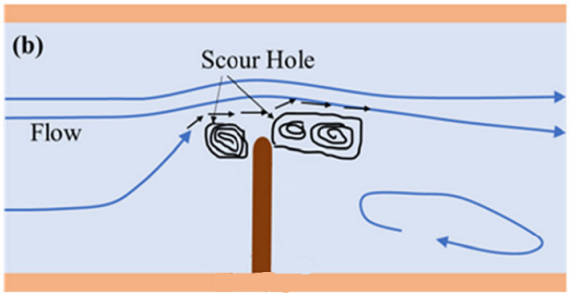

(a) Top view of groyne structure (Nandhini et al., 2024)

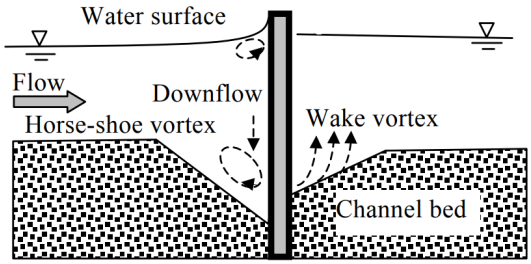

(b) Side view of scour at rectangular groyne (Zhang & Nakagawa, 2008). Erosion magnitudes are less significant for sloped groynes

Figure 2.3: Comparison of top and side views of scour development around groynes

In zones where the flow velocity and bed shear stress are sufficiently low, deposition of sediment occurs. As erosion removes material from high-energy regions, such as near the groyne head or within the mixing layer, this sediment is often redistributed downstream. In the wake zone behind the groyne, flow deceleration and the presence of recirculating eddies make deposition of sediment possible. These sheltered areas are characterised by reduced turbulence and bed shear stresses. Over time, this leads to the accumulation of sediment in the groyne field.

Whether erosion or deposition occurs depends not only on the magnitude of the bed shear stress, but also on the sediment characteristics. The Shields parameter provides a method to assess whether the local bed shear stress exceeds the threshold required to initiate sediment motion. When the computed bed shear stress exceeds the critical shear stress corresponding to the sediment size, sediment transport is likely to occur. If below this value, deposition is expected.

2.3.2. Bed shear stress formulations

Bed shear stress (τ_0), expressed in pascals, is a key parameter for assessing sediment mobility and the onset of scour. It represents the force per unit area exerted by flowing water on the bed surface and is critical for determining whether sediment particles remain at rest or are entrained into the flow (Schiereck & Verhagen, 2019). There are two common methods to estimate τ_0. The first formulation is expressed as:

$$\tau_0 = \rho g h i_b \tag{2.6}$$

with h the flow depth and i_b the bed slope. This method is suited for uniform or depth-averaged flow conditions. Alternatively, bed shear stress can be expressed using the shear velocity u_*, a quantity that

characterises the intensity of near-bed turbulence:

$$\tau_0 = \rho u_*^2 \tag{2.7}$$

The shear velocity u_* can be derived from velocity profiles near the bed or from turbulence models in numerical simulations. It is particularly useful in estimating the initiation of sediment motion and is often used with the dimensionless Shields parameter θ, which relates the bed shear stress to the gravitational forces acting on sediment particles:

$$\theta = \frac{\tau_0}{(\rho_s - \rho)gD} \tag{2.8}$$

Here, ρ_s is the sediment density and D the characteristic particle diameter. Sediment motion typically begins when θ exceeds a critical value θ_c, known as the critical Shields stress. This critical threshold depends on factors such as grain size, bed packing and flow regime, but for sand-sized particles, a typical value is around $\theta_c \approx 0.055$. Comparing computed values of θ to θ_c allows for the prediction of erosion (if $\theta > \theta_c$) or deposition (if $\theta < \theta_c$).

2.4. Spiral flow effects

Spiral flow generation

In river bends, the curvature of the flow path introduces a centrifugal acceleration of approximately u^2/R, where u is the streamwise velocity and R is the radius of curvature of the bend (Graf & Blanckaert, 2002). To balance this outward-directed centrifugal force, the water surface develops a transverse slope: it rises toward the outer bank and lowers toward the inner bank. This creates an inward-directed pressure gradient across the channel cross-section.

However, streamwise velocity varies with depth, with flow going faster near the surface and slower near the bed due to bottom friction, as indicated by the pink region in Figure 2.4. As a result, the centrifugal force is stronger near the surface and weaker near the bed. In contrast, the pressure force resulting from the water surface slope is approximately uniform with depth.

These two create a distribution of transverse flow: near the bed, the inward pressure force dominates, pushing water toward the inner bank, while near the surface, the outward centrifugal force dominates, pushing water toward the outer bank. The result is a cross-sectional circulation: inward flow along the bed and outward flow near the surface, as indicated by the blue region in Figure 2.4. Over the width of the channel, this secondary flow shows an upward motion near the inner bank and a downward motion at the outer bank, as indicated by the green region in Figure 2.4. This forms the classic spiral flow known in river bends.

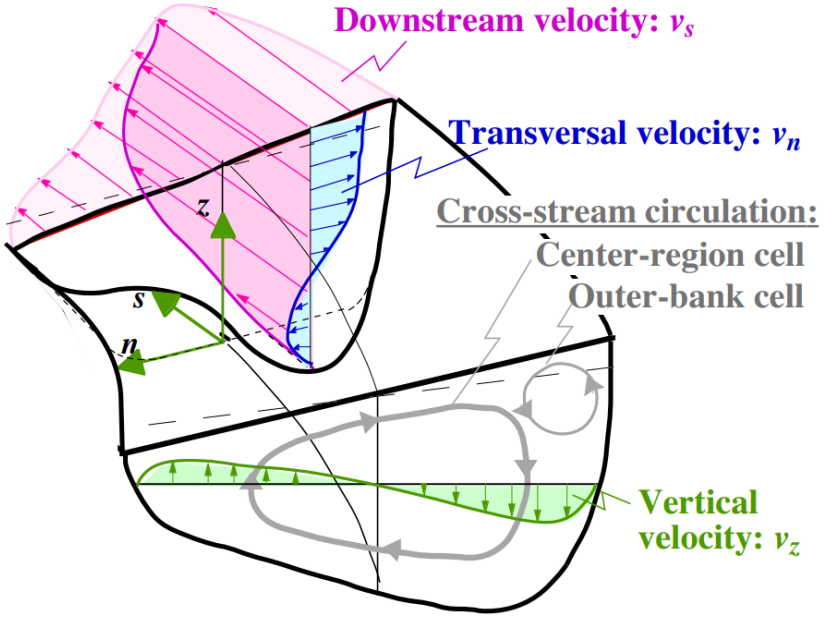

Figure 2.4: Spiral flow representation (Graf & Blanckaert, 2002)

Spiral flow representation

As explained in the previous section, the transverse water surface gradient plays a central role in balancing the outward centrifugal force in a river bend. Its magnitude can be estimated using a simplified lateral force balance:

$$\frac{\partial h}{\partial r} \approx \frac{\bar{u}^2}{Rg} \tag{2.9}$$

In addition to the pressure gradient, the strength of the transverse velocity component is closely related to channel geometry. Theory presented by van Bendegom et al. (1978) shows that the transverse velocity v_n is proportional to the curvature ratio h/R, where h is the flow depth and R is the bend radius. This relationship reflects how secondary flow becomes more pronounced in deeper channels and tighter bends. A commonly used approximation is given by:

$$v_n(z) = 6 \cdot h \cdot (\frac{2z}{h} - 1)\frac{\bar{u}}{R} \tag{2.10}$$

Here, $v_n(z)$ is the transverse velocity at depth z and $\bar{u}$ is the depth-averaged streamwise velocity. For simplicity, this formulation neglects the effect of boundary friction, which can lead to inaccurate values, especially near the bed. However, it remains valuable as an approximation of the transverse velocity gradient over the depth.

3

Site analysis

3.1. Approach to the site analysis

To analyse the hydrodynamic and morphodynamic effects of the Xstream groyne, a field-based data approach was adopted. This approach is essential to provide an empirical interpretation of the key physical mechanisms influencing flow and sediment development in the area. These insights are used to better understand the behaviour of the Xstream groyne concept and to parameterise the numerical model that follows.

All field data were provided as part of the Xstream pilot project near Kampen. The available datasets include multibeam-derived bed level measurements, ADCP flow velocity data, and surface tracer tests. Although the measurements themselves were not performed during this research, significant post-processing and interpretation were carried out to gain insight into the local flow and sediment dynamics and to better understand what is happening in the area.

Before analysing the measurements in detail, several geometric and hydraulic parameters of the site were determined. These include the radius of curvature of the river bend, local discharge and water levels, groyne geometries, and sediment grain size. These parameters are necessary for both interpreting the physical processes and defining the boundary conditions of the numerical model.

Three types of field data were processed using dedicated tools:

- **Bed level measurements** were handled using QGIS (QGIS Development Team, 2024). Digital elevation models were constructed from multibeam data. These were then used to generate bed level difference maps, slope plots, and sediment volume balances. Raster-based tools were applied to extract quantitative measures of erosion and deposition throughout the groyne field and main channel.
- **ADCP measurements** were translated using a combination of MATLAB (MathWorks, 2024) and Python (Python Software Foundation, 2024). These scripts were developed to decrypt, clean, and convert the raw velocity transects into interpretable data. From this, quiver plots, velocity profiles, and transverse flow structures were constructed. The ADCP data served as a key source for evaluating recirculation patterns, mixing layers, and potential spiral flow signatures.

- **Float tracking experiments** were conducted using oranges placed at three different groynes (including the Xstream groyne). Each test was recorded with a drone, producing short overhead videos. The motion of each tracer was analysed, and the most relevant observations were captured by tracing the floaters across the video frames to extract their paths.

Together, this method provides both spatial and temporal insight into flow and sediment development around the Xstream groyne. It serves as a basis for the interpretation of observed patterns and supports the explanation of the physical mechanisms at work.

3.2. Area overview

3.2.1. General information

The study area is located along the IJssel River, where the Xstream groyne is situated just downstream of the bend near Kampen, in the province of Overijssel. The investigated groyne is part of a pilot project (SSRS, 2025) aimed at testing the hydraulic and morphological performance of more adaptable groyne designs. That is why a wide variety of measurements is available, which is discussed in this chapter. Figure 3.1 shows a satellite overview of the area, including the position of the Xstream groyne in relation to the surrounding groynes. The figure shows that the observed area is located at the end of a bend, which could possibly influence the flow characteristics and bed shape in the area.

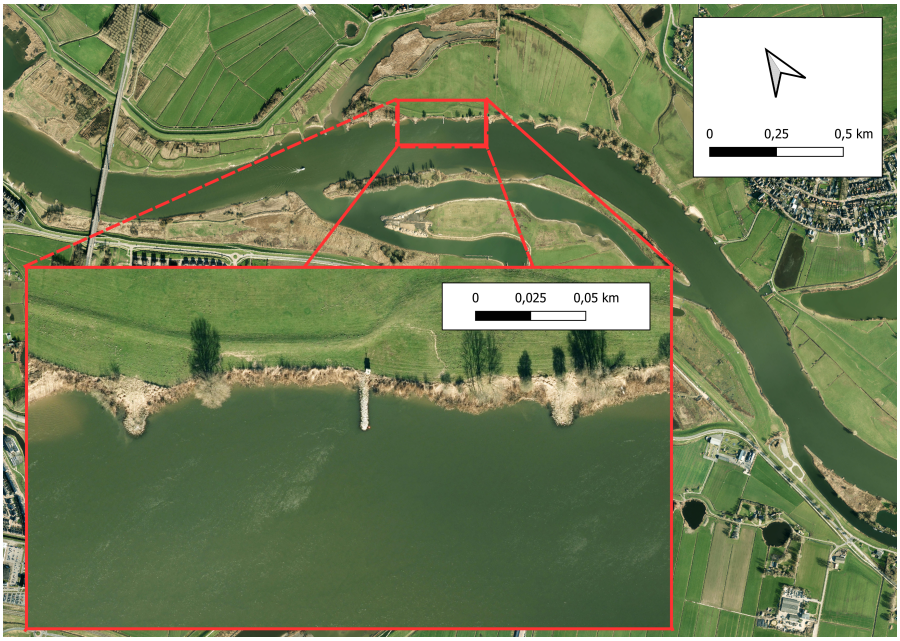

Figure 3.1: Xstream groyne area

3.2.2. Hydrograph

Figure 3.2 shows a hydrograph at Olst, which is the nearest discharge measurement location that keeps track of river discharges. The figure displays the discharge over multiple years, including all depth measurements (multibeam) in the Xstream groyne area that were relevant to this research.

The first measurement was taken before the implementation of the Xstream groyne in 2017. A subsequent measurement in 2020 corresponds to the period when the shorter version of the Xstream groyne was present. Two measurements were conducted in 2022, with one approximately a month before

and one a few days after the groyne was extended. All remaining measurements were taken after this extension. The date of the ADCP measurement, which is further described in Section 3.4.1, is also indicated. Additionally, the hydrograph shows two reference discharge lines: an average discharge line (Q_{average}) at $Q = 365$ m^3/s, and a discharge at which the groynes become submerged (Q_{overflow}) at $Q = 871$ m^3/s, calculated in Section 3.2.4.

Rijkswaterstaat defines the discharge terminology as follows: raised discharges occur at values above approximately 750 m^3/s and high discharges are identified above 1150 m^3/s (Buschman, 2024). However, as shown in Figure 3.2, actual discharge values did not reach this high value. Therefore, when the term “high discharge” is used in this report, it refers to conditions that would typically be defined as “raised discharge” under the official classification by Rijkswaterstaat.

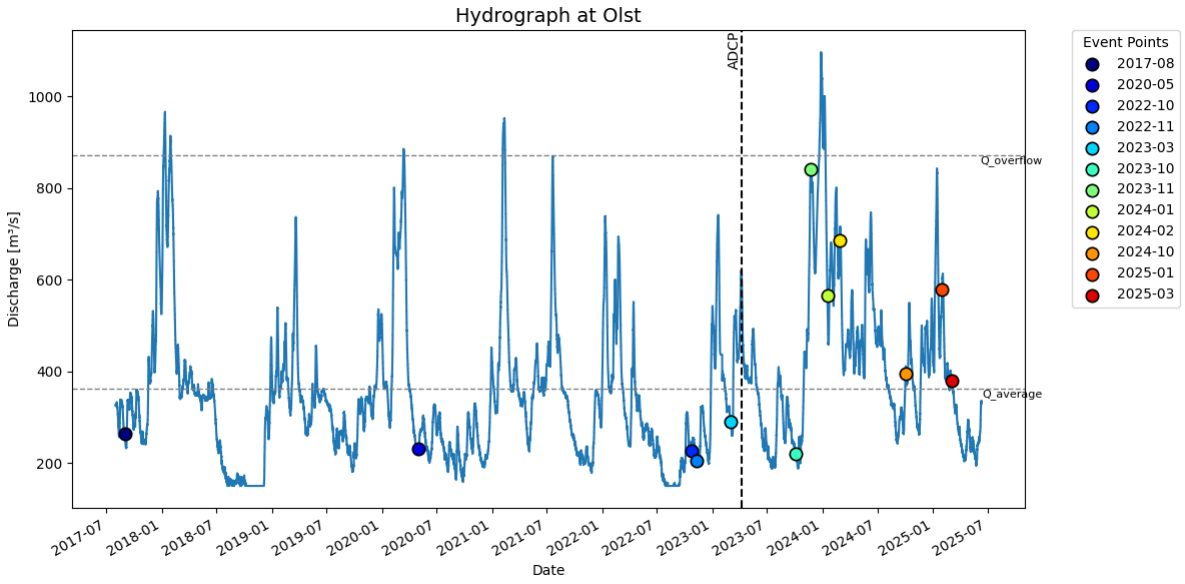

Figure 3.2: Hydrograph at Olst including all relevant measurements

3.2.3. River and groyne geometries

The transverse profile of the river near the Xstream groyne, shown in Figure 3.3, reveals a typical bed geometry associated with river bends. The inner bend is relatively shallow, while the outer bend features a significantly deeper channel. A steep depth gradient is visible near the outer riverbank, illustrating the asymmetrical cross-section that is characteristic of curved rivers. Based on the riverbed profile, the average water depth across this section was calculated to be approximately 5.2 metres. This value provides a useful reference for evaluating flow conditions and sediment dynamics in the area.

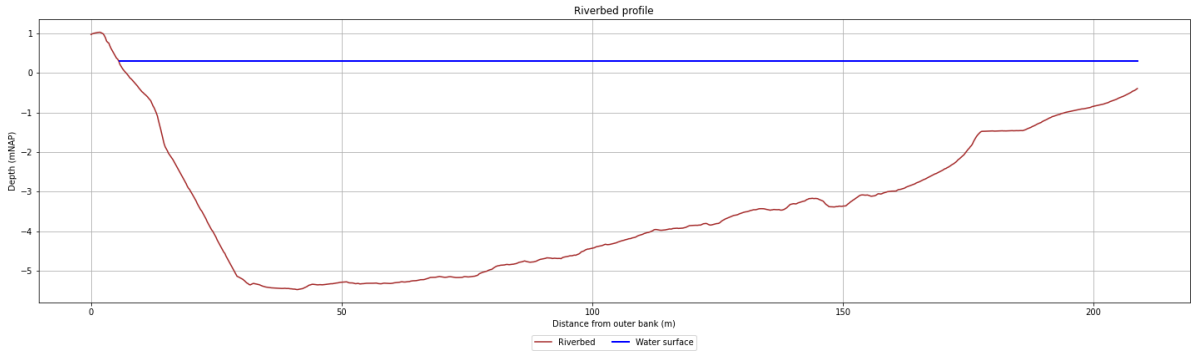

Figure 3.3: Transverse profile of the river bed near the Xstream groyne

The geometries of the traditional and the Xstream groynes show distinct characteristics. The traditional groyne shown in Figure 3.4a is composed of layered materials including a sand core, filter layer, pitched rock and rock armour, reinforced by timber piles. This design features a gentler 1:3 slope and a crest width of 3 metres, a total height of 6 metres, with a transverse base width of 36 metres and a groyne length (at bed level) of 30 metres. It also contains fascine mattresses on the slope to increase stability. In contrast, the Xstream groyne, shown in Figure 3.4b, consists of Xstream blocks with a compact trapezoidal shape, 1:1 side slopes, a crest width of 1 metre, and a base width of 12 metres. Its height is 6.5 metres and it extends 24 metres into the main channel. This groyne is fully made from Xstream blocks, meaning it does not contain a sand core or fascine mattresses for extra stability.

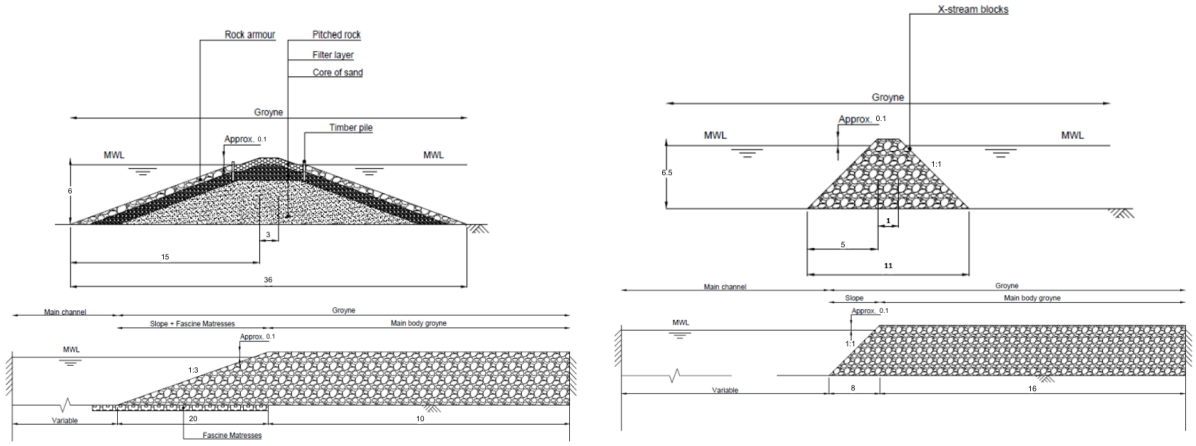

(a) Schematics of traditional groyne

(b) Schematics of Xstream groyne

Figure 3.4: Schematics of both groynes with dimensions (van Alderwegen, 2021) (not scaled!)

3.2.4. Average water height and flow characteristics

Table 3.1 shows water levels and discharges for several discharges at Lobith, which is the location where the Rhine enters the Netherlands. This location is often used to determine discharges at other places. In this case, the table refers to the water levels and discharges at the Xstream groyne. For a discharge of 2000 m^3/s, the discharge at the Xstream groyne is 370 m^3/s. With a mean discharge of 365 m^3/s, found from the hydrograph data, the average water level of -0.10 metres is used.

A second-degree polynomial fit is applied to the available water height and discharge data to estimate the discharge at which the Xstream groyne is overflown. The crest level of the groyne is located at

+0.75 metres NAP, which does not directly correspond to a value in the dataset. Therefore, a quadratic fit approximates the relationship between water height and discharge across the measurements. By evaluating the fitted polynomial at a water height of 0.75 metres, the estimated discharge is approximately 871 m^3/s. This value represents the point at which the groyne is expected to begin overflowing under rising water levels. The data used to construct the polynomial fit are presented in Table 3.1.

Table 3.1: Water height above NAP and discharge at the Xstream groyne for several Lobith discharges (Arnhem, 2022)

Name	S_600	S_1020	S_2000	S_4000	S_6000	S_8000	S_10000	S_13000	S_16000
Water Height (m)	-0.35	-0.29	-0.10	0.29	0.84	1.34	1.72	2.32	3.11
Discharge (m^3/s)	78.3	176.3	369.3	636.7	958.4	1230.4	1520.3	2034.3	2660.7

Based on the ADCP data (Section 3.4.1), a depth-averaged velocity of approximately U = 0.8 m/s was observed near the Xstream groyne. A corresponding average water depth was estimated at h = 4.0 m, derived from the multibeam measurements. These two parameters provide the necessary input to evaluate the local flow regime using the standard dimensionless indicators Froude and Reynolds.

Froude number:

$$Fr = \frac{U}{\sqrt{gh}} = \frac{0.8}{\sqrt{9.81 \times 4.0}} \approx 0.128$$

This result indicates that the flow was subcritical ($Fr < 1$). Subcritical flow is typical for Dutch lowland rivers. The Froude number may be higher near the groyne structures due to flow acceleration and water build-up, but will most probably not lead to a Froude number above 0.5.

Reynolds number:

$$Re = \frac{Uh}{\nu} = \frac{0.8 \times 4.0}{1.0 \times 10^{-6}} = 3.2 \times 10^6$$

This value confirms that the flow is fully turbulent, as expected in a river system with this velocity and depth.

3.2.5. Radius of curvature & spiral flow

The area of the Xstream groyne is located just at the end of a river bend, as shown in Figure 3.1. This bend has a certain radius of curvature that can impact the flow distribution and, with that, the sediment transport. This will mainly be translated into the magnitude of spiral flow, as explained in Section 2.4. From Figure 3.1, the radius of curvature is calculated, and a value of approximately 1200 metres was found. The river's width is approximately 200 metres. With the equations from Section 2.4, the gradient of the water surface over the transverse can be determined.

Using a depth-averaged streamwise velocity of u = 0.79 m/s (Determined value with the flow velocity measurements in Section 3.4.1) and a bend radius of R = 1200 metres, the transverse water surface slope can be estimated using the relation $\partial h/\partial r \approx u^2/(Rg)$ (from Section 2.4). Substituting these values gives a slope of approximately 5.3×10^{-5}. Over a channel width of 200 metres, this corresponds to a water level difference $\Delta h \approx 0.0106$ metres or 1.06 centimetres between the inner and outer banks. While small in magnitude, this difference could be enough to induce a cross-stream pressure gradient that drives the development of spiral flow.

The slope of the transverse velocity over the depth can also be determined. With a flow depth of h = 5.2 metres, the transverse velocity varies linearly from the bed to the surface. For this case, the slope over depth becomes $\frac{dv_n}{dz} = \frac{12\bar{u}}{R}$. Assuming a depth-averaged velocity of $\bar{u}$ = 0.79 m/s and a bend radius of $R = 1200$ metres, this results in a slope of $\frac{dv_n}{dz}$ = 7.90×10^{-3}. Consequently, the transverse velocity varies from approximately -0.0206 m/s near the bed to +0.0206 m/s near the surface. This function neglects the friction parameter at the boundaries, which could lead to inaccurate values, primarily near the bed level. However, for an approximation of the transverse velocity slope over the depth, this can still be considered valuable.

3.2.6. Sediment distribution and river slope

The mean sediment size regularly becomes finer over the transect of a river. That is why finer sediment sizes are found at the Xstream groyne location. Figure 3.5 shows the results of a sediment research in the area by Deltares (Buschman & Kosters, 2021). They found that the soil was made up of a large range of sediment sizes, including several shell banks. An average sediment size can be set to 0.5 millimetres for the median (D_{50}). This also corresponds to the statements made in a report of Rijkswaterstaat (Wilbers, 1997) that showed the same values. This report states that the bed has a slope of 0.83×10^{-4}.

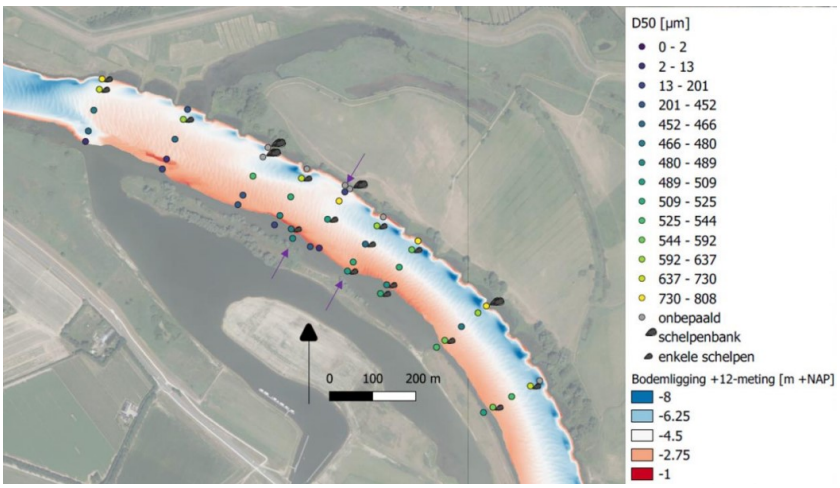

Figure 3.5: Median sediment size D_{50} (Buschman & Kosters, 2021)

Based on this median grain size, the critical bed shear stress for sediment motion can be estimated using the Shields criterion from Section 2.3.2. For fully turbulent river flow, the critical Shields parameter θ_c is typically taken as 0.055. Using this and assuming a sediment density of $\rho_s = 2650\,\mathrm{kg/m^3}$ and water density $\rho = 1000\,\mathrm{kg/m^3}$, the critical shear stress τ_c can be calculated as:

$$\tau_c = 0.055 \cdot (2650 - 1000) \cdot 9.81 \cdot 0.0005 \approx 0.44\,\mathrm{Pa}$$

This means that bed shear stresses exceeding approximately 0.44 pascals are expected to initiate sediment transport.

3.3. Bed level measurement analysis

The implementation of the Xstream groyne has been divided into two phases. Phase 1 (Buschman & Kosters, 2021) extends to the three smaller Xstream groyne versions in the area, while phase 2 (Buschman, 2024) is when the two groynes in the inner bend were removed and the outer bend groyne was extended to its current length. Before and during these phases, extensive measurements have been carried out in the area to get a clear perspective on the morphological behaviour around the Xstream groyne.

3.3.1. Before and during Phase 1

Phase 1 involved the implementation of three smaller Xstream groynes: two in the inner bend and one in the outer bend, each approximately 10 metres long. Observations on morphological changes during this phase are made by making use of three multibeam measurements: before groyne implementation (2017-08), shortly after groyne placement (2020-05) and just before groyne extension (2022-10).

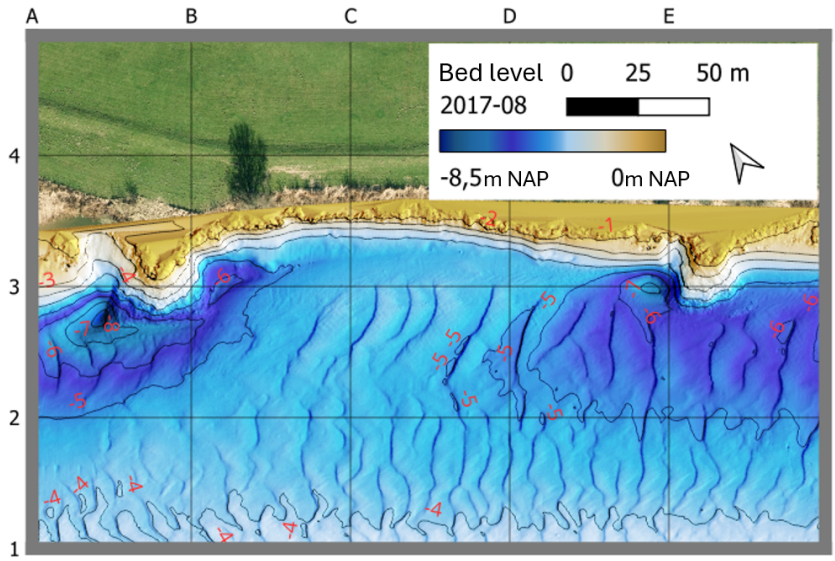

Figure 3.6: Bed topography from 2017-08

Before the groyne installation, a shallow area inside the groyne field was observed, which was surrounded by clear scour patterns visible at the existing groyne heads. Figure 3.6 shows a depth map of the area before the implementation of the groyne. A significantly large scour pit at the downstream groyne and a second scour pit located upstream of this groyne are identified. These unusual formations may result from a higher aspect ratio that was present before the placement of the Xstream groyne.

A difference map in Figure 3.7 shows the amount of erosion and sedimentation in the area between the date of the bed topography map of Figure 3.6 (2017-08) and just before extension of the groyne. Here, the impact of the smaller groyne on the area is visible. During this period, morphological changes became apparent, primarily by erosion around the groyne head, indicating morphologic behaviour as explained in Section 2.3.1. Partial sediment deposition occurred within the downstream scour pits. A sediment transport balance was done to see the erosion and sedimentation in the groyne field area. The area indicated by raster-squares A2 to D3 (excluding boundaries with excessive changes due to measurement inconsistencies) amounts to approximately 14,000 m^2. Over this period, the volume of eroded sediment was around 1,920 m^3, while sedimentation accounted for roughly 445 m^3. This results

in a net sediment export of approximately 1,475 m³ from the groyne field.

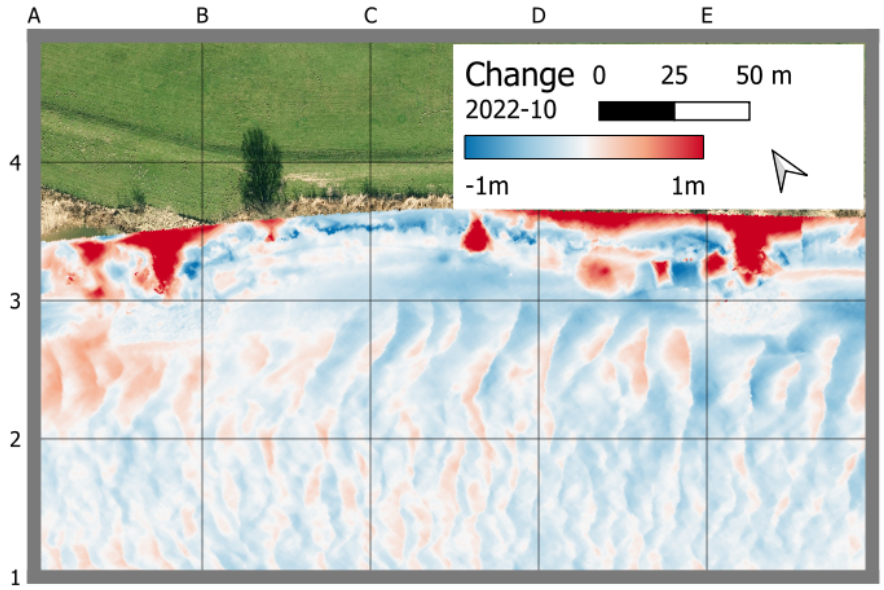

Figure 3.7: Bed level difference between 2017-08 and 2022-10 (Blue areas show erosion, while red areas show sedimentation)

3.3.2. During Phase 2

In the first year after extending the Xstream groyne to 25 metres long, substantial morphological changes were seen. In the first few months, large-scale erosion prominently developed in front of the groyne head, as shown in Figure 3.8, which became a distinct feature throughout the year. To quantify this, another sediment balance for the area, consisting of 16,500 m^2, was made. It showed again more erosion (1,650 m^3) than accretion (1,330 m^3), resulting in a net sediment export of approximately 325 m^3.

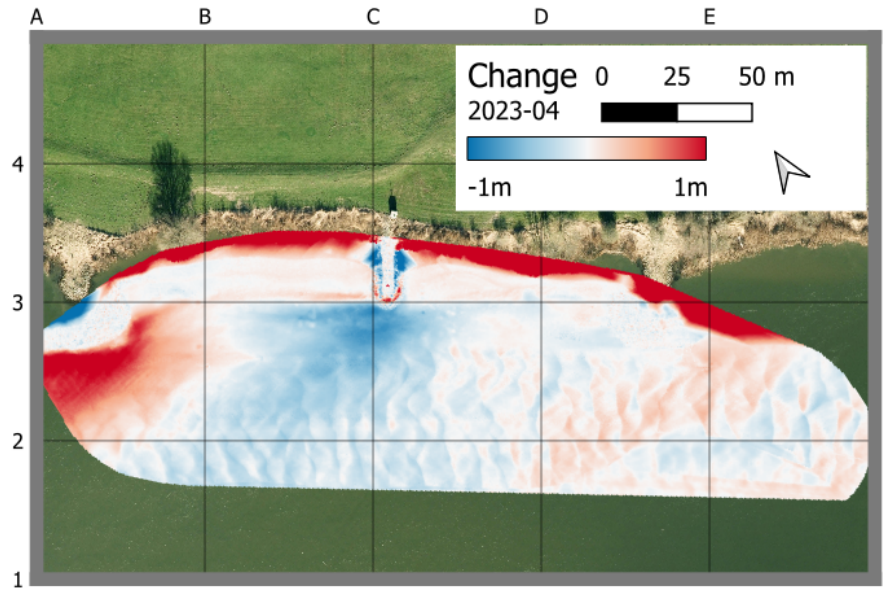

Figure 3.8: Bed level difference between 2022-11 and 2023-03 (Blue areas show erosion, while red areas show sedimentation)

Following the groyne extension, the sediment line was first observed forming downstream of the groyne. Figure 3.9a shows the cross-section of the base of the sediment line. In the first four months, the line formed a sharp peak near the groyne head. According to the hydrograph in Figure 3.2, the first year (till 2023-10) coincided with relatively low discharge. Toward the end of the year, the sediment line flattened and broadened. During these few months, the depth changes in the main channel and the groyne field are relatively small. The measurement taken in 2023-11 is during a much higher discharge, at which the groyne is almost submerged, showing immediate changes at the riverbed. During this period, again erosion is observed in the main channel, causing the riverbed to be a full metre lower than the year before.

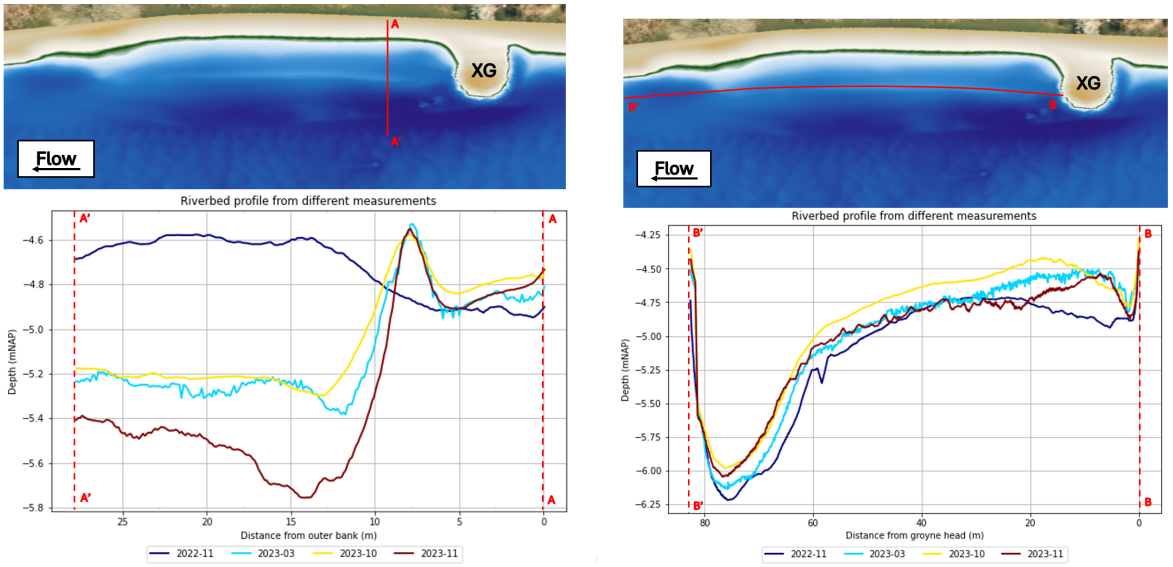

(a) Cross section base of sediment line

(b) Cross section full sediment line

Figure 3.9: Two cross sections that present the movement of the sediment line in the first year

Figure 3.9b shows a cross-section along the full sediment line (through the groyne field). Near the groyne head, the sediment line forms, reaching its largest height (of approximately 0.3 metres). At the end of the groyne field, around 60 metres from the groyne head, the upstream scour pit is located. Apart from the formation of the sediment line, no larger changes are observed during these measurements.

In the second year after the extension of the Xstream groyne, morphological changes continued to develop. The measurement from 2023-11, precisely one year after the extension, captured a high discharge scenario at around 850 m^3/s, which led to more erosion and shifted the sediment line closer to shore. Two months later, in 2024-01, discharge had decreased slightly after a short period where groynes were submerged. Using Table 3.1, the water level was estimated at +1.12 metres NAP, meaning the groynes were submerged by approximately 0.37 metres. The influence of groyne submergence appeared to be limited, as only minor changes in sedimentation were observed within the downstream groyne field. However, notable erosion continued near the groyne head, accompanied by sedimentation further into the groyne field.

The 2024-02 measurement, taken during another raised discharge, revealed the deepest bed levels observed in the area so far. Figure 3.10 presents the local bed level slopes. Several notable features are visible:

1. Two rings near the groyne show high slopes, likely indicating the presence of glacial boulders

known to occur in this part of the IJssel (van der Heide & Hellinga, 1954).

2. A groove running parallel to the sediment line, forming a boundary between the groyne field and the main channel.
3. This area between the sediment line and the grooves shows different morphological behaviour than in the channel. No ripples are present, and the gradients are lower.
4. The groyne field near the river bank also seems flat relative to the channel. This flattening seems to go hand in hand with the sediment line formation, as this also occurred in the first months after the groyne extension.

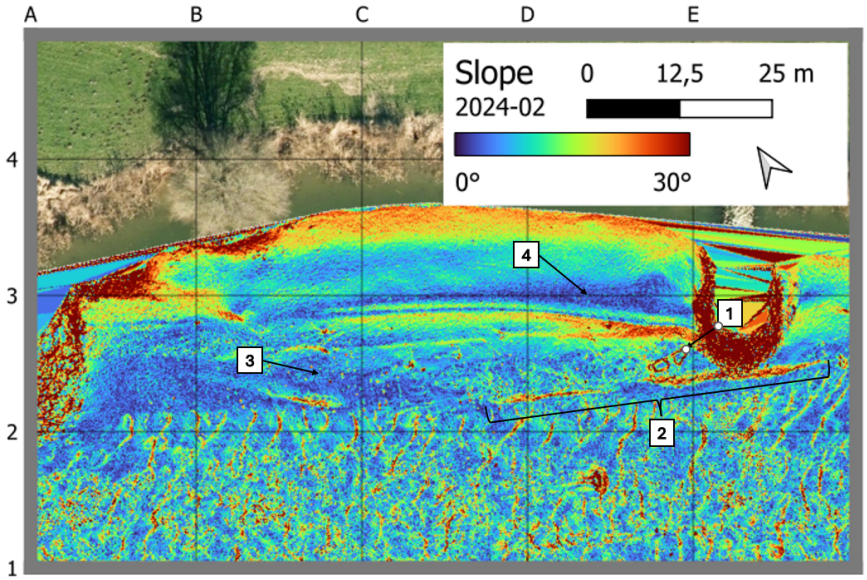

Figure 3.10: Slope figure of 2024-02

Figure 3.11a indicates a shift of the sediment line towards the shore during higher discharges, while maintaining its height and width. However, after a period of lower discharges (2024-10), the height of the base of the sediment line decreased significantly. Toward the channel, even more erosion can be observed. With another cross-section of the sediment line in Figure 3.11b, its change through the second year can be better observed. The figure shows that the groove near the groyne increased significantly, mainly due to a period of low discharge, while the average height of the line is still higher than the year before.

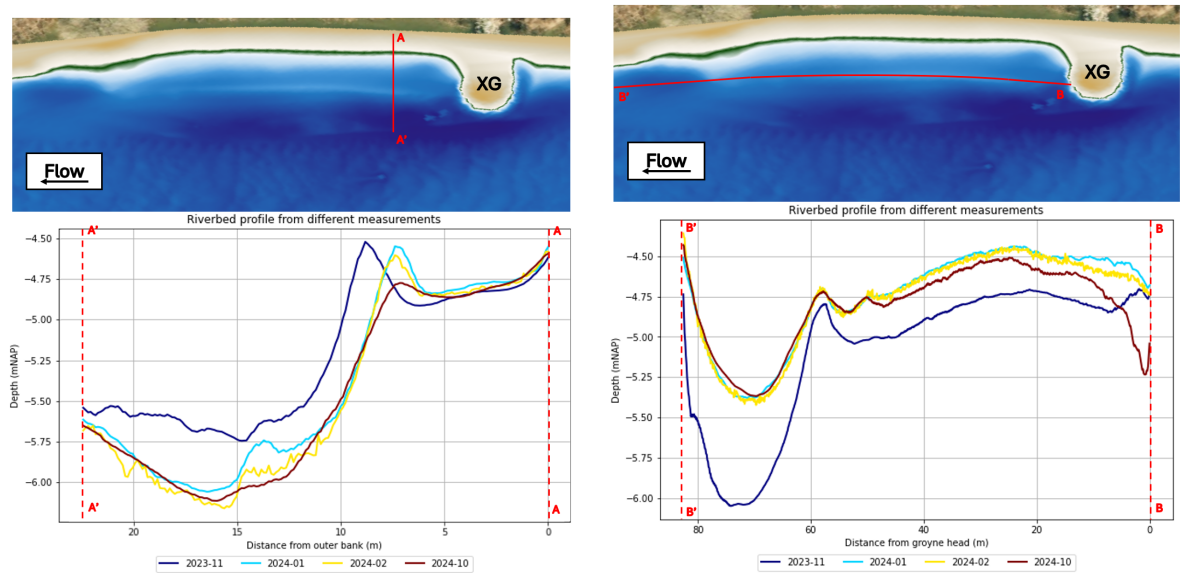

(a) Cross section base of sediment line

(b) Cross section of full sediment line

Figure 3.11: Two cross sections that present the movement of the sediment line in the second year

An additional measurement was done in March 2025. A bed topography map of March is shown in Figure 3.12a. The overall depth changes were relatively minor during this period. This could indicate that the area is slowly heading towards an equilibrium state. Nevertheless, erosion was predominant.

Figure 3.12b shows the full lifetime of the base of the sediment line through a cross-section. The line is formed just outside the groyne field, shifting towards the shore through the years. The higher discharges around January 2024 have a larger effect on its movement. After some time, when the area near the channel is also partially eroded, the sediment line decreases in height, although changes become less significant. This indicates an equilibrium pattern. From February 2024 onward, a secondary ridge is observed near the groyne head. Together with the sediment line, it borders an area where accelerated flow is expected, possibly marking the outer boundary of the mixing layer. From the slopes in Figure 3.10, this was also observed.

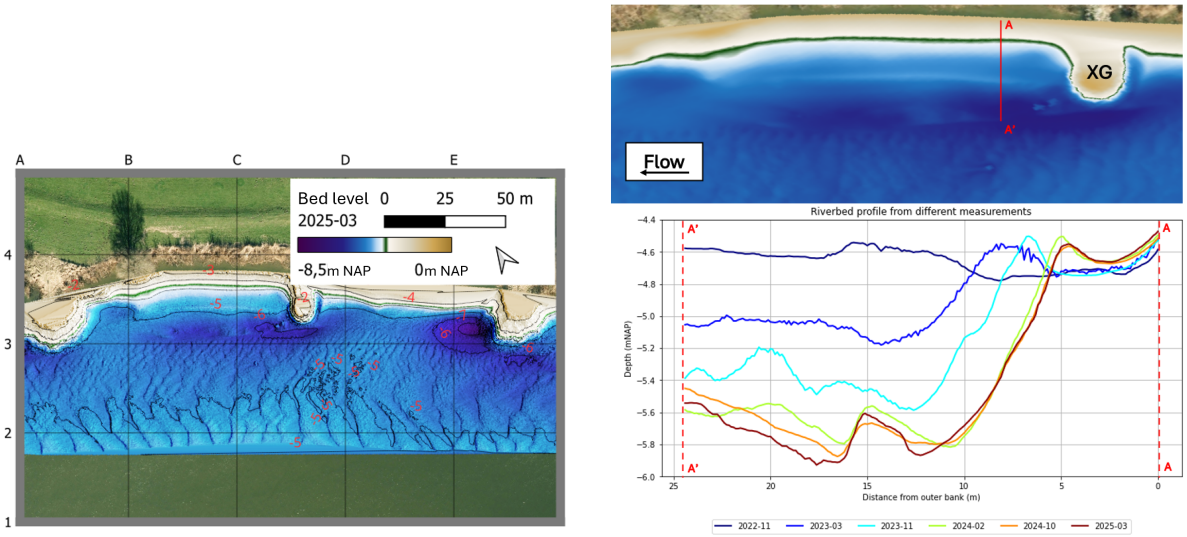

(a) bed topography in 2025-03

(b) Cross section base of the sediment line

Figure 3.12: Left: bed level measurement of 2025-03, right: complete lifetime of the base of the sediment line

3.3.3. Summary on the morphodynamic findings

The multibeam measurements taken before and after the construction and extension of the Xstream groyne reveal a structured morphodynamic evolution. The most relevant observations are:

1. **Initial scour patterns**: Before implementation, the groyne field was shallow and contained multiple scour pits near adjacent traditional groynes.
2. **Phase 1 response**: The introduction of the shorter Xstream groyne caused immediate erosion near the groyne head. Some of the displaced material settled in the downstream scour pit, while the upstream pit remained largely unchanged.
3. **Phase 2 response**: After extension to 25 metres, erosion intensified in front of the groyne, particularly during high discharge periods. Near the groyne head, a second ridge formed. Together with the sediment line, it borders an area where accelerated flow is expected.
4. **Sediment line evolution**: A distinct sediment ridge developed downstream of the groyne, separated from it by a groove. This ridge shifted toward the riverbank during high discharges and flattened during low-flow conditions.
5. **Stability of the groyne field**: The interior of the groyne field remained relatively stable, with erosion concentrated on the channel side and near the groove boundary.

3.4. Flow velocity analysis

This section presents the velocity distribution at the Xstream groyne area, based on the ADCP measurements and float tracking experiments. These provide detailed insights into the velocity distribution across different depths and river sections. The goal is to evaluate the flow patterns in and around the downstream Xstream groyne field and compare them to nearby traditional groyne fields. The ADCP measurements were taken during a raised discharge of approximately 630 m^3/s, which corresponded to a water level of 0.29 metres above NAP.

3.4.1. ADCP measurements

Depth averaged flow

Figure 3.13 shows three vector plots of the depth-averaged velocity field: around the Xstream groyne (a) and the two groyne fields upstream (b) and downstream (c) of this area.

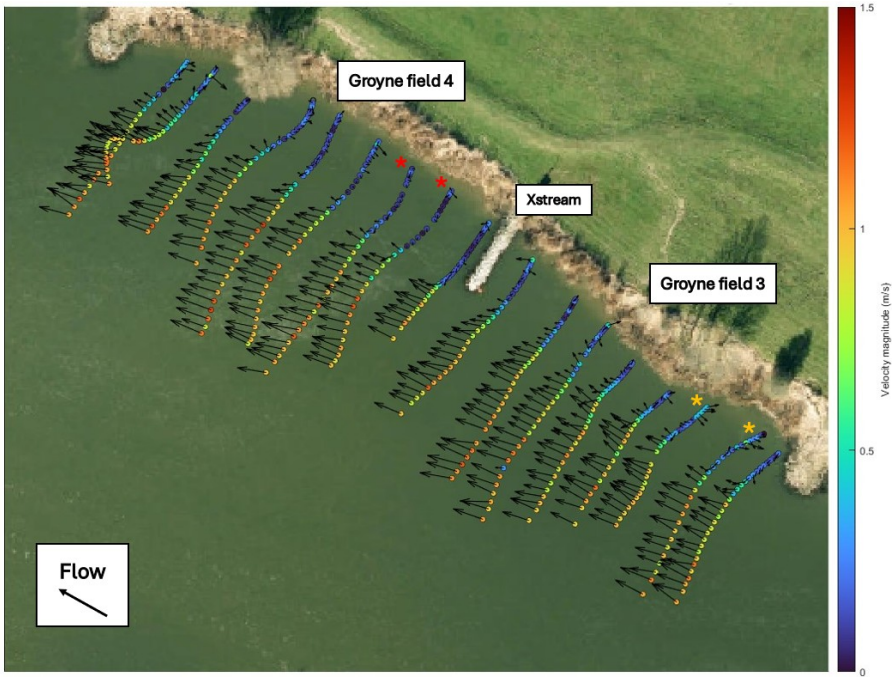

(a) Quiver plot around Xstream groyne

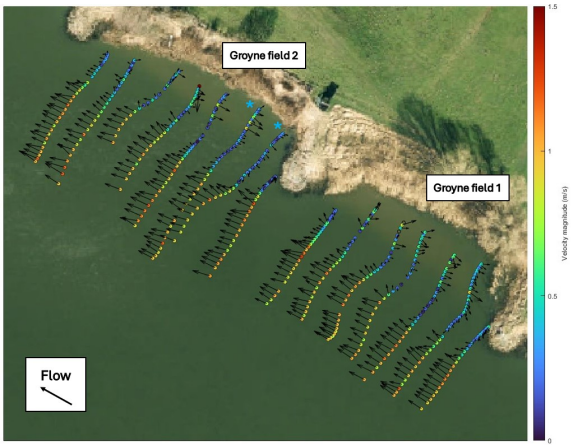

(b) Quiver plot upstream groyne fields

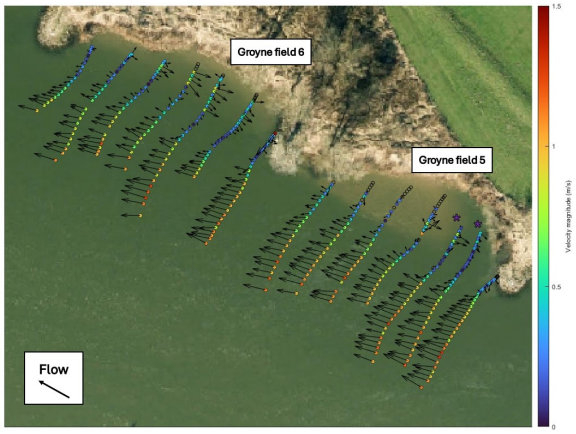

(c) Quiver plot downstream groyne fields

Figure 3.13: Quiver plots showing depth-averaged velocity patterns around the Xstream groyne (a), upstream groyne fields (b) and downstream groyne fields (c)

All groyne fields show a clear contrast between the velocities inside the groyne field and in the main channel. In the channel, velocities exceed 1.0 m/s, while inside the groyne fields, they drop below 0.5 m/s. All groyne fields show similar flow patterns and follow the theory described in Section 2.2, with recirculation zones and flow that follows the groyne heads. Another observation is the low velocities directly downstream of the base of the Xstream groyne. At other groynes, the velocities at this location are more significant, which can be observed in Figures 3.13b and 3.13c. Possibly, due to a mild flow through the permeable structure, the recirculating pattern is suppressed, causing flow speeds to be

close to zero. Just upstream of the Xstream groyne, the flow is primarily pushed towards the channel around the groyne head, despite its permeability.

Figure 3.14 shows the depth-averaged streamwise velocities around the recirculating zones of four groyne fields. The transects that have been used are indicated with stars in Figure 3.13. Near the main channel, velocities are similar for the groyne fields, approximating around 1.0 m/s. Toward the main channel, the velocity decreases and even becomes negative near the riverbank. The table of Figure 3.14 explains the decrease in velocity toward the channel. Notably, the relatively weak slope of groyne field 4, which is the groyne field downstream of the Xstream groyne, is also notable. Also, the groyne field does not indicate negative velocities.

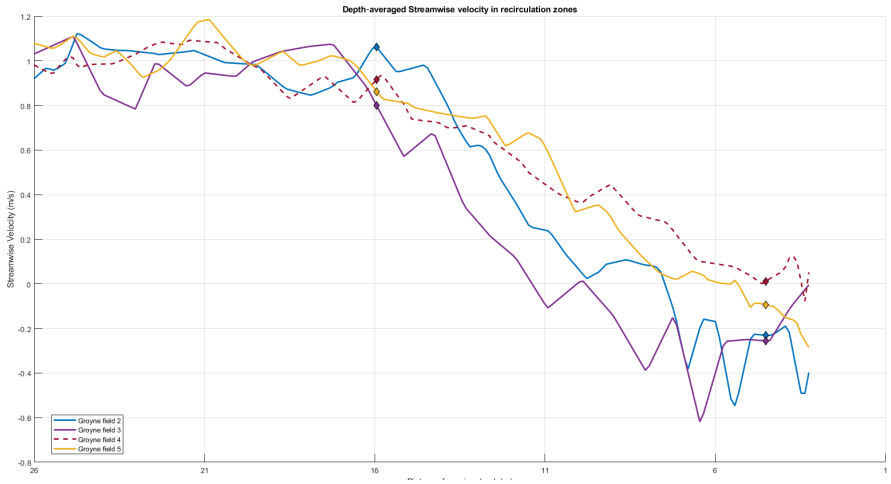

Field	Slope (m/s per m)
Groyne field 2	0.108
Groyne field 3	0.110
Groyne field 4	0.077
Groyne field 5	0.093

Figure 3.14: Streamwise velocity magnitudes near the groyne heads. Left: depth-averaged streamwise velocity in recirculation zones (dashed line indicates downstream of Xstream groyne). Right: slope of velocity decline, with values corresponding to diamonds shown in the graph

Depth specific flow

Besides the general depth-averaged patterns, the flow characteristics at specific depth levels also reveal important insights. Local variations in streamwise, transverse, and vertical velocities highlight fine-scale flow dynamics. These localised patterns can provide valuable explanations for the flow processes occurring near the Xstream groyne, as discussed in the following chapter.

It is important to note that the measurements were taken over a relatively short time period. As a result, the data represent a transient flow state, rather than a time-averaged condition. In regions with highly turbulent structures, such transient figures may not fully capture long-term behaviour, but they can still offer meaningful insights into momentary flow features and instabilities. It should also be noted that for small magnitudes, the measurement becomes more sensitive to errors, which is mostly the case for the vertical velocities.

Streamwise velocity profiles near groyne heads:

Figure 3.15a shows velocity profiles measured near the Xstream (blue) and traditional (orange) groynes. The Xstream groyne shows an overall higher velocity profile. Near the bed, the velocity profiles show linear shapes, but the velocity distribution at the traditional groyne profile is much wider. That is why velocities are lower at the traditional groyne near the bed. Near the surface, both velocity profiles show velocities of approximately 0.75 to 0.85 m/s. However, the traditional groyne shows a uniform shape,

while the Xstream profile decreases toward the surface, suggesting higher surface friction than at the Xstream groyne.

The measured velocity of approximately 0.8 m/s can be compared with a simple calculation of the flow speed by dividing the discharge by a river cross-section near the Xstream groyne. Using the bed level profile of Figure 3.3, a river cross-section at a water level of 0.29 metres is found of 796 m^2. With a discharge of 630 m^3/s, the calculated flow velocity is 0.79 m/s. This shows a similar approximation of the velocity as the measurements.

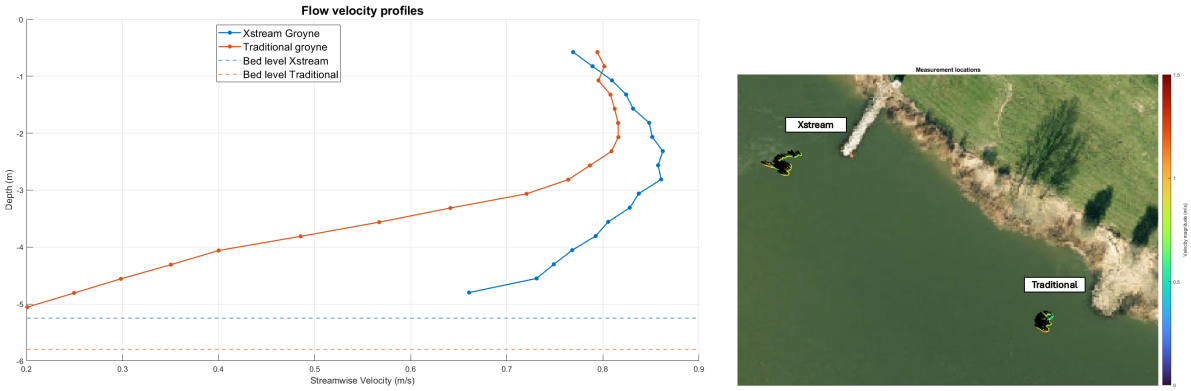

(a) **(b)**

Figure 3.15: (a) Streamwise velocity profiles with bed levels, (b) Measurement locations of the two flow velocity profiles

Near the traditional groyne:

Figures 3.16 and 3.17 show cross-sections near the upstream traditional groyne (in between groyne fields 2 and 3) and near the Xstream groyne. The colours indicate the streamwise velocities with red positive values and blue negative values. Also, the transverse and vertical velocities are indicated with quivers.

Figure 3.16a shows a cross-section just downstream of the traditional groyne. Here, the flow inside the groyne field is directed toward the channel going downward. The blue colors indicate a clear recirculating pattern. Figure 3.16b shows a cross-section just upstream of the traditional groyne. Here, the recirculation zones are only slightly visible. This is a measurement default, as the measured transect did not reach deep enough in the groyne field. A flow direction toward the main channel can be observed, suggesting that the flow wants to go around the groyne head. However, no clear vertical flow patterns are present.

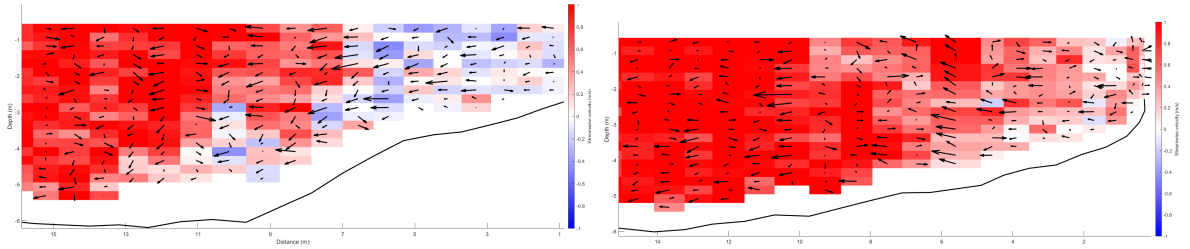

(a) Velocities just downstream **(b)** Velocities just upstream

Figure 3.16: Velocities at the upstream traditional groyne. (Colour bar: streamwise direction, with positive values in the direction of the main flow. The quivers show a combined direction of transverse and vertical flow components)

Near the Xstream groyne

Around the Xstream groyne, the flow exhibits several deviations from the patterns described above. Figure 3.17a shows the flow patterns just downstream of the Xstream groyne. Around 8 meters from the riverbank, the flow shows a clear flow direction that is directed toward the channel, while the other vector shows inconsistent behaviour that could be caused by the transient behaviour of the measurement or the low velocities here. At approximately 11 meters from the riverbank, a slight downward flow can be observed, which could be due to a present spiral flow. Overall, Figure 3.17a does not show any clear vertical velocity patterns. Figure 3.17b shows the flow patterns just upstream of the Xstream groyne head. Here, the most present flow pattern is the transverse directed flow toward the main channel at around 8 to 12 meters. This larger flow may be caused by the groyne obstruction of the flow field due to the Xstream groyne, which directs the main flow around the groyne head. More towards the channel, the transverse velocities are highly variable, both in direction and magnitude. Again, the vertical velocities are not clearly visible.

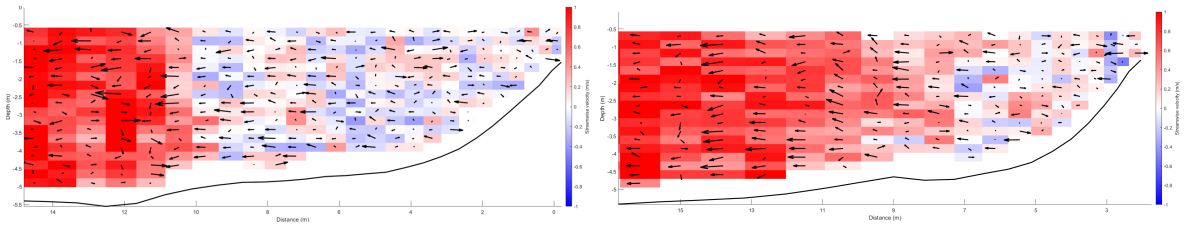

(a) Velocities just downstream

(b) Velocities just upstream

Figure 3.17: Velocities at the Xstream groyne (Colour bar: streamwise direction, with positive values in the direction of the main flow. The quivers show a combined direction of transverse and vertical flow components)

Near the sediment line:

The ADCP measurement also gives a description of the specific flow patterns near the sediment line. Figure 3.18 shows this flow behaviour around the sediment line. It can be described at four distinct locations: the base (1), the middle (2), the tail (3) and the wake (4), as illustrated in the figure.

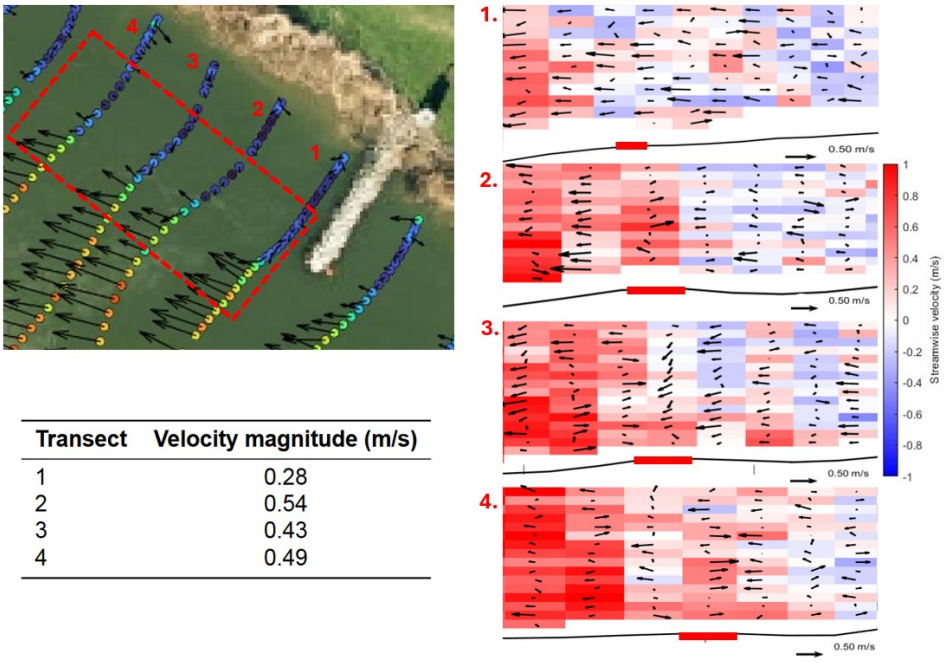

Transect	Velocity magnitude (m/s)
1	0.28
2	0.54
3	0.43
4	0.49

Figure 3.18: Flow analysis of the sediment line. **Left:** Aerial view showing the four ADCP transects near the sediment line. **Right:** Velocity cross-sections, with the red bar on the channel wall indicating the sediment line location. **Table:** Near-bed (three-dimensional) velocity magnitudes at the line

Near the base, flow is primarily directed toward the main channel, potentially contributing to the formation of the groove separating the groyne from the sediment line. The 3D velocity magnitude at this part is, however, relatively weak. Around the middle, the groyne-field side exhibits a negative streamwise velocity due to recirculation, with negligible transverse and vertical velocities. On the channel side, however, streamwise flow remains positive, accompanied by significant transverse velocities directed away from the sediment line. As a result, the sediment line's middle segment would experience minimal flow disturbance even though the velocity magnitude is strongest here. Near the tail, flow directions on either side of the line converge: flow within the groyne field moves outward towards the channel, whereas the channel-side flow is directed inward toward the groyne field. Additionally, vertical velocities at this location are downward-directed, further contributing to flow convergence at the tail of the sediment line. Where flow converges, an increase in energy is expected, which is translated into an increase in flow velocity. In the fourth figure, the velocities above the line seem higher and the three-dimensional magnitude is also relatively high, which indicates that the flow indeed converges in the wake of the sediment line.

Figure 3.19 is added to give a representation of these flows around the sediment line. The black arrows show flow deflection around the groyne. The red arrow represents the flow toward the channel, indicating the observation near the base of the line. The orange arrows are around the middle of the line, weak and straight in the groyne field and strong and curved near the channel. The yellow arrows indicate the flow convergence at the tail.

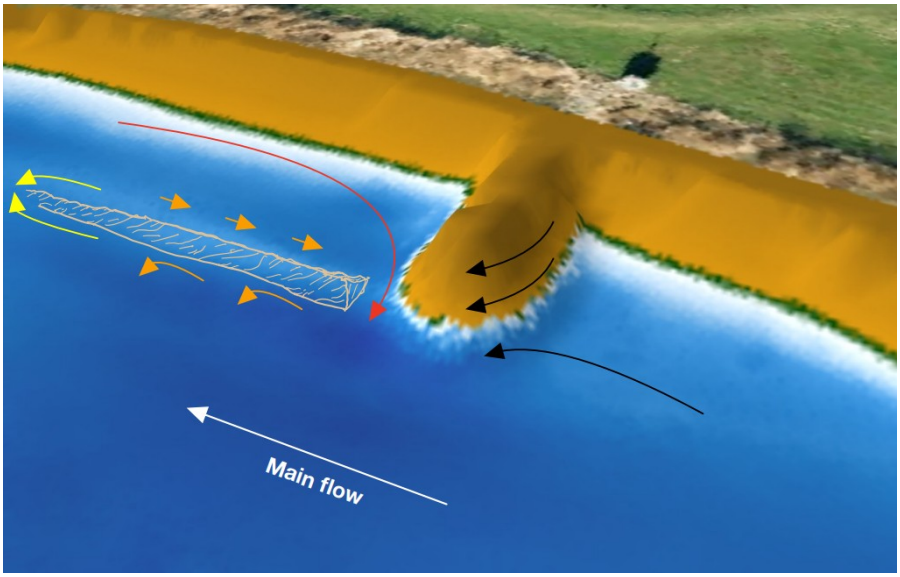

Figure 3.19: Three-dimensional view of streamlines near the sediment line at the Xstream groyne

Spiral flow

The ADCP measurements could possibly tell something about the magnitude of spiral flow in the area. Most of the data was collected near groynes, where turbulence can strongly influence the transverse velocity profile, potentially altering the spiral flow pattern. Additionally, the relatively short duration of each measurement may hinder accurate characterisation of vertical velocity structures. Therefore, the analysis focused only on the five depth profiles of each transect located closest to the main channel, where flow is generally less disturbed by groyne-induced turbulence. By averaging all depth profiles per groyne field, these selected profiles are expected to reflect the spiral flow structure more reliably.

The results are shown in Figure 3.20, which displays the depth profiles of transverse velocity for all groyne fields shown in Figure 3.13. A clear presence of spiral flow is not directly observable due to the small number of measurement points across the depth. However, slight gradients in the profiles are visible, which could suggest the presence of spiral flow. Observed transverse velocity magnitudes range between -0.05 m/s and $+0.05$ m/s.

These observed values can be compared with the theoretically calculated transverse velocity from Section 3.2.5. There a velocity range, from approximately -0.0206 m/s at the bed to $+0.0206$ m/s at the surface, was determined.

The calculated values lie within the same order of magnitude as the observed data, but are approximately twice as large. The difference may be attributed to local flow disturbances caused by groynes, measurement resolution limitations or neglecting friction effects.

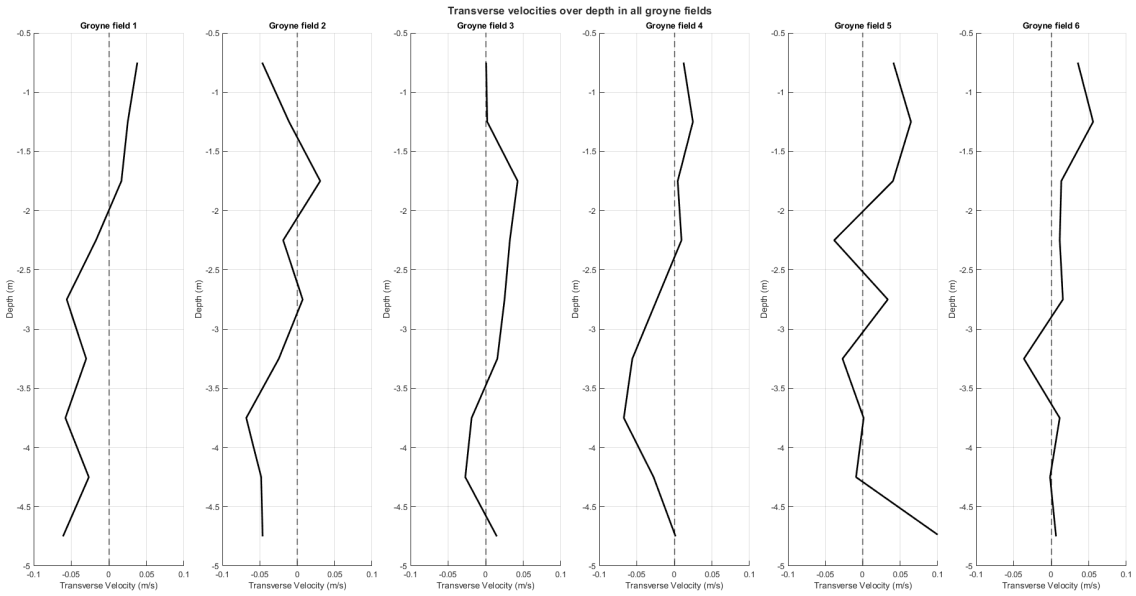

Figure 3.20: Spiral flow representation from ADCP measurements. From left to right: the most upstream groyne field to the most downstream groyne field

3.4.2. Float tracking tests

Figure 3.21 compares the flow paths near two different groyne types: a traditional groyne (upstream) and the Xstream groyne. At the traditional groyne, the orange trajectories curve strongly toward the groyne field after passing the groyne head, indicating a clear recirculating pattern. This behaviour is characteristic of a well-developed horizontal eddy and horizontal mixing layer flow.

In contrast, at the Xstream groyne, the tracer paths remain more aligned with the main channel direction. Instead of being diverted into the groyne field, the flow continues downstream along a narrower band closer to the main channel axis. This suggests a weaker return vortex or reduced horizontal entrainment at the Xstream groyne. That means the Xstream groyne appears to create a less obstructive hydrodynamic footprint. These observations support the modelled flow field results and suggest that the Xstream groyne shows reduced mixing at the water surface.

(a) Tracked path of the oranges around traditional groyne **(b)** Tracked path of the oranges around Xstream groyne

Figure 3.21: Comparison of float tracking tests at Xstream and traditional groynes

3.4.3. Summary on hydrodynamic findings:

The hydrodynamic behaviour around the Xstream groyne was analysed through ADCP measurements and float tracking tests. These results confirmed the presence of flow features associated with groynes. The primary observations have been summed up:

1. **Suppressed recirculation and milder mixing layer:** Flow behind the Xstream groyne shows a weaker and more elongated recirculation zone compared to traditional groynes. The velocity gradient across the mixing layer was observed to be milder than in adjacent groyne fields.
2. **Altered velocity profile:** The streamwise velocity profile near the Xstream groyne differs from the profile at the traditional groyne. At the Xtream groyne, the velocities near the bed were higher. Near the surface, the profiles showed similar flow speeds. However, a more uniform profile was observed near the traditional groyne.
3. **Flow deflection into main channel:** Flow is pushed around the Xstream groyne head, despite its permeability resembling the behaviour seen at traditional groynes.
4. **Distinct flow separation near sediment line:** A flow transition zone is observed along the sediment line: flow inside is stagnant or weakly circulating, while outside it accelerates sharply into the main channel. This boundary aligns with the outer edge of the mixing layer and is consistent across discharge conditions.
5. **Weaker surface return flow:** Float tracking reveals short, but clear recirculation loops at the traditional groyne compared to a stronger, tighter flow at the Xstream groyne, confirming suppressed surface vortex activity.

4

Software selection

This chapter presents the software selection process used to choose the most appropriate numerical modelling tool for simulating the flow behaviour around the Xstream groyne. While later chapters detail the full model setup and results, this chapter focuses on evaluating and comparing different hydrodynamic modelling packages using a multi-criteria analysis.

The model aims to:

- Investigate how groyne characteristics such as permeability and slope affect flow separation, recirculation strength and mixing layer development.
- Explore the three-dimensional structure of the flow, including vertical and transverse velocity components, which are difficult to measure comprehensively in the field.
- Identify the hydrodynamic and morphodynamic conditions that lead to the formation of a sediment ridge and scouring patterns observed near the Xstream groyne.
- Compare the performance of the Xstream groyne concept to that of a traditional groyne under similar hydraulic conditions.

This chapter is structured as follows. Section 4.1 defines and evaluates relevant modelling criteria. A multi-criteria analysis (MCA) in Section 4.2 is performed to score and compare five software packages. Based on this analysis, a final selection is made that best aligns with the modelling objectives.

Several 3D hydrodynamic modelling tools were considered. The options include three CFD packages: ANSYS Fluent, OpenFOAM and FLOW-3D. Also, two flow models with integrated morphodynamic capabilities are taken into account: Delft3D FLOW and MIKE3. The focus is on these five modelling packages and evaluating them with a multi-criteria analysis to identify the most suitable one. Each model is assessed on modelling capabilities, which are based on information found in the manuals of ANSYS Fluent (ANSYS, 2025), OpenFOAM (The OpenFOAM Foundation, 2024), FLOW-3D (Flow Science, 2019), Delft3D FLOW (Deltares, 2025) and MIKE3 (DHI Group, 2025).

4.1. Software criteria

This section defines general modelling criteria relevant for the hydrodynamic simulations on which each software's capabilities are compared. These baseline criteria include the solving methods, morphodynamic coupling, representation of permeability, wall functions, free surface boundary and the practicality of the models.

Solving methods

One of the key distinctions for numerical modelling lies in the governing equations they solve and whether they support hydrostatic or non-hydrostatic flow assumptions. This is particularly important in the context of sloped groynes, where the flow structure can vary significantly with depth due to separation, turbulence, and vertical shear (Section 2.2). Models that can resolve three-dimensional and non-hydrostatic effects are therefore more suitable for accurately simulating flow behaviour for this research.

ANSYS Fluent solves the full three-dimensional Navier–Stokes equations and includes turbulence modelling through RANS (Reynolds Averaged Navier-Stokes) and LES (Large Eddy Simulation). It is non-hydrostatic and well-suited for resolving vertical flow structures over complex geometries. FLOW-3D also uses the full non-hydrostatic Navier–Stokes equations, making it highly applicable to flows with strong vertical dynamics. OpenFOAM provides a similar option to the other two with various solvers and turbulence models. Delft3D, in contrast, is based primarily on depth-averaged shallow water equations, with a 3D hydrostatic extension that does not resolve vertical accelerations, which limits its use in strongly three-dimensional flows. MIKE3 supports both hydrostatic and non-hydrostatic formulations, offering the ability to model vertical flow variations when needed, though the non-hydrostatic option is still based on a layered grid structure and simplified vertical momentum formulation, making it less detailed than the full CFD approaches used in ANSYS Fluent, FLOW-3D or OpenFOAM.

Morphodynamic coupling

Simulating morphodynamic processes, such as sediment transport and bed level change, can be highly valuable when assessing how structures like groynes influence long-term river morphology. While not always a requirement, having an integrated morphodynamic module allows a more direct estimation of bed evolution without interpreting flow results separately for sediment response.

ANSYS Fluent does not include integrated morphodynamic capabilities. While there are options to script sediment transport or couple with external tools manually, this is not typically practical. FLOW-3D offers built-in sediment transport and scour modules, supporting bedload and suspended load transport. It allows for bed changes, making it well-suited for local morphodynamic studies around structures. OpenFOAM offers custom-implemented models, which are developed through its community (Chauchat et al., 2017). These offer coupling between hydrodynamics and bed evolution, but are technically more complicated to master. Delft3D has an integrated morphodynamic module, capable of simulating sediment transport with feedback to the flow field. It supports multiple grain sizes and cohesive and non-cohesive sediments and has been widely applied in real-world coastal and riverine morphodynamic studies. MIKE3 similarly includes a sediment transport module that can model both suspended and bedload transport, as well as bed level changes.

Permeability representation

The ability to represent a permeable structure is important when simulating the Xstream groyne. A model that supports internal flow through permeable domains enables more realistic simulation of flow

dynamics through and around a permeable groyne.

ANSYS Fluent includes advanced porous media modelling capabilities, allowing users to assign porosity and permeability directly to zones within the mesh. It can define a given permeability so that flow through the groyne is modelled by their 'superficial velocity porous formulation'. FLOW-3D and OpenFOAM provide porous media modelling mainly via the Forchheimer equation. This equation defines resistance characteristics within specified regions of the domain. Implementation is flexible but may require manual setup and parameter tuning. Delft3D, in contrast, offers only limited support for internal flow through porous structures. Permeability effects are typically approximated using increased bed roughness or a special "porous plate" object to represent partially transparent barriers. A porous plate in Delft3D is essentially a thin structure where a user-specified porosity and hydraulic friction factor determine the flow passing through. This is, however, not compatible with the complex groyne structure. MIKE 3 does not provide a similar porous media element for open channel flow. Permeability requires a culvert with a certain head loss, which is hard to determine. Overall, the CFD packages score better on this criterion.

Wall functions

Accurate representation of near-wall flow behaviour is essential for modelling friction, shear stress, and turbulence effects close to boundaries. Wall functions serve as a numerical approximation of near-wall turbulence without resolving the entire viscous sublayer, which would otherwise require extremely fine meshes and excessive computational resources.

ANSYS Fluent, FLOW-3D, and OpenFOAM all include standard wall function formulations that interact with their turbulence models and allow users to define wall roughness. While they differ slightly in implementation and flexibility, their capabilities are broadly comparable in how they handle near-wall flow. In contrast, Delft3D and MIKE3 apply friction through empirical coefficients such as Manning or Chezy, without resolving boundary layers. These approaches are suitable for large-scale hydrodynamics but offer less detail near boundaries, which is relevant for groyne flow dynamics.

Free-surface modelling

Approaches to free-surface modelling vary depending on the numerical framework and intended use of the model. ANSYS Fluent and OpenFOAM offer multiple free-surface modelling options, most notably the Volume of Fluid (VOF) method and level-set (rigid lid) approaches. This flexibility allows users to select the method that best fits their mesh resolution and physical requirements. FLOW-3D, in contrast, uses only the VOF method for free-surface modelling. Its implementation, known as TruVOF, is tailored for hydraulic and open-channel flows and is highly accurate for modelling sharp surface gradients and multiphase interactions. However, it does not offer level-set interface tracking methods, so users have less flexibility if a less sophisticated approach is desired.

Delft3D and MIKE3 do not use interface-capturing techniques. Instead, they compute a free surface elevation field based on hydrostatic (or simplified non-hydrostatic) assumptions. This surface elevation approach is suitable for broad-scale flow and wave modelling, but it does not capture local surface deformation in detail.

Practicality

The practicality itself can be divided into three parts: accesibility, user friendliness and parallel run capabilities.

Accessibility: The accessibility of modelling packages varies widely depending on their licensing options. ANSYS Fluent is a commercial package that requires a paid license. However, licensing is available for this research. FLOW-3D is also a commercial product and offers research licenses for students only on request. This license is only available for four months and extensions are only available through paid academic licenses. OpenFOAM is fully open-source and freely available, with no licensing restrictions. It can be installed, modified, and redistributed without cost, making it highly accessible to both students and professionals. Delft3D is partialy open-source, however, the full version is available for this research. MIKE3 is a commercial package developed by DHI, and it requires a license for use. Like ANSYS Fluent and Delft3D a license is available for MIKE3.

User friendliness: The ease of using a modelling package depends on how straightforward it is to set up geometry, generate a mesh, define physical conditions, and manage simulations, as well as whether a graphical interface is available and what level of technical support can be expected. ANSYS Fluent provides a fully integrated GUI. Mainly, off-line technical support is available. FLOW-3D also includes a dedicated GUI designed for hydraulic modelling. Support is only provided through licensed access, which is not available via student licensing. OpenFOAM does not include a GUI. Instead, users define simulations through text files and scripts, which offer flexibility but come with a larger initial learning threshold. Technical support is not available. Delft3D includes a GUI, though it is less modern in design compared to commercial tools; It does, however, offer a wide variety of technical support. MIKE3 features a comprehensive GUI and provides access to technical support through DHI, as well as offline support options.

Parallel run capabilities: Given the expected scale and complexity of the model, the ability to run simulations in parallel on high-performance computing clusters is an important practical consideration. ANSYS Fluent supports parallel processing and is available on the cluster of Delft University of Technology named DelftBlue (Delft High Performance Computing Centre (DHPC), 2024) and a cluster from Royal BAM Group (DCW). FLOW-3D also supports parallel computing, but no institutional access is available on clusters for this research. OpenFOAM is designed with parallel execution in mind and runs efficiently. For this research it is supported on the cluster of Deltares named hydra7 (h7) and DelftBlue. Delft3D also supports parallel runs and is available on h7 and DelftBlue. MIKE3 supports parallel runs as well, and is accessible on DCW.

4.2. Multi-criteria analysis

This multi-criteria analysis (MCA) evaluates each software package across a set of relevant technical and practical criteria. Scores are assigned to each model based on software capabilities and the specific requirements of this research.

Weight determination

The weights assigned to the criteria are based on the modelling objectives and expected computational setup.

- **Solving methods (0.25):** This criterion has been given the highest weight, as it determines whether the model can resolve depth-dependent, three-dimensional, and non-hydrostatic flow, which is essential for accurately simulating flow structures around the groynes.
- **Morphodynamic coupling (0.05):** While not essential for the core objectives of this study, an integrated morphodynamic module could be useful for directly estimating bed level changes. How-

ever, the main focus lies on hydrodynamic behaviour rather than sediment transport. Morphological trends can still be inferred (though less specifically) by analysing hydrodynamic output such as velocity patterns and bed shear stress. As a result, this criterion is assigned a relatively low weight.

- **Permeability representation (0.10):** The ability to simulate internal flow through permeable groyne structures is important for accuracy, but less critical than flow resolution.
- **Wall functions (0.15):** This criterion reflects the ability to model shear stress and turbulence near walls. It is moderately weighted due to its relevance to near-bed flow and resistance.
- **Free-surface modelling (0.10):** This criterion has a modest weight. No waves or rapidly changing surface features are expected, so detailed surface deformation is not critical. While a water level slope may occur near the groynes, which would be directly visible in a VOF model, a rigid-lid model would by default reconstruct and output water-level elevations from pressure. That way, the slope near the groynes is still visible even without a full free-surface solver.
- **Practicality (0.20):** This criterion captures non-technical but important aspects of model usability. It consists of three equally weighted sub-criteria: accessibility, user friendliness and parallel run capabilities. Even though these fall under the practicality, each sub-criterion is used individually in the scoring table and contributes one-third to the total practicality score, resulting in a combined weight of 0.20.

Criteria scores

Each software package was scored on a scale from 1 (poor) to 5 (excellent) for each evaluation criterion, as shown in Table 4.1. The weights are also added to the table. For each modelling package, the score for a criterion was multiplied by the weight of that criterion to produce a weighted score. The total weighted score for each model was then computed by summing all individual weighted scores. To express the results on a 0–100 scale, each model's raw total score was divided by the maximum possible total (which is 5 × 100 = 500). This resulted in a normalised performance score, making it easier to compare the overall capabilities of the software packages directly.

Table 4.1: Final MCA with scores on a 0–100 scale

Criterion	Weight (%)	Fluent	FLOW-3D	OpenFOAM	Delft3D	MIKE3
Solving methods	25	5	5	5	2	3
Morphodynamic coupling	5	1	4	2	5	4
Permeability representation	10	5	5	5	2	2
Wall functions	15	5	5	5	2	2
Free-surface modelling	10	5	5	5	2	3
Practicality						
Accessibility	6.67	5	1	4	5	5
User friendliness	6.67	4	2	1	5	4
Parallel run capabilities	6.67	5	1	4	4	3
Total score (0–100)		**79.68**	**69.34**	**74.01**	**47.68**	**51.01**

Selected model

Based on the results of the multi-criteria analysis (Table 4.1), ANSYS Fluent and OpenFOAM emerge as the best performing modelling packages, with normalized scores of 79.68 and 74.01, respectively.

Both show strong performance across the most relevant criteria, particularly in solving methods, wall functions, and permeability representation.

While OpenFOAM is highly appealing for its open-source nature and flexibility and it performs nearly equally in technical capabilities, it comes with a significantly steeper learning curve, lacks a graphical interface, and offers limited technical support. These aspects make it less practical for this research, where efficient setup, troubleshooting, and computational performance are critical.

Given its top score and its strength in both modelling capabilities and practical use, **ANSYS Fluent** is selected as the preferred modelling package for this research. It combines robust 3D flow modelling, reliable porous media representation and strong wall treatment. Its integrated GUI and technical support options further increase its suitability. While OpenFOAM remains a strong open-source alternative, ANSYS Fluent offers a more complete and accessible solution for the objectives of this project.

5

Numerical modelling

This chapter presents the development, configuration, and results of the three-dimensional numerical model used to simulate the flow around the Xstream and traditional groynes. It outlines the modelling choices, including geometry design, mesh refinement, turbulence modelling, and boundary conditions. Through sensitivity analysis and validation against field measurements, the model's reliability is assessed. The final part of the chapter provides a detailed analysis of the simulated flow and sediment responses to understand the hydraulic impact of the Xstream groyne in comparison to a conventional design.

5.1. Approach to the numerical modelling

5.1.1. Model set-up

Following the selection of ANSYS Fluent as the preferred modelling package, this section presents the full setup of the hydrodynamic model. The goal is to construct a representative 3D simulation that captures the flow behaviour around the Xstream groyne under realistic river conditions. The setup includes all key modelling components, such as geometry construction, mesh generation, numerical and physical parameter settings and boundary condition definitions.

Geometry design

The geometry is the base of the model, which functions as a hull through which the water flows. This is also where the first and one of the main choices must be made: designing a schematized or a representative model? A schematized version is an idealised model containing simplified aspects, for example, a straight trapezoidal channel. For these models, the focus is laid on understanding physical processes or theoretical behaviour without being tied to a specific practical case. A representative model aims to reproduce a specific real-world case that incorporates characteristics like river bathymetry. The objective of a representative model is to investigate principles that are highly specific to that real-world case. The main objective of a numeric model in this research is to represent the flow around the Xstream groyne in the IJssel area. For that reason, it has been more useful to design a representative model using data already discussed in Chapter 3.

One of the multibeam datasets has been used as a starting point for the model geometry. The dataset used was from October 2022, just one month before the Xstream groyne was extended. Two reasons support this choice. A first reason is that choosing a depth measurement shortly before extension of the groyne can support the morphologic changes in the first months, where some of the more apparent changes occurred. Even though it seems contradictory, choosing a depth map that only contains a smaller version of the groyne makes it easier to implement the full version. The dataset has a pixel size of 0.1x0.1 m^2, which means that there is a data point for every 10 centimetres. To prevent excessive data usage in the model, this dataset is converted to a pixel size of 2x2 m^2, meaning a data point every 2 metres. The implemented dataset is shown in Figure 5.1. With this dataset, the model will also contain the upstream and downstream traditional groynes and the bed topography over the whole river width. The figure shows the inner river bank (bottom side), where two old Xstream groynes from Phase 1 are included and some inconsistencies in the measurements to the left of the downstream Xstream groyne (raster A1). These have all been deleted from the geometry, as they are irrelevant for the research.

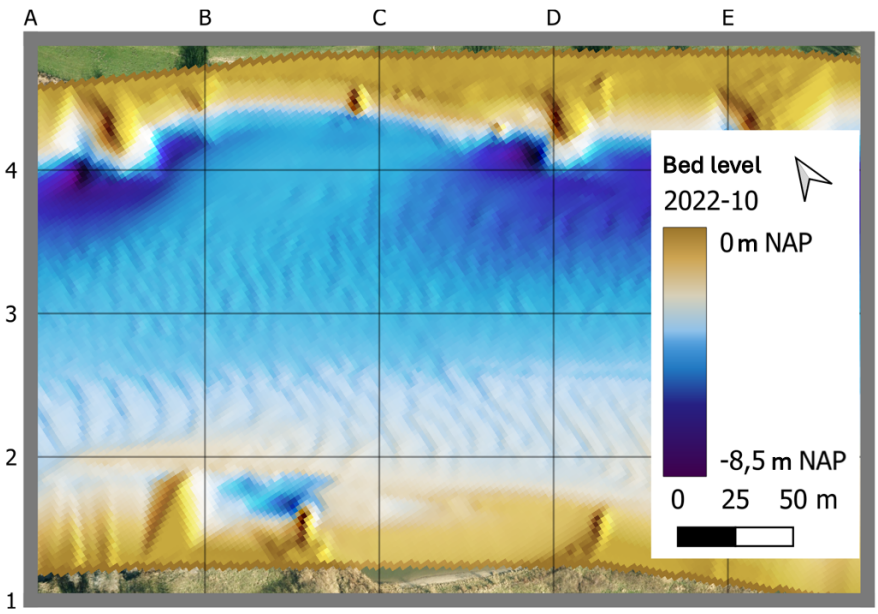

Figure 5.1: Bed topography map used for geometry

At the upstream and downstream sides, the geometry is extended. At the upstream side, a bend is added to represent the bend of the IJssel. The 500 metre long bend is added on this side with a radius of curvature of 775 metres. The bend was meant to have the same curvature as the IJssel bend, but unfortunately, due to human errors, this did not occur. A larger effect of spiral flow may be expected due to this consequence and must be taken into account in the results and discussion. At the downstream side, the river is extended with a 150 metre long straight reach. This is done to prevent any influence that the downstream boundary condition may have on the area of interest. For the topside of the model, which should represent the water surface, a 'rigid lid' is chosen. A further explanation of this choice is provided in Section 5.1.1. The slope of this rigid lid is set to a zero angle slope to keep it highly simplified and prevent the creation of difficult geometries. The riverbed slope at the extended upstream and downstream parts is also set to a zero slope, while the measured part is highly variable. However, the extended parts are not at the same height, causing a small height difference between the

two.

The groyne structure can be added as a secondary geometry (or solid) inside the river reach. This groyne is made as a separate solid, so in the calculation set-up phase, it can be given a certain permeability. On the wall and riverbed boundaries, the groyne has the exact shape as the river reach to prevent any gaps or inconsistencies that may influence the calculations. The groyne slope successfully represents the Xstream groyne at a 45-degree slope (1:1) and its dimensions are also similar. Another geometry was designed, which represents the exact shape of the traditional groyne. This groyne was made impermeable with an 18-degree slope (1:3). More information on this geometry shape is found in Appendix B.

Mesh generation

The mesh generation process began with the creation of a surface mesh, where cell sizes were varied between 0.5 and 1.5 metres depending on location. This adaptive sizing allowed the model to better resolve key flow features without generating an unnecessarily large number of cells. From this surface mesh, a full three-dimensional volume mesh was constructed.

A crucial element in the volume mesh design was the inclusion of boundary layers. These are thin layers of mesh near walls and the riverbed, designed to capture velocity gradients more accurately. Ten boundary layers were applied along these surfaces, with a gradually increasing cell size moving away from the boundary. This ensures better resolution of near-wall flow characteristics, which are especially important for simulating shear stress and turbulence close to groynes.

The volume mesh type used was a poly-hexcore mesh. This combines structured hexahedral cells in the bulk flow regions—offering efficient and accurate flow calculation—with polyhedral cells near complex geometries such as groynes and the riverbed. This hybrid approach was selected to enhance flow resolution and numerical stability, while keeping the total number of cells lower than in a fully unstructured mesh.

To further improve accuracy in critical zones, two levels of local refinement were applied around the groynes. ANSYS Fluent refines a three-dimensional poly-hexcore mesh by halving all edges, which splits up a single cell into 8 child cells. To elaborate on the fineness compared to the largest grid area, the first refinement leads to a refined area with 8 times the number of cells and leads to a doubled resolution. The area with two refinements will have 64 times more cells, while having a resolution that is 4 times better.

Calculation set-up

This section describes the numerical and physical settings used in the CFD model. These settings directly influence the model's accuracy, stability, and how well it represents the hydrodynamics in the IJssel near the Xstream groyne.

General:

The CFD model was designed as a three-dimensional, single-phase flow simulation to reflect the hydrodynamics in the IJssel near the Xstream groyne. Since the study focuses on long-term, stable flow characteristics rather than short-term fluctuations, a steady-state solution was chosen. This approach assumes that flow properties such as velocity and turbulence remain constant over time.

The simulation domain includes only water as the fluid phase. Given the low compressibility of water under river conditions, it was treated as an incompressible fluid, which allowed the use of a pressure-

based solver in ANSYS Fluent. This type of solver is suitable for solving incompressible flow problems efficiently and accurately.

Additionally, gravity was applied in the vertical (negative z) direction, as it plays a crucial role in the overall pressure distribution and flow dynamics in open channel flows like rivers.

Turbulence models:
Modelling turbulence accurately near the groynes is one of the more challenging objectives in the simulations. These flows behave highly three-dimensionally with phenomena like flow separation and recirculation, as was explained in Section 2. Capturing these principles properly is essential to realistically predicting bed shear stress and flow patterns behind the groyne. Most engineering simulations use Reynolds-Averaged Navier-Stokes (RANS) turbulence models, which average the effects of turbulence over time and solve for the mean flow. This makes them much more computationally efficient than time-resolved models, but it comes at the cost of reduced accuracy in capturing fine-scale turbulent structures.

ANSYS Fluent offers a wide range of RANS-based and hybrid turbulence models, each with its own complexity and accuracy. Four available models (in increasing complexity and accuracy) have been analysed:

- **k–ε:** In fluid dynamics, one of the more famous methods is the two-equation k–ε model, where k is the kinetic turbulence and ε is the kinetic dissipation rate. This method is commonly used due to its simplicity and low computational cost. It works well with reasonable predictions for many general engineering flows (Saberi & Galoie, 2017), especially where the flow remains attached and isotropic. Studies like (Zhang et al., 2005) and (Kumar & Malik, 2016) successfully applied k–ε models to spur dike and groyne flow problems, showing that they can provide reasonably accurate predictions of large-scale flow features. However, it is known that they often underpredict turbulent fluctuations and the width of mixing layers, especially in flows with strong vortex interactions. As such, while k–ε is computationally efficient, it can be too simplified for the detail needed here.
- **k–ω SST:** The k–ω SST (Shear Stress Transport) model is another two-equation RANS model that combines the strengths of the k–ε and k–ω models, where ω is the specific dissipation rate. It uses the k–ω formulation near boundaries, all the way down to the wall through the viscous sub-layer, which improves the accuracy of boundary layer flows. It also gradually transitions to the k–ε formulation away from the boundaries, offering stability and robustness in the outer flow region.

  This hybrid approach makes k–ω SST particularly effective for flows with separation, recirculation zones, and adverse pressure gradients. Shampa et al. (2020) demonstrated that three-dimensional flow simulations using the k–ω SST turbulence model were able to reproduce key hydraulic features in slit-type groyne fields, showing that this model could be a viable option.
- **Reynolds Stress Model (RSM):** The Reynolds Stress Model (RSM) provides greater detail by solving transport equations for each component of the Reynolds stress tensor, allowing it to better capture anisotropic turbulence and circulating flows. This is especially useful in highly three-dimensional flows around groynes. However, RSM comes with a significant computational cost and is also more sensitive to mesh quality, making it less practical for large, complex river domains.

- **Large Eddy Simulation (LES):** Large Eddy Simulation (LES) is a highly sophisticated approach to turbulence modelling by directly resolving the larger turbulent structures while parameterizing only the smaller scales. This allows LES to capture detailed flow phenomena such as vortex shedding, unsteady separation and turbulent mixing. For example, Koken and Constantinescu (2008) applied LES to study the flow and scour mechanisms around spur dikes. They, however, did their research at a relatively low Reynolds number, requiring fewer resources. For most cases with higher Reynolds numbers, LES requires extremely fine meshes and small time steps, especially in 3D domains, resulting in very high computational costs. Detached Eddy Simulation (DES) is sometimes used as a hybrid method that combines aspects of RANS near walls with LES in the free stream, offering a compromise between detail and efficiency.

Boundary conditions:

In a numeric model constructed in Fluent, boundary conditions are set to describe how the flow enters, exits, and interacts with the domain. The choice of boundary conditions is another influence on both the accuracy and stability of the simulation. Every boundary in the geometry is set with certain conditions. There will be one upstream boundary that works as an inlet and a downstream boundary as an outlet. Another boundary must be set to define the free surface boundary. All other boundaries are walls (groynes and outer walls) or the riverbed.

- **Free surface boundary:** The free surface is the boundary on the top side of the water. This is called a free surface, as water is able to move towards that direction much more easily than through other surfaces like walls. To schematize this surface, there are two well-known options: the rigid lid or the volume of fluid. The rigid lid method fixes the free surface at a certain height, preventing any deformations in this boundary. A volume of fluid method sees the model as a multi-phase flow where water can mix with a secondary layer filled with air. Even though this second method gives a better approximation, as the water surface has more freedom, defining an extra layer would also increase the total mesh size. This makes the computations much larger and complex.

  Khosronejad et al. (2019) did a study on numerical comparisons between rigid-lid and level-set methods for the free surface boundary using LES. Their results suggest that for higher Reynolds numbers, the rigid-lid assumption can lead to non-negligible differences for the turbulence statistics. They do, however, state that this is only expected when significant backwater is anticipated and the inconsistencies are more significant for an LES study. Koken and Constantinescu (2008) makes use of the rigid-lid approximation for a DES simulation. It is stated that for low Froude numbers ($Fr \leq 0.5$), this approximation is still a valid option (which was determined to be $Fr \approx 0.128$ in Section 3.2.4).
- **Upstream boundary:** The upstream boundary is defined as a **velocity inlet**, where the velocity magnitude is given. A velocity inlet helps initiate flow development. The model must simulate a flow that represents the conditions during the ADCP measurement.
- **Downstream boundary:** The downstream boundary is modelled as a **pressure outlet** with a gauge pressure set to zero. This boundary condition allows fluid to exit the domain freely and is commonly used when the exact downstream pressure is unknown. It also helps with avoiding reflections that could disturb the flow near the boundary.
- **Permeability:** To incorporate permeability for the Xstream groyne, ANSYS Fluent needs three specific variables: porosity, viscous resistance coefficient and inertial resistance coefficient. The

porosity was determined by Wetser (2016) at a value of 0.6, where she also found a permeability value of approximately 0.47 m/s. This permeability value was validated for CFD simulations by ten Oever (2023), where he iterated both the viscous and inertial resistance to eventually get the correct permeability values, as shown in Figure 5.2.

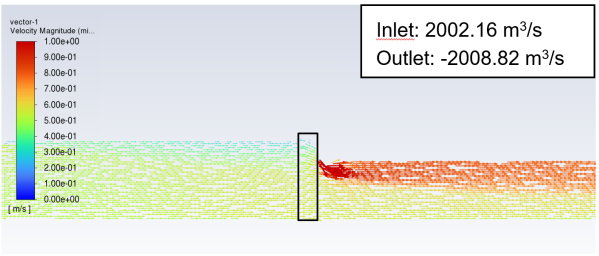

Figure 5.2: Hydraulic Xstream tests

- **Wall Boundary Condition with Roughness:** The riverbed and groyne surfaces were modelled using the standard wall function with roughness modifications, suitable for high-Reynolds-number flows where resolving the viscous sublayer in detail is computationally excessive (ANSYS, 2025). Instead of directly computing near-wall turbulence, ANSYS Fluent applies an empirically derived log-law velocity profile normal to the wall:

$$U^+ = \frac{1}{\kappa} \log(Ey^+) - \Delta B \tag{5.1}$$

where:

  - $U^+ = \frac{U}{u_\tau}$ is the dimensionless velocity,
  - $y^+ = \frac{yu_\tau}{\nu}$ is the dimensionless wall distance,
  - $\kappa \approx 0.41$ is the von Kármán constant,
  - $E \approx 9.8$ is an empirical constant,
  - ΔB is the roughness function.

The influence of roughness is characterised by the non-dimensional roughness height $k_s^+ = \frac{k_s u_\tau}{\nu}$, for which:

  - Hydrodynamically smooth: $K_s^+ \leq 2.25$
  - Transitional roughness: $2.25 < K_s^+ \leq 90$
  - Fully rough: $K_s^+ > 90$

In rough wall treatment, the roughness function ΔB is computed using:

$$\Delta B = \frac{1}{\kappa} \ln(f_r) \tag{5.2}$$

where f_r is a function of k_s^+ and the roughness constant C_s. This correction adjusts the velocity profile near the wall to account for momentum loss from rough surface drag.

A final note about friction implementation in ANSYS Fluent is that it does not permit simultaneous use of permeability and wall roughness. Due to this, when applying permeability to the groyne, it

cannot have friction and must be assumed to have smooth walls.

Groyne case comparison

To compare the effects of the groynes, three groyne configurations are simulated:

1. **Base case:** A simulation without any groyne in the domain. This serves as a reference to assess the unaltered flow and validate pre-intervention conditions.
2. **Traditional case:** Incorporates a typical groyne with 1:3 slopes and no permeability (fully impermeable structure).
3. **Xstream case:** Includes the Xstream groyne with 1:1 slopes and a permeability similar to the real groyne structure.

These configurations are kept identical in terms of flow rate, boundary conditions, mesh resolution, and turbulence models. By comparing these cases, the contributions of groyne slope and permeability can be understood. The key characteristics of the groyne designs are summarised below:

Table 5.1: Overview of groyne configurations used in the model simulations

Case	Groyne type	Slope	Permeability	Porosity
Base Case	No groyne	–	–	–
Traditional	Traditional groyne	1:3	0	0%
Xstream	Xstream groyne	1:1	$\sim$0.47 m/s	60%

5.1.2. Sensitivity analysis

The following sections present the outcomes of each sensitivity test. These tests were conducted to assess how critical modelling choices influence key hydrodynamic outputs such as velocity gradients, turbulence structures and bed shear stress. By evaluating the impact of mesh resolution, turbulence modelling and surface representation, the analysis ensures that the simulation outcomes are both numerically stable and physically meaningful. The results guide the selection of modelling settings used in the final simulations and increase confidence in the physical accuracy of the model.

Mesh resolution

Implementing a grid dependency test is critical in ANSYS Fluent to confirm that the results are not significantly influenced by the mesh resolution. Inadequate mesh density can lead to a poor representation of flow features, especially in regions with complex geometry or high turbulence, such as around a groyne. On the other hand, overly fine meshes result in excessive computational time and resource usage without necessarily improving the accuracy of the solution.

Four different mesh densities were created and tested, each finer than the last. The aim was to observe how some of the flow characteristics improved with increasing mesh quality and to identify the point at which further refinement gives insignificant improvements. The precision of a grid can be classified by the number of grid cells and the minimum grid cell size. Also, the location of the refined mesh is fundamental for the model results. Table 5.3a describes this information for every mesh. Figure 5.3b shows the different refinement areas.

Mesh Type	Total Cells	Min. Cell Size [mm]	Implemented Refinements
Extra coarse	≈ 4.2 million	17.8	No refinements applied; the entire domain uses the base grid (grey area).
Coarse	≈ 7.1 million	9.0	Two refinement levels: the white and red sections are both refined once.
Fine	≈ 10.7 million	2.7	Three refinement levels: the white section is refined once, the red section twice.
Extra fine	≈ 25.5 million	1.9	Four refinement levels: the white section is refined once, the red section three times.

(a)

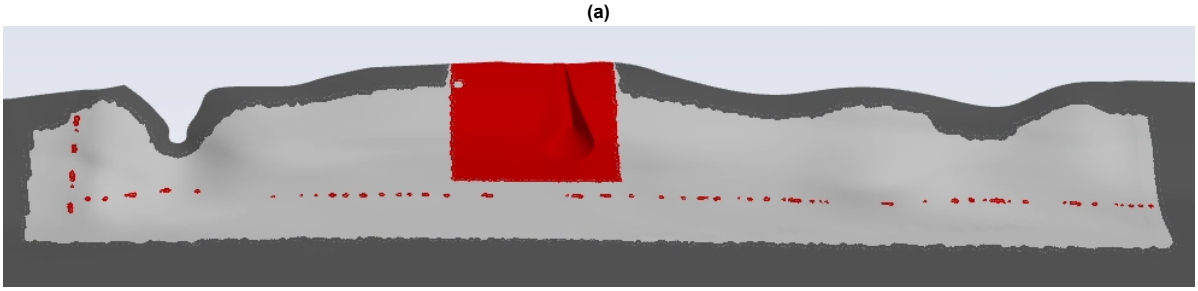

(b)

Figure 5.3: Overview of mesh resolution: (a) Table showing mesh settings and refinement levels, (b) Visualisation of refined areas in the model domain

The mesh has been checked by observing the changes through three key flow parameters under the various meshes. The first parameter is the velocity magnitude over the vertical to see if the profile captures the expected shape of a boundary layer with low velocities near the bed and increasing toward the surface. Second, the turbulent viscosity is analysed to assess the mesh's ability to resolve turbulence structures and gradients. Lastly, the bed shear stress is evaluated along the riverbed, as it plays a crucial role in determining morphologic changes and is highly sensitive to near-wall mesh refinement. These parameters are observed at two different locations, as shown in Figure 5.4. The velocity and the turbulent viscosity are checked over the depth indicated by the vertical lines. For the bed shear stress, the mesh is checked over the bed indicated by the horizontal lines.

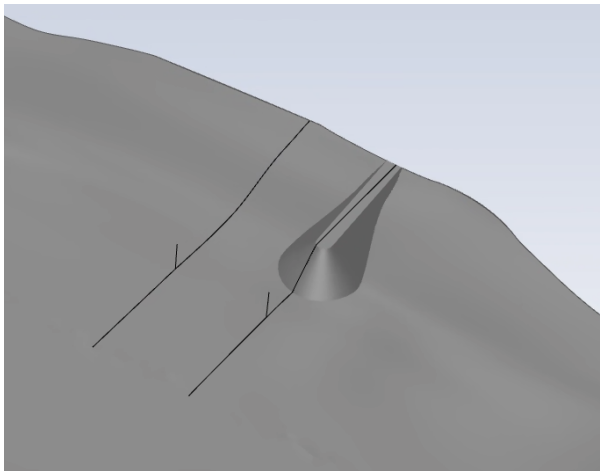

Figure 5.4: Groyne area showing plot locations. **vertical lines:** vertical profiles for velocity and turbulent viscosity. **horizontal lines:** riverbed transects for bed shear stress

Turbulence model

To evaluate the sensitivity of turbulence modelling on flow results, a comparison was made between the k–ε and k–ω SST turbulence models. These models were evaluated based on their output for three parameters: velocity, turbulent kinetic energy (TKE), and bed shear stress. The turbulent viscosity was excluded due to its inconsistent order of magnitude across models, which made direct comparison unreliable. All evaluations were performed at the same two locations used in the mesh sensitivity test (see Figure 5.4).

In addition to these two models, the applicability of the Reynolds Stress Model (RSM) and Large Eddy Simulation (LES) was considered. Short trial simulations using RSM led to multiple convergence errors, and LES was not attempted due to its high computational demand and mesh resolution requirements. These higher-fidelity models were therefore excluded from the final analysis.

Free-surface approximation

Instead of using multiphase approaches such as Volume of Fluid for the free-surface, this study applies a simplified method known as the rigid-lid approximation. To assess the suitability of the rigid-lid approach, the static pressure was examined along the top boundary, which represents the location of the water surface.

In a true free-surface simulation, the pressure at the air–water interface would be constant and equal to atmospheric pressure. Any significant spatial variations in the pressure under the rigid lid could indicate surface fluctuations that are not captured by this simplified method.

5.1.3. Model validation

To evaluate the accuracy and reliability of the numerical model, a series of validation steps were carried out using available measurement data. These comparisons focus on key hydrodynamic parameters such as depth-averaged velocity fields, vertical velocity profiles, bed shear stress distributions, and secondary (spiral) flow structures.

Depth-averaged velocity field

The modelled velocities in the groyne field upstream and downstream of the Xstream groyne can be validated using the ADCP measurements. Velocities in the area can be compared both qualitatively and quantitatively. qualitatively, the quiver plot from Figure 3.13a can be compared with a velocity contour plot including streamlines, enabling the identification of the main flow structures in the area and their deviations.

Quantitatively, the gradients of these groyne fields from Figure 3.14 can be used to make a comparison. To assess the model's ability to reproduce the transverse velocity gradients, two statistical indicators were used: the Root Mean Square Error (RMSE) and the coefficient of determination (R^2).

The RMSE quantifies the average magnitude of the differences between the modelled and experimental velocities. It provides a direct measure of the model's accuracy in terms of velocity prediction. A lower RMSE indicates that the model predictions are closer to the measured data:

$$\mathrm{RMSE} = \sqrt{\frac{1}{n}\sum_{i=1}^{n}\left(u_{\mathrm{exp},i} - u_{\mathrm{mod},i}\right)^2} \tag{5.3}$$

where $u_{\text{exp},i}$ and $u_{\text{mod},i}$ are the experimental and modelled velocities at point i, respectively, and n is the number of comparison points. The RMSE is sensitive to larger errors, making it particularly useful for identifying regions where model performance deviates significantly.

The coefficient of determination, R^2, expresses the proportion of variance in the measured data that is captured by the model. It reflects how well the model reproduces the spatial trends in the velocity field. An R^2 value of 1 indicates a perfect fit, whereas values closer to 0 indicate poor agreement between model and measurements. Finally, a negative R^2 value can occur when the model predictions are worse than simply using the mean of the observed data as a constant prediction.:

$$R^2 = 1 - \frac{\sum_{i=1}^{n} \left(u_{\text{exp},i} - u_{\text{mod},i}\right)^2}{\sum_{i=1}^{n} \left(u_{\text{exp},i} - \bar{u}_{\text{exp}}\right)^2} \tag{5.4}$$

where $\bar{u}_{\text{exp}}$ is the mean of the experimental velocities. Unlike RMSE, R^2 is dimensionless and indicates how well the model explains the variability of the observations, rather than the absolute error.

Vertical profile comparison

The measured depth profiles from Figure 3.15a can be used as validation for the model. At similar locations, the velocity magnitude over the velocity can be plotted for the model results. These are combined with the measurements and can statistically be determined, by also using the RMSE and R^2. These metrics offer an assessment of the model's performance in simulating the characteristic depth profile.

Initial scour pattern comparison

The simulation without the groyne structure, referred to as the base case, is used to assess the bed shear stress distribution in the area. Bed shear stress serves as a key indicator for potential sediment transport and erosion patterns. This output can be qualitatively validated by comparing it with the observed bed topography shown in Figure 3.6. In particular, zones of elevated bed shear stress can be linked to morphological features such as scour pits, while areas of reduced shear stress may correspond to sediment deposition zones. This comparison provides insight into whether the model reasonably predicts the morphologic trends in the absence of the groyne.

Spiral flow structure

The presence of spiral flow is evaluated by examining multiple transverse velocity profiles along the length of the groyne fields. These depth profiles are taken at various locations to account for potential disturbances caused by the Xstream groyne. By comparing the profiles from groyne fields 3 and 4, as shown in Figure 3.20, the development and possible disruption of secondary flow patterns can be assessed. The specific locations of these depth lines are indicated in Figure 5.5.

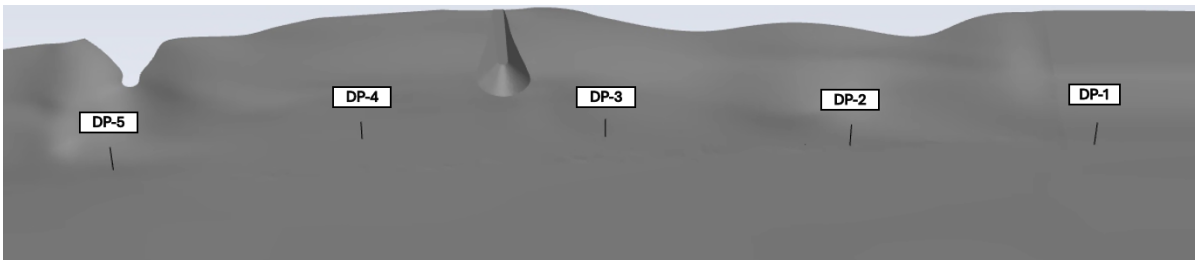

Figure 5.5: Depth profile locations in the groyne area

5.1.4. Flow field analysis

Recirculation zone characteristics

Velocity contours and streamlines were extracted at two horizontal planes: near the free surface (z=+0.5m) and near the bed level (z=−4m). These plots were used to identify vortices, flow separation zones and streamline curvature around the groynes.

In addition, streamwise velocity profiles were extracted at four representative positions: A, B, C, and D. Profiles at A and B describe the transverse velocity distribution across the downstream groyne fields, while C and D show the vertical velocity distribution near the groyne heads. All data were post-processed and visualised using (Tecplot, 2022) to compare the flow behaviour between the traditional and Xstream groyne designs.

Turbulence patterns and intensity

To analyse the turbulence characteristics near the riverbed, contours of turbulent kinetic energy (TKE) were extracted from the bed level of the numerical model results. This was done for both the traditional and Xstream groyne configurations. The visualisations were used to identify areas of elevated turbulence around the groynes and to assess the spatial distribution of TKE within the groyne fields.

5.1.5. Sediment response analysis

Bed shear stress patterns

Bed shear stress distributions were extracted from the numerical model to evaluate the potential for erosion and sediment deposition around the groynes. Contour plots were generated at the bed level for both the traditional and Xstream groyne configurations to visualise the spatial distribution of shear stress across the domain.

In addition to the spatial contours, quantitative shear stress profiles were extracted along selected cross sections within the groyne field (Locations A and B). These profiles allowed for a direct comparison of shear stress magnitudes between the two configurations. The critical threshold for sediment motion, determined in Section 3.2.6, was used to interpret zones of likely erosion or deposition.

Behaviour at the sediment line

To investigate the formation of the sediment line and the associated flow structures, bed shear stress contours were analysed in the groyne field downstream of both groyne types. These contours were extracted from the numerical model at the bed level to identify regions of low shear stress where sediment deposition is likely to occur.

To further explain the flow conditions in these zones, a series of cross-sectional slices were taken perpendicular to the flow direction in the area surrounding the sediment line. For each cross-section, streamwise velocity contours and streamlines (derived from transverse and vertical velocity components) were plotted to reveal eddy structures and flow convergence patterns. These cross-sections were spaced along a 20-metre stretch.

A comparison was also made with the traditional groyne case. Cross-sectional profiles were extracted in the same region and included in Appendix C to assess the presence and development of eddies. This analysis helped explain why sediment is able to settle near the Xstream groyne but not in the case of the traditional design.

5.2. Results of the numerical modelling

5.2.1. Model set-up

The model setup serves as the foundation for the numerical analysis and determines how well the simulation represents realistic river conditions. This section summarises the final configuration of the geometry, mesh, boundary conditions, and numerical settings used in the hydrodynamic simulation of the IJssel near the Xstream groyne.

Geometry design

The final geometry includes both the natural bathymetry and the added Xstream and traditional groynes. Figure 5.6 shows the complete river reach, including the upstream bend and downstream extension. Figure 5.7 provides a closer view of the Xstream groyne geometry used in the simulation. These geometries form the basis of the computational domain and ensure that key physical features are realistically represented in the model.

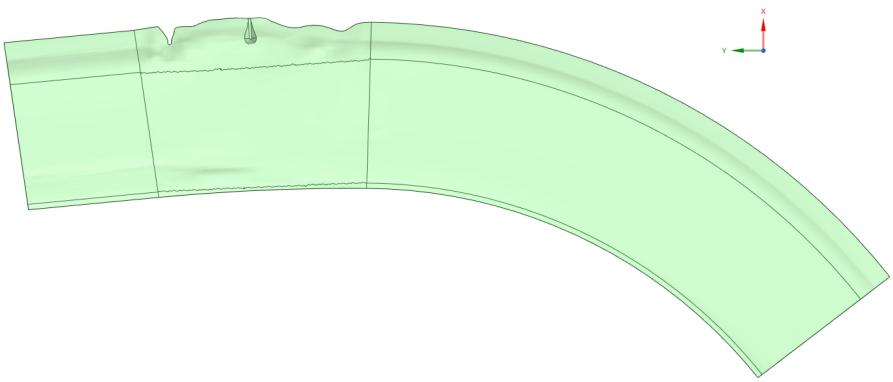

Figure 5.6: River geometry

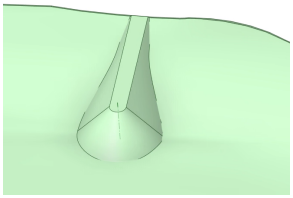

Figure 5.7: Xstream groyne geometry

Mesh generation

The result of the mesh is illustrated in Figure 5.8. Here, the refinements are visible, going from large hexes outside the groyne area (this area is indicated by the yellow colour) to a first refinement in the area. A second refinement is done near the groyne and shown by the black box or a zoomed-in version in Figure 5.9.

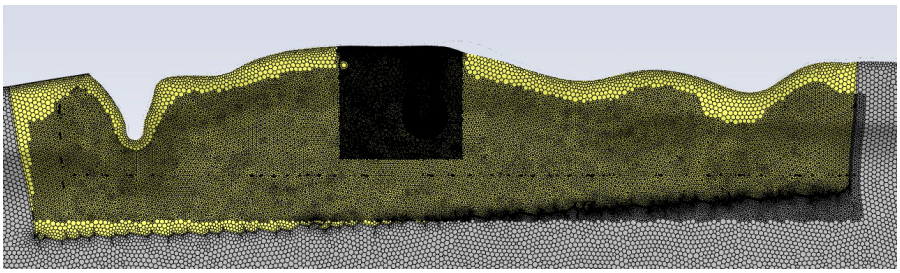

Figure 5.8: Indication of three mesh sizes in the area

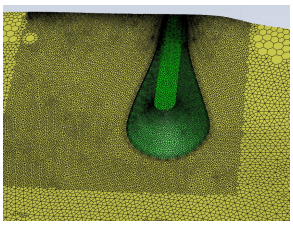

Figure 5.9: Mesh refinement area near the Xstream groyne

Table 5.2 shows key mesh metrics used to evaluate the model. Low skewness and high orthogonal quality indicate good numerical stability and minimal numerical diffusion. While the average aspect ratio is relatively high, this is acceptable in boundary layer regions. The total number of cells is a result of the two refinement areas.

Table 5.2: Mesh quality metrics

Metric	Value	Interpretation
Skewness (average)	0.102	Excellent quality
Orthogonality (average)	0.864	Good
Aspect ratio (average)	9.10	Acceptable
Total cells	10,662,691	Highly refined mesh
Minimum cell size [mm]	2.7	Small cells near boundaries

Calculation set-up

The final numerical and physical parameters used in the simulation are defined. It includes general settings, turbulence modelling approach and the applied boundary conditions. These settings determine how the model interprets and calculates the flow behaviour within the domain and directly affect both the accuracy and stability of the simulation.

General set-up:

The general parameter configuration of the model is summarised in Table 5.3. These general parameters have all been kept at their default values.

Table 5.3: General simulation setup parameters

Parameter	Value / Description
Flow type	3D, steady-state, single-phase (water only)
Solver	Pressure-based
Gravity	9.81 m/s² in the negative z-direction
Water density	998.2 kg/m³
Dynamic viscosity	1.003×10^{-3} Pa·s

Turbulence models:

After evaluating all available turbulence models, the **k–ω SST turbulence model** was selected for this study as it offers a well-balanced compromise between accuracy and computational cost. This model is particularly effective in capturing key flow features near groynes, such as flow separation and recirculation, which are critical for realistic simulation of river hydrodynamics. Its near-wall formulation allows for accurate resolution of boundary layers, while its hybrid structure ensures numerical stability in both near-wall and free-stream regions. Compared to more advanced models like LES or RSM, the k–ω SST model remains computationally manageable for the scale and complexity of the riverine domain used in this study.

Boundary conditions:

The applied boundary conditions are summarised in Table 5.4. The rigid lid at the top of the domain was implemented as a symmetry boundary, effectively mirroring the solution and preventing vertical deformation. Despite this simplification, changes in local water surface elevation can still be interpreted indirectly from pressure gradients near the surface.

The upstream flow condition was defined through a velocity inlet, set to 0.75 m/s after calibration iterations. This resulted in a discharge of approximately 610 m^3/s, closely matching the ADCP-measured

discharge of 630 m^3/s. The downstream condition was set as a pressure outlet with zero gauge pressure, allowing natural flow exit and avoiding artificial reflections.

Porous media settings were applied to the Xstream groyne to represent its permeability. Wall roughness effects were implemented on the riverbed and impermeable groynes using standard roughness corrections.

Table 5.4: Overview of applied boundary condition settings

Boundary/Setting	Applied Configuration
Free surface	Rigid lid, fixed at 0.3 m with a symmetry boundary condition
Upstream	Velocity inlet: 0.75 m/s
Downstream	Pressure outlet: 0 Pa gauge pressure
Groyne permeability	Porosity = 0.6 Viscous resistance = 500 $1/m^2$ Inertial resistance = 60 1/m
Wall roughness	Roughness height k_s = 0.0005 m Roughness constant C_s = 0.5
Note	No roughness applied to permeable groynes due to ANSYS Fluent limitations

5.2.2. Sensitivity analysis

Mesh resolution

Figure 5.10 compares velocity profiles at the two locations. At both locations, the vertical profiles show that the extra coarse and coarse meshes underpredict surface velocities by 0.05 m/s to 0.1 m/s. The fine and extra fine meshes resolve the velocity profile accurately. They both follow a similar velocity path over the depth and are also able to show the velocity gradients near the bed, which are affected by the groyne. The difference between the velocity profiles of the fine and extra fine meshes is negligible.

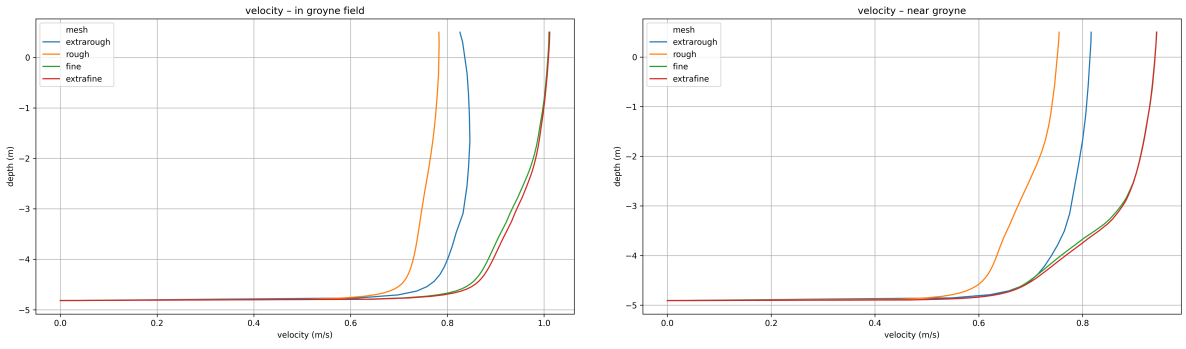

(a) Velocity profile near groyne

(b) Velocity profile in groyne field

Figure 5.10: Velocity profiles for different mesh resolutions

Figure 5.11 compares the turbulent viscosity distributions over depth at the two locations. The extra coarse and coarse meshes visibly smooth out the vertical gradients and under-represent localised peaks in turbulence intensity, especially near the free-surface boundary. In contrast, the fine and extra fine meshes produce similar distributions and better resolve the turbulence structure. The added

refinement in the extra fine mesh, again results in only slight improvements compared to the fine mesh.

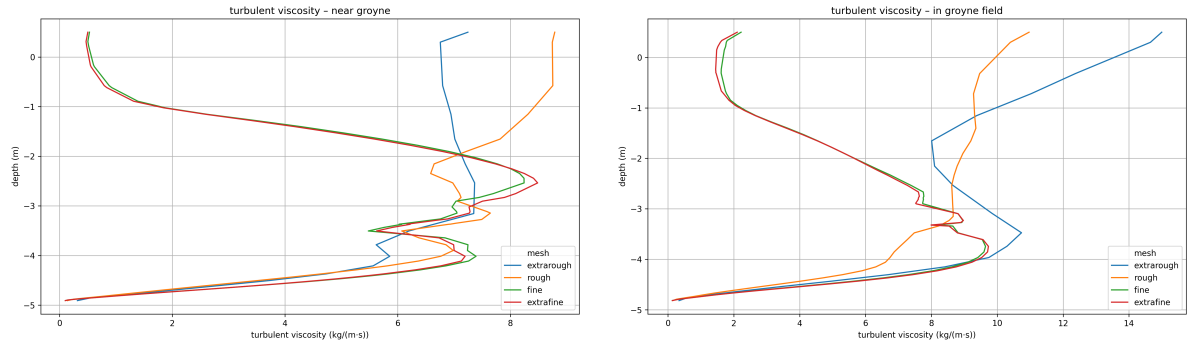

(a) Turbulent viscosity near groyne

(b) Turbulent viscosity in groyne field

Figure 5.11: Turbulent viscosity profiles for different mesh resolutions

Figure 5.12 shows the bed shear stress distributions along the riverbed at both locations. The extra coarse and coarse meshes consistently underestimate peak shear stress values, which would indicate the zones influenced by flow separation near the groyne. The curves are overly smoothed, indicating an inability to capture sharp shear gradients. In contrast, the fine and extra fine meshes yield higher-resolution profiles that reveal distinct peaks. As with the other parameters, the difference between the fine and extra fine meshes is small, only observing a slightly higher bed shear stress for the extra fine mesh in the groyne field. Figure 5.12a shows a flat line over the top of the groyne indicating zero stress. This is due to the model setup that does not allow water to flow over the groyne.

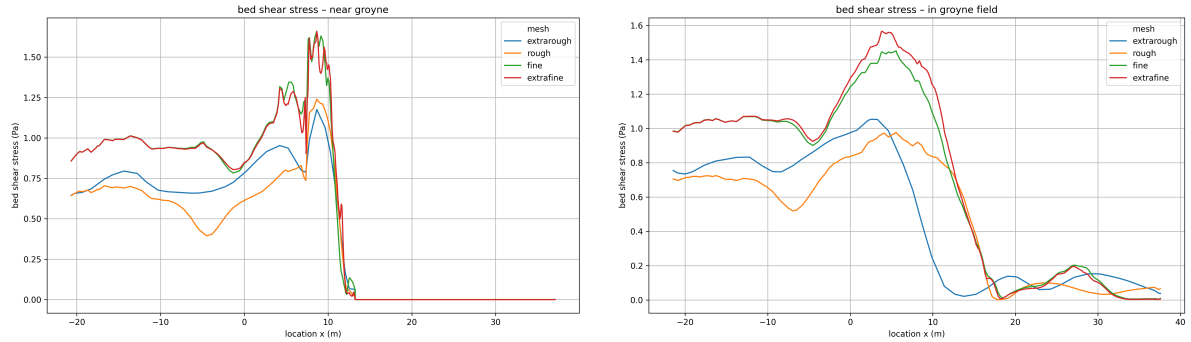

(a) Bed shear stress at groyne

(b) Bed shear stress in groyne field

Figure 5.12: Bed shear stress profiles for different mesh resolutions

The mesh sensitivity analysis demonstrates that the coarse and extra coarse meshes are insufficient to resolve velocity gradients, turbulence, and bed shear stress with enough accuracy. Both fine meshes provide consistent and reliable results across all examined parameters, capturing key flow characteristics effectively. Although the extra fine mesh offers even more detail, the improvements are minimal relative to the significant increase in computational cost. Therefore, the fine mesh (with approximately 10.7 million cells) is selected for further simulations. It offers a well-balanced compromise between numerical precision and computational efficiency.

Turbulence model

As shown in Figure 5.13, velocity profiles are nearly identical between both turbulence models. Minor differences appear near the bed and surface, but the general flow structure is well captured in both cases. This confirms that the velocity field is not highly sensitive to the choice between k–ε and k–ω SST in this setup.

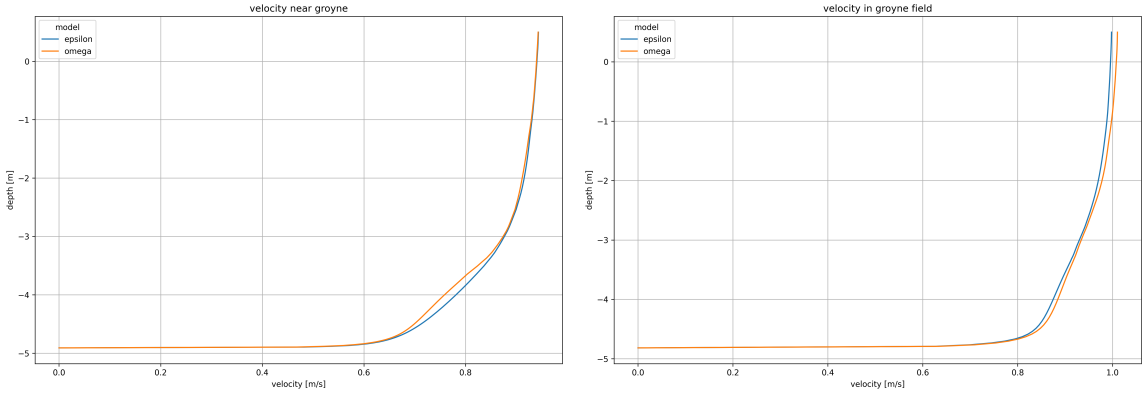

Figure 5.13: Velocity profiles for k–ε and k–ω SST turbulence models

Figure 5.14 reveals more significant differences in TKE distribution. The k–ε model exhibits slightly higher turbulence intensities near boundaries, consistent with its known tendency to over-predict near boundaries, as it can act more diffusively. These differences are moderate but could affect local flow patterns around groynes and in mixing layers.

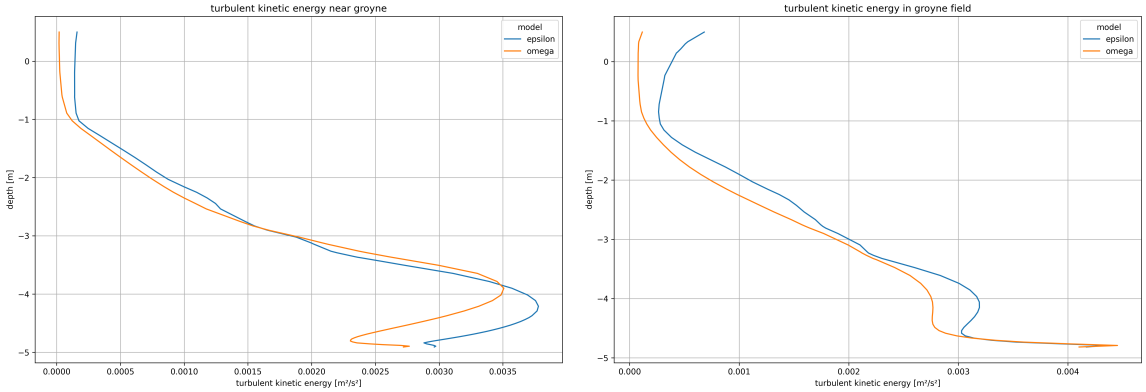

Figure 5.14: Turbulent kinetic energy (TKE) profiles for k–ε and k–ω SST turbulence models

In Figure 5.15, the bed shear stress distribution is nearly identical between the two models. Slight deviations are visible at peak locations, mainly in the groyne field, but the overall shape and intensity are consistent. This indicates that for the purpose of estimating bed stresses, both models could be used with limited impact on the results.

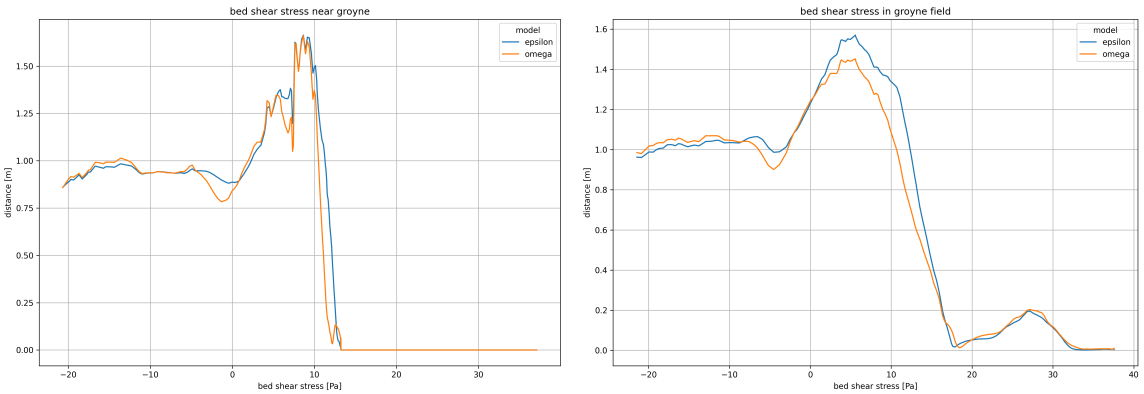

Figure 5.15: Bed shear stress comparison between k–ε and k–ω SST models

Overall, both the k–ε and k–ω SST turbulence models produce similar results for large-scale hydrodynamic behaviour. However, the k–ω SST model provides a more refined and physically realistic representation of turbulence near boundaries, particularly in the TKE distribution. It offers the best balance between accuracy and computational efficiency for this study.

Free-surface approximation

Figure 5.16 shows the static pressure distribution along the top lid of the model domain. The figure reveals a pressure gradient from high pressure at the upstream end to lower pressure downstream. It can be observed that the static pressure increases toward the upstream end of the model, with values reaching approximately 250 pascal near the outer bend. This build-up is expected due to the centrifugal effects in the bend geometry and upstream momentum.

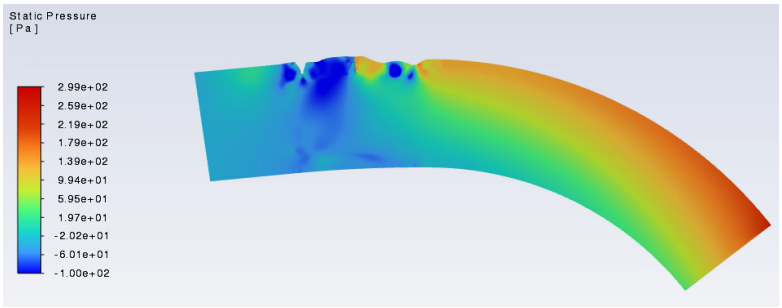

Figure 5.16: Static pressure distribution along the rigid-lid surface

These two expected causes for the increased pressure are further explained:

1. A first cause would be the flow curvature in the river bend. The large pressure values are observed around the outer bend. Due to curvature in the bend, the flow will be pushed toward the outer bend, as explained in Section 2.4. In the model, the water surface elevation change is approximately 2.5 centimetres, using the hydrostatic relation $\Delta h = \Delta p/(\rho g)$. When determining this from Section 2.4, the water level gradient becomes 8.5×10^{-5}. Over a 200 metre channel width, this results in a total elevation difference of about 1.7 centimeters. This shows that the water level setup can be partially explained by the spiral flow.
2. A second likely cause for the pressure build-up near the outer bend is the backwater effect induced by the groynes. These structures obstruct the flow locally, particularly in the main channel and

near-bank zones, causing a slight upstream water level rise. As water is forced to decelerate and move around the groynes, the increased flow resistance leads to elevated pressure and water surface upstream of the structures. This could have caused the additional pressure increase of approximately 80 pascal (0.8 centimetres) over the outer bend.

Conclusion on the sensitivity

This sensitivity analysis investigated three key modelling aspects: mesh resolution, free-surface treatment and turbulence model selection.

1. The mesh resolution test showed that coarse and extra coarse meshes were insufficient to resolve velocity gradients and near-wall turbulence accurately. The fine mesh provided nearly identical results to the extra fine mesh, making it the optimal choice for balancing computational cost and result quality.
2. The turbulence model comparison demonstrated that both the k–ε and k–ω SST models deliver comparable results for velocity and bed shear stress. However, the k–ω SST model offered a more accurate representation of turbulent kinetic energy, suggesting it is better suited for capturing detailed turbulence effects in complex flow zones.
3. The rigid-lid approximation used for the free-surface was validated through analysis of static pressure distribution, which revealed a minor surface elevation gradient. This gradient could be attributed to spiral flow and backwater effects and was found to be within acceptable limits.

5.2.3. Model validation

Depth-averaged velocity field

The velocity field around the Xstream groyne, shown in Figure 5.17, reveals distinct velocity contrasts between the main channel and the groyne fields. In the traditional groyne fields, the streamlines indicate the presence of recirculating flow patterns, which are characteristic of flow separation behind rigid structures. Such recirculation is absent downstream of the Xstream groyne, where the low-velocity region appears more elongated and aligned with the flow direction. These spatial patterns were also observed in the ADCP measurements of Figure 3.13a, indicating strong qualitative agreement between the numerical model and the field data.

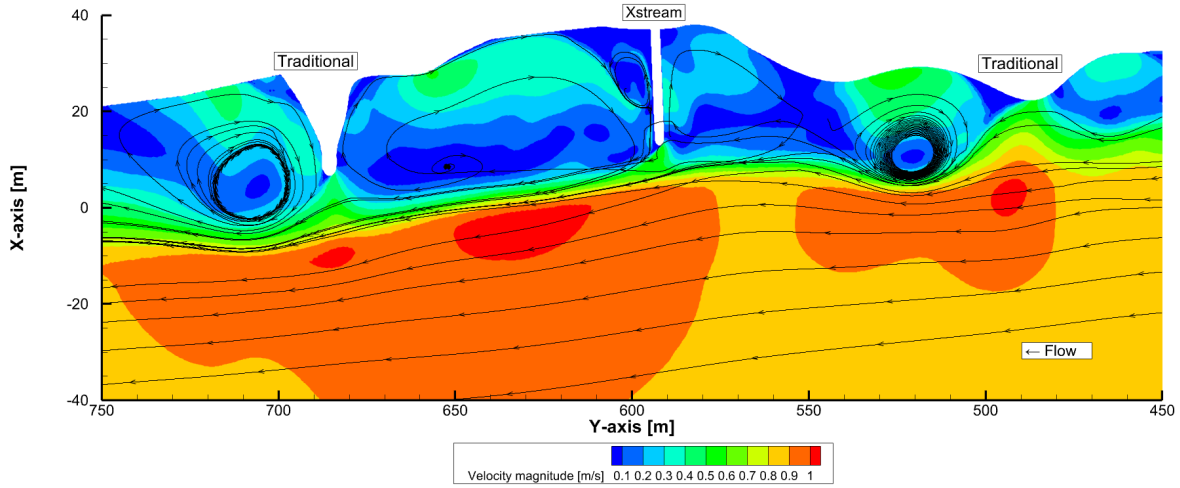

Figure 5.17: Velocity magnitude around the Xstream groyne

Figure 5.18 shows the profiles of the velocity gradients between the main channel and groyne field near the traditional groyne and the Xstream groyne. On first sight the fit of the Traditional groyne field seems to be good. The Xstream groyne clearly shows a different pattern, where the slope of the numerical data is much steeper and follows the same shape as observed at the traditional groyne. The observation done in the ADCP measurement that showed a milder slope in the groyne field at the Xstream groyne is therefore contradictory.

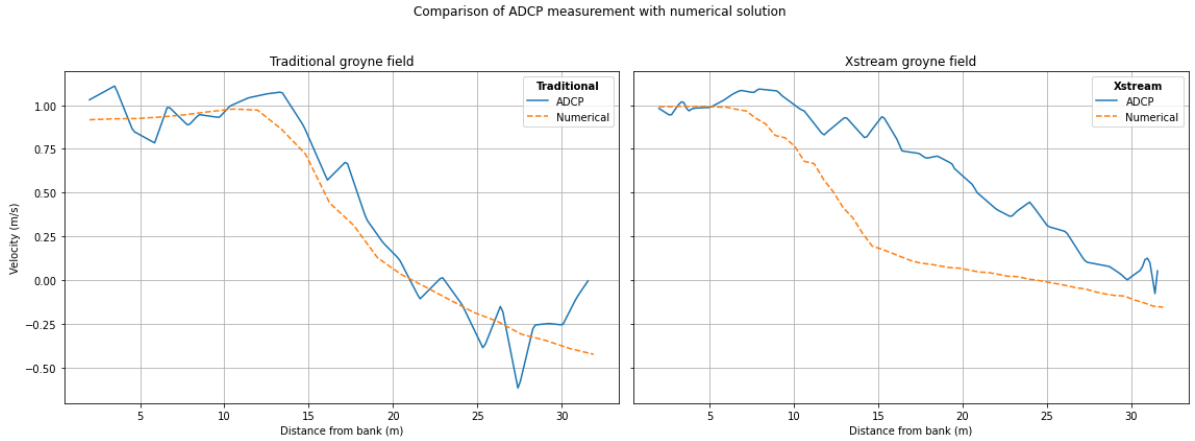

Figure 5.18: Comparison of velocity gradient between main channel and groyne field near groynes

Quantitative validation of the model performance is summarized below. The statistical comparison includes the Root Mean Square Error (RMSE) and the coefficient of determination (R^2).

- **Traditional vs ADCP:** RMSE = 0.156 (27.0%), $R^2 = 0.918$. The Traditional groyne field shows strong agreement between modelled and measured velocities. The low RMSE indicates that the absolute deviations are minor, while the high R^2 suggests the model effectively captures the shape and trend of the observed velocity gradient.
- **Xstream vs ADCP:** RMSE = 0.376 (58.2%), $R^2 = -0.082$. In contrast, the Xstream case displays a much poorer fit. The RMSE is significantly higher, indicating large deviations between the simulation and measurements. The negative R^2 suggests the model performs worse than a simple average, failing to reproduce the observed pattern and potentially introducing misleading trends.

These statistics highlight both strengths and limitations in the model's predictive performance. The velocity profile near the traditional groyne shows a good fit with the measurements, indicating that the model is capable of accurately capturing the lateral velocity gradient in this configuration. In contrast, the Xstream groyne field exhibits a much weaker fit. Although the modelled profile follows a similar shape to that observed near the Traditional groyne, it deviates significantly from the ADCP measurements taken at the Xstream location. This error may be partly caused by the highly transient nature of the measurements, which introduces additional uncertainty into the comparison. Nevertheless, the good agreement in the Traditional case provides a positive indication of the model's overall capability.

Vertical profile comparison

Figure 5.19 presents the depth profiles of flow velocity near both groynes, comparing ADCP measurements with the corresponding model results. For the traditional groyne, the model shows notable deviations from the measurements, particularly near the bed, where the observed velocity decreases

more sharply than the simulation predicts. Closer to the surface, however, the agreement between model and measurement improves.

In the Xstream case, the model and measurement display similar overall shapes, but the model consistently overestimates the velocity by approximately 0.05 m/s across most of the profile. It is also important to note that the ADCP data lacks values near the surface and the bed, likely due to limitations of the measurement equipment in capturing velocities close to boundaries.

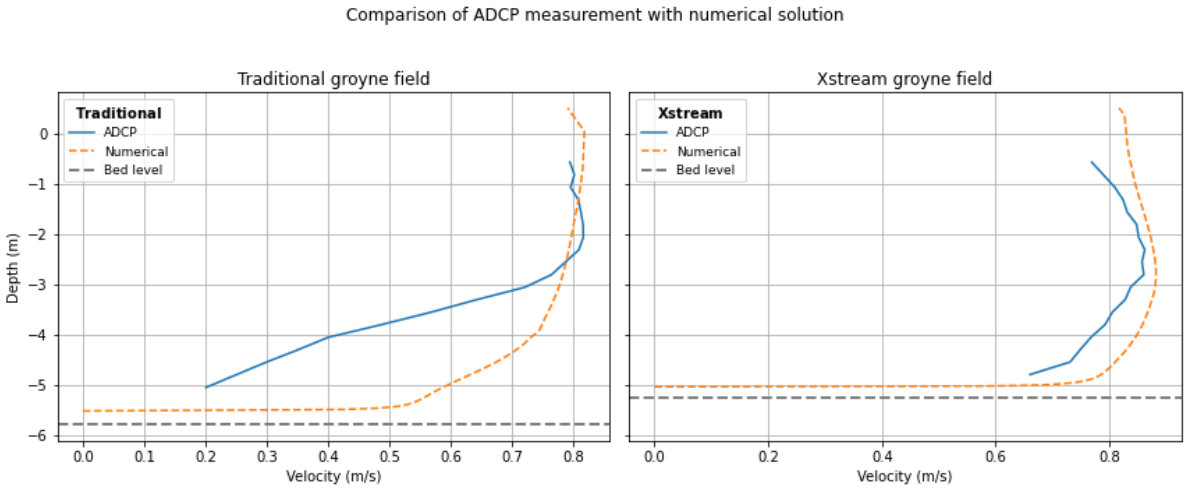

Figure 5.19: Comparison of depth profiles near groynes

Quantitative validation of the model performance is summarized below. The statistical comparison includes the Root Mean Square Error (RMSE) and the coefficient of determination (R^2).

- **Traditional vs ADCP:** RMSE = 0.205 (32.7%), $R^2 = 0.108$. The modelled velocity profile near the traditional groyne shows moderate agreement with the measured profile. While the RMSE suggests a reasonable match in magnitude, the low R^2 value indicates that the model does not accurately reproduce the shape or trend of the observed depth-dependent velocity distribution.
- **Xstream vs ADCP:** RMSE = 0.058 (7.1%), $R^2 = -0.232$. Despite the relatively low RMSE, which indicates small absolute differences in velocity magnitude, the negative R^2 suggests that the model fails to capture the vertical trend observed in the measurements. However, the measured profile at this location is relatively uniform and lacks strong curvature, which can diminish the sensitivity of the R^2 metric and lead to a misleadingly low or negative value even when absolute agreement is acceptable.

These statistics again reflect contrasting model performance. For the traditional groyne, the velocity magnitudes are fairly well reproduced, but the model lacks the ability to resolve the detailed vertical variation in velocity. In the Xstream case, although the modelled velocities are close in magnitude to the measured values, the vertical structure deviates in shape, resulting in a poor correlation with the measured trend. Since the ADCP measurements at this site are relatively steady and consistent over time, the errors are more likely due to limitations in the model's ability to resolve the vertical flow structure rather than measurement uncertainty. An example is that the depth profiles of the model are insignificantly altered by friction, which may cause the difference in the shape.

Initial scour pattern comparison

Figure 5.20 presents the bed shear stress distribution for the base case simulation. Distinct peaks in shear stress appear near the groyne heads, indicating zones of intensified flow interaction where sediment transport is more likely to occur. These high-stress regions align with expected hydraulic behaviour around groyne structures. A comparison with the morphological features that were observed from Figure 3.6 reveals that the locations of scour pits partially correspond to these shear stress peaks. In particular, the high shear stress downstream of the groyne matches the position of the scour pit.

To assess the likelihood of sediment transport, the computed bed shear stresses can be compared to the critical shear stress derived from Shields' theory. For the median sediment size of 0.5 millimetres, this corresponds to a critical shear stress of about 0.44 pascal. In Figure 5.20, this value is exceeded in the main channel, where bed shear stresses are found of approximately 0.9 pascal. In the groyne field, this critical stress is not exceeded, causing sediment to be deposited. This behaviour is valid for river morphodynamics.

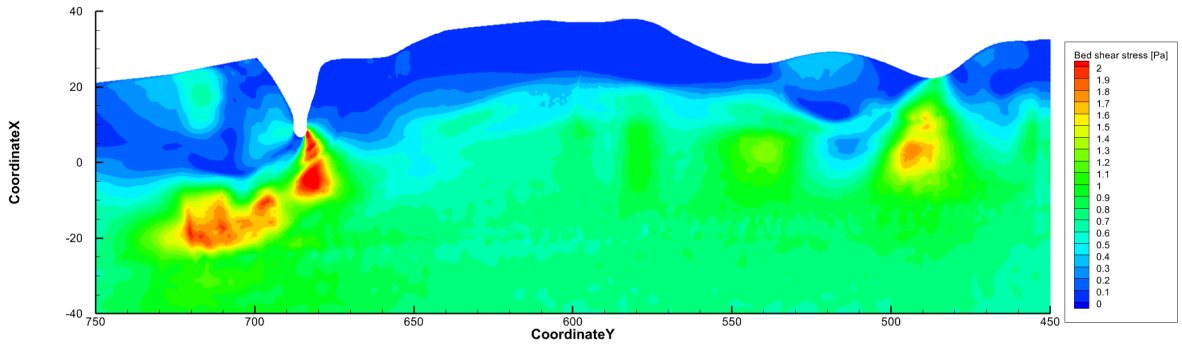

Figure 5.20: Bed shear stress contour from base case

Spiral flow structure

Figure 5.21 shows the transverse velocity profiles at five locations along the groyne fields. A clear spiral flow pattern is visible in the first three profiles (DP-1 to DP-3), characterised by negative transverse velocities near the bed—indicating flow toward the inner bend and positive velocities near the surface, indicating outward flow. This vertical circulation is consistent with the secondary flow structure expected in curved channels and matches the transverse velocity magnitudes of approximately ±0.05 m/s observed in the ADCP measurements (Section 3.4.1).

Further downstream, beyond the Xstream groyne (DP-4 and DP-5), the spiral flow pattern becomes disrupted. Here, the transverse velocity profile predominantly shows flow directed toward the inner bend throughout the depth, with no clear sign of upward return flow near the surface. This matches the general inward-directed flow observed in the ADCP profile at this location. However, unlike the measurements, which still display a weak spiral flow structure, the model does not produce a secondary circulation in this region.

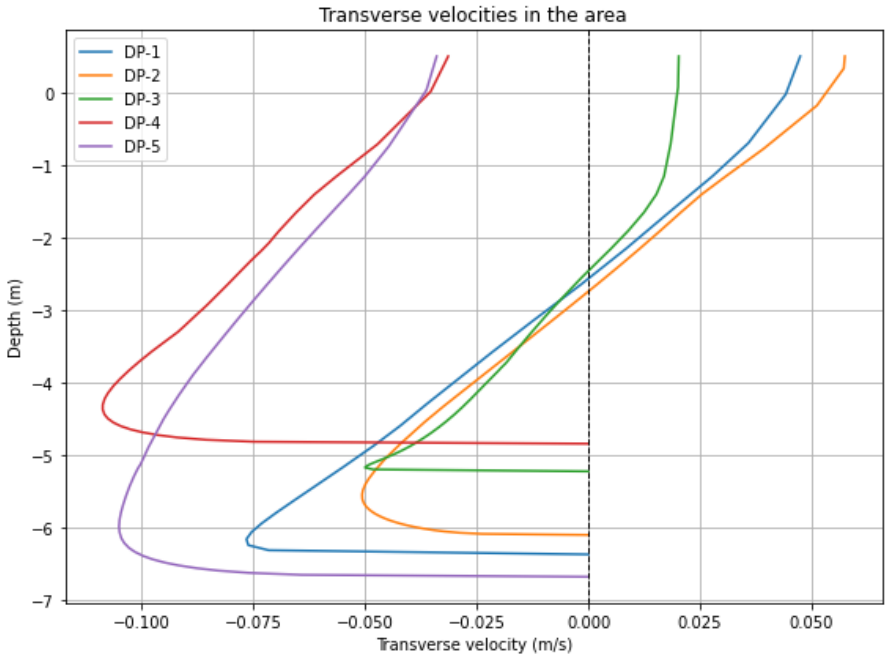

Figure 5.21: Depth profiles of transverse velocities in the groyne field area

5.2.4. Flow field analysis

Recirculation zone characteristics

Figure 5.22 shows the velocity contours at the free surface (z = +0.5m) for both groyne configurations, with streamlines added to indicate flow direction. In the upstream groyne field, both cases exhibit similar flow patterns, including the two vortices. Velocity magnitudes in this region are also comparable between the two cases.

In contrast, the downstream groyne field reveals notable differences. The traditional groyne case exhibits two well-defined vortices and a third smaller eddy near the groyne base. The largest of these resembles the upstream vortex and represents a typical feature of flow past a traditional groyne. In the Xstream case, only a single, broad vortex is present, extending over most of the downstream groyne field, with its centre located approximately 60 meters from the groyne. These differences are partly explained by the groyne geometries. The more gradual slope of the traditional groyne allows greater flow connectivity between fields, moving water around the groyne head more freely. In contrast, the steeper slope of the Xstream groyne restricts flow passage near the head, resulting in a sharp velocity gradient in this region. It is notable that the slight permeability of the Xstream groyne does not contribute to an easier flow passage as the streamline curve toward the main channel or recirculate in the upstream groyne field.

The contour colours highlight differences in velocity magnitude. While both cases show low velocities within recirculation zones, the Xstream configuration exhibits a significantly larger low-velocity area. For the traditional groyne, velocities around the eddies reach up to 0.5 m/s, with slower flow appearing further downstream. In the Xstream case, velocities near the bank are around 0.5 m/s, but within the recirculation zone drop below 0.2 m/s. Meanwhile, the main channel shows velocities exceeding 0.8 m/s in both cases, though the Xstream case shows a larger accelerated velocity zone in the channel.

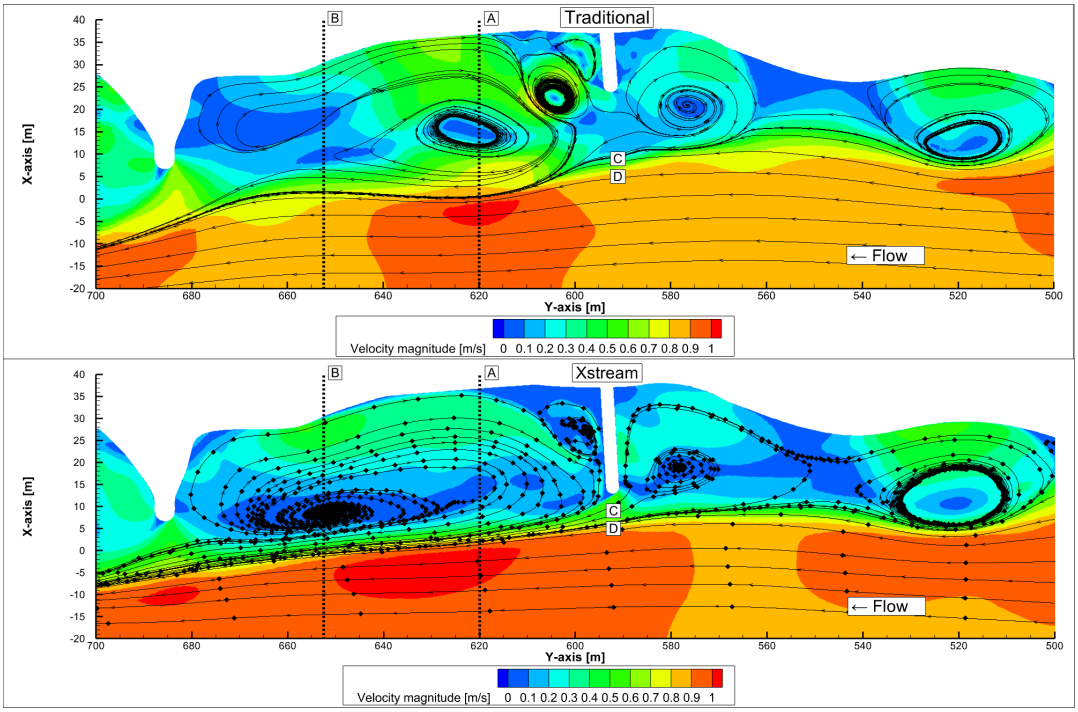

Figure 5.22: Velocity contours including streamlines at the free-surface. Top: Traditional groyne case, bottom: Xstream groyne case

Another contour plot displays the velocities and streamlines near the riverbed (at $z = -4\,\mathrm{m}$) in Figure 5.23. As with the surface flow, the most notable differences occur in the downstream groyne field. Near the traditional groyne head, a small vortex is present, associated with locally reduced flow magnitudes, while adjacent to this vortex, a concentrated patch of higher velocity is present.

In contrast, no clear vortex is visible downstream of the Xstream groyne. The low-velocity zone observed at the traditional groyne is shifted closer to the riverbank in this case. The streamlines suggest that flow penetrates through the permeable Xstream groyne, which may contribute to the absence of the formed downstream eddy (observed at the traditional groyne). Instead, a narrow band of elevated velocity is observed near the groyne toe, extending downstream along the bed.

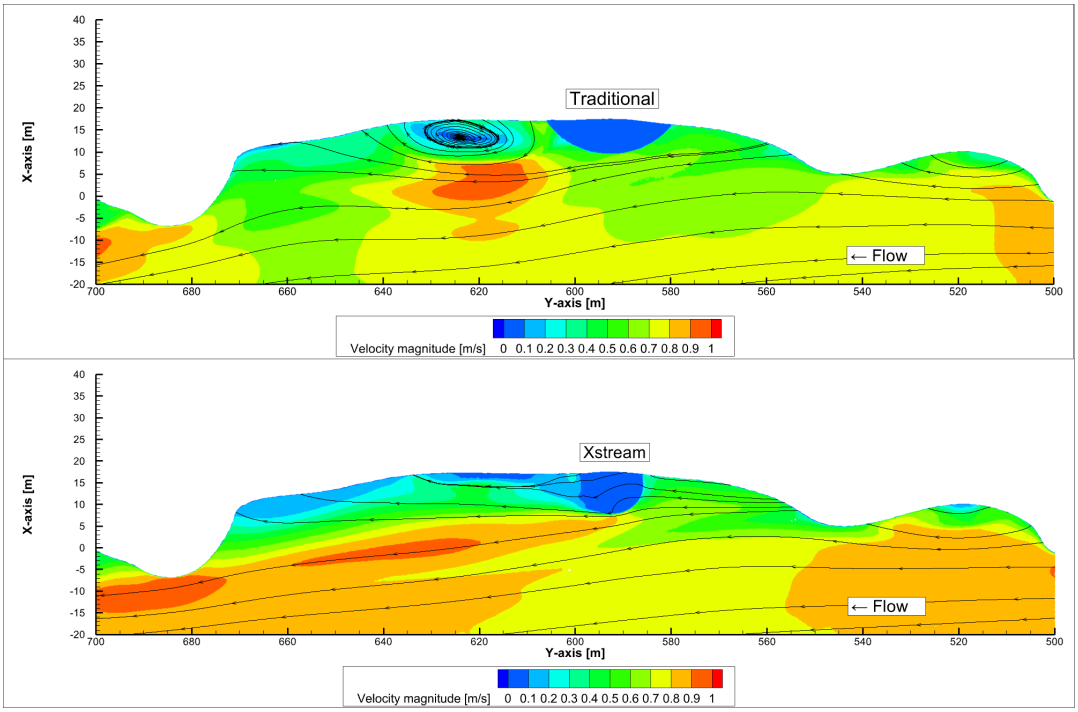

Figure 5.23: Velocity contours including streamlines near the bed level. Top: Traditional groyne case, bottom: Xstream groyne case

Figure 5.24 presents the streamwise velocity profiles at three representative locations: A, B, C and D (as indicated in Figure 5.22). Locations A and B are positioned at the centres of the two main recirculating vortices in the downstream groyne fields. Location C and D display vertical depth profiles near the groyne head at the toe and at the middle of the Xstream slope.

The left-hand panel shows the streamwise velocity across the groyne field width for both locations A and B. At both sites, the Xstream and traditional configurations exhibit high and relatively uniform velocities in the main channel, ranging from approximately 0.9 to 1.0 m/s. Moving into the groyne field, distinct differences emerge. At location A, the traditional groyne shows a steeper velocity gradient, with the velocity dropping to zero in the eddy centre and a wide zone of upstream-directed flow near the riverbank reaching up to 0.5 m/s. The Xstream configuration follows a similar shape but with less intensity; the upstream flow near the bank only reaches -0.35 m/s. At Location B, a reverse pattern is observed. The Xstream groyne shows a stronger negative velocity near the riverbank, exceeding that of the traditional case by approximately 0.2 m/s. Notably, the velocity gradient near the traditional groyne is shifted approximately 5 metres closer to the riverbank compared to that of the Xstream groyne which can also be observed in Figure 5.22.

The right-hand panel (Locations C and D) displays the vertical distributions of streamwise velocity near the groyne head, illustrating how velocity varies with depth for different slope configurations. At location C, the velocity profile for the Xstream groyne is significantly lower over much of the depth due to the influence of the groyne structure. Within the groyne itself, flow velocities remain below 0.025 m/s. However, immediately beyond the groyne head, the velocity increases sharply to values exceeding 0.6 m/s, which is higher than those observed in the traditional groyne case at the same location. Despite differences in water depth between the groynes, both profiles show a similar trend: velocity peaks near the groyne head and decreases toward the free surface. At location D, near the toe of the groyne, the

profiles diverge more clearly. Below -2 metres depth, the Xstream groyne exhibits higher velocities, whereas the traditional groyne displays a velocity profile shaped by friction, with decreasing values toward the riverbed. Near the free surface, the velocity associated with the Xstream groyne once again shows a damped pattern, consistent with the behaviour observed at location C.

Note: A numerical error shows a velocity increase inside the traditional groyne (z=-4.4m to z=-5.2m), which should be neglected. This error did not harm the solution and is present due to internal physics inside the impermeable traditional groyne structure that ANSYS Fluent assumes as flow.

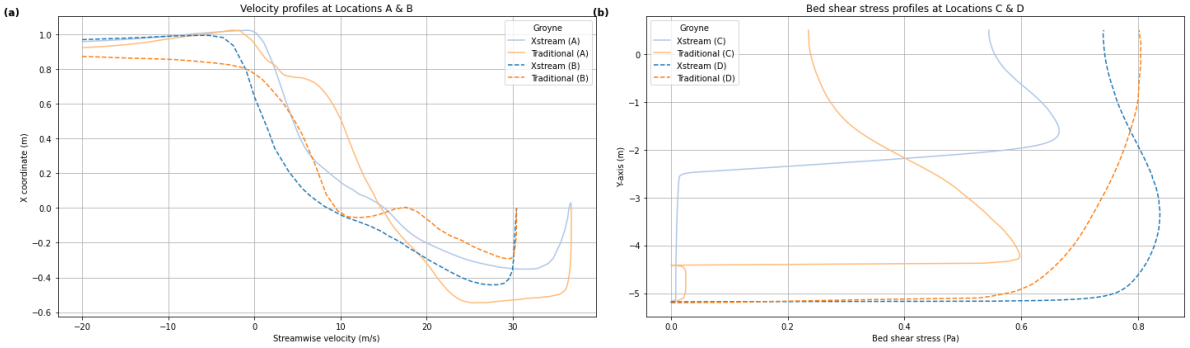

Figure 5.24: Velocity profiles. Left: Streamwise velocities in the groyne fields, right: velocity magnitude at the groyne heads

Turbulence patterns and intensity

Figure 5.25 shows the contours of turbulent kinetic energy (TKE) near the bed level for both the traditional and Xstream groyne configurations. In the traditional case, TKE levels are notably elevated around the groyne head, forming a concentrated region of turbulence that aligns with the high-velocity zone shown in Figure 5.23. Elevated TKE magnitudes are also present within the groyne field, particularly near the base of the groyne, indicating turbulent activity in this area.

In contrast, the Xstream groyne produces a much more subdued turbulence field. TKE levels are generally lower and more evenly distributed, with a single, narrow band of higher energy following the path of elevated velocity seen in Figure 5.23. Within the groyne field, TKE remains relatively low, suggesting that the Xstream design generates significantly less turbulence near the bed compared to the traditional groyne.

Both configurations exhibit a high-TKE patch near the downstream groyne. However, this region appears smaller in the traditional case, suggesting a larger shadow zone behind the groyne, which effectively shields the downstream structure from turbulent flow.

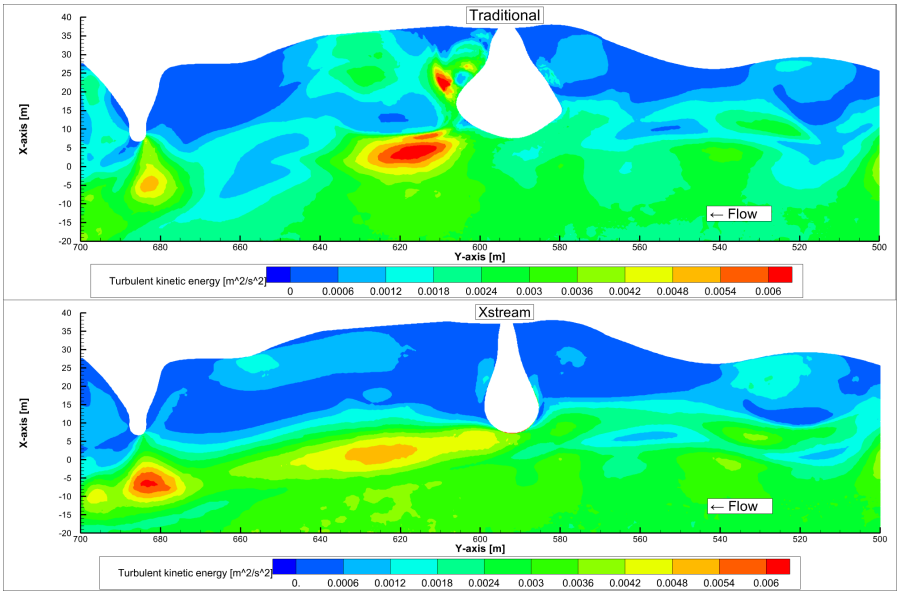

Figure 5.25: Turbulent kinetic energy contours near the bed level. Top: Traditional groyne case, bottom: Xstream groyne case

5.2.5. Sediment response analysis

Bed shear stress patterns

Figure 5.26 presents the bed shear stress contours for both the traditional and Xstream groyne configurations. The patterns show a strong resemblance to those observed in Figure 5.25. As established in Section 3.2.6, sediment movement initiates when the bed shear stress exceeds approximately 0.44 Pa.

In the traditional groyne case, shear stress values exceed this threshold in several regions near the groyne. Most notably, a large high-stress patch is present around the groyne head, indicating potential erosion. This coincides with the typical development of a scour pit—commonly observed at the head of traditional groynes. Within the groyne field, elevated shear stress is also found near the groyne base, which likely prevents sediment deposition. Further downstream, however, the groyne field shows a broader zone of low shear stress, suggesting favourable conditions for sediment accumulation.

In contrast, the Xstream groyne produces a distinctly different shear stress pattern. A long, continuous region of elevated shear stress originates at the toe of the groyne and extends along the downstream groyne field. This indicates potential erosion not just at the head but along the entire interface with the main channel. These high-stress patterns closely align with the erosion features seen in the bed topography maps from 2024 onward, discussed in Section 3.3. Within the groyne field itself, shear stress values are generally lower and most areas remain below the critical threshold for sediment motion, indicating that sediment deposition is more likely to occur there.

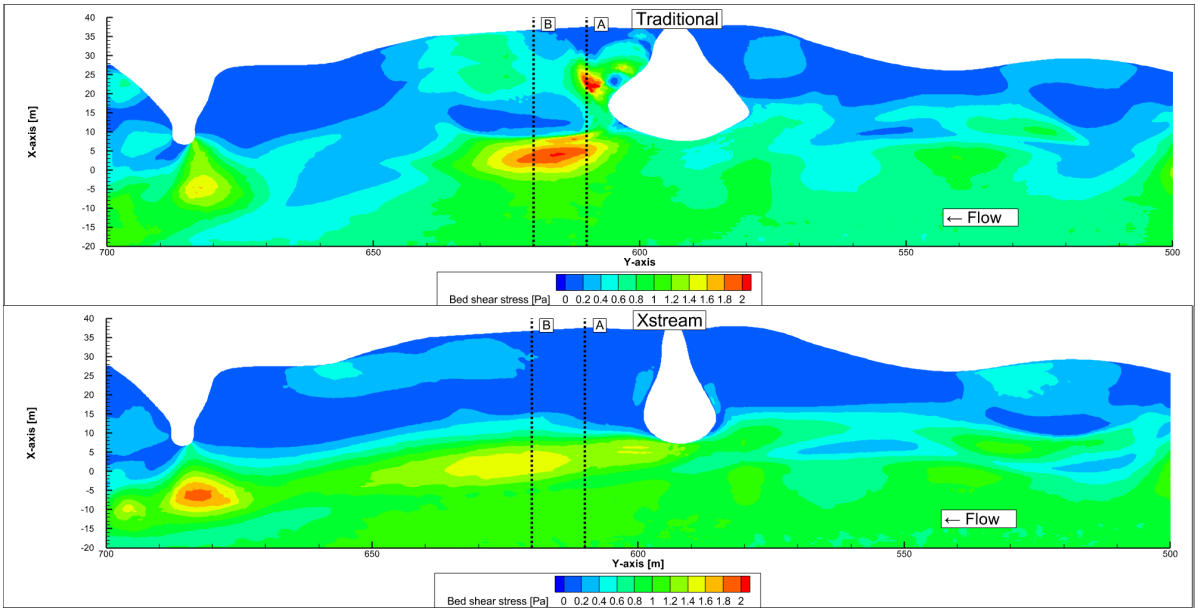

Figure 5.26: Bed shear stress contours at the bed. Top: Traditional groyne case, bottom: Xstream groyne case

Graphs shown in Figure 5.27 describe the magnitude of the bed shear stresses. At location A, the bed shear stresses in the traditional groyne case show values above 0.5 pascals in most of the area, with two distinct regions reaching peak values between 1.8 and 2.0 pascals. The Xstream groyne, on the other hand, shows much lower bed shear stresses in the same area, with a peak around 1.5 pascals and deeper in the groyne field reaching maximum values around 0.25 pascals.

For the transect at B, low bed shear stresses are also observed for the traditional groyne. However, these values are still approximately 0.3 pascals higher than those of the Xstream groyne. At the peak locations, the Xstream groyne case consistently shows lower maximum values than the traditional groyne, indicating a reduced capacity for sediment transport in the Xstream configuration. In the main channel, the bed shear stresses show similar magnitudes for both groyne types.

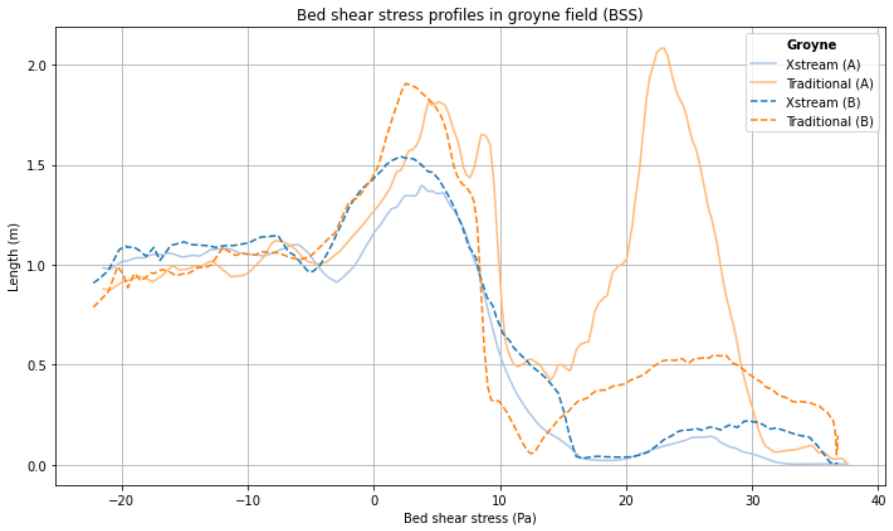

Figure 5.27: Bed shear stress profiles in the groyne field

Behaviour at the sediment line

Figure 5.28 describes the bed shear stress just downstream of both groynes. Due to the legend settings of the contour plot the largest part of the traditional groyne field shows excessive bed shear stresses. However, a larger patch of blue and green is visible near the main channel that indicates bed shear stresses below 0.35 pascals, where sediment deposition is possible. Comparing it with the Xstream groyne this is however negligible, where the full groyne field shows lower bed shear stresses. Interestingly a wider and longer blue area follows the main channel direction, which is also the location where the sediment line is formed. The bed shear stresses close to zero therefore give a good indication of how this line came to be. Near the groyne a patch of higher bed shear stresses is observed. This patch acknowledges the existence of the groove that separates the groyne from the sediment line.

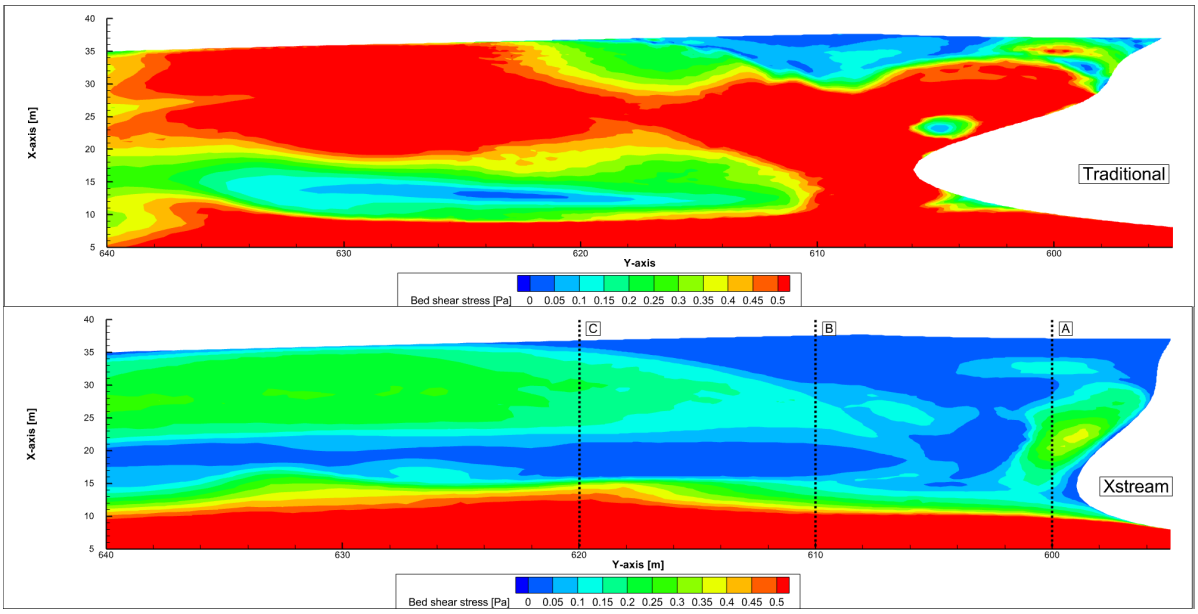

Figure 5.28: Bed shear stress contours in the groyne field. Top: Traditional groyne case, bottom: Xstream groyne case

To describe the flow patterns at the location of the sediment line, Figure 5.29 shows multiple cross sections near the groyne with the locations of the cross-sections described in Figure 5.28. The contours indicate the streamwise velocity, where blue is upstream directed and red downstream directed. The streamlines show the combined transverse and vertical velocity. A clear pattern is visible in all cross-sections, where a large eddy is observed in the area of low streamwise velocity. The presence of the eddy causes flow to leave the groyne area from the upper part of the water column. The flow convergence between the groyne field and eddy is located in the middle of the water column, which causes a small area at the bed to be shielded from the stronger flows, which can be observed at approximately x = 14 to 15 metres. Combined with the lower streamwise velocities, this area makes it ideal for sediment to be deposited. The last cross-section shows a secondary eddy inside the groyne field. Even though it causes a certain circulation in the field its flow is obstructed by the primary eddy, which indicates the higher strength of this primary eddy. The cross sections are taken over a length of 20 metres and are able to explain the blue band of low shear stresses from Figure 5.28. Similar profiles were made for the traditional groyne and were added to Appendix C. These cross sections show no presence of eddies near the groyne, while further away from the groyne, a similar eddy is present. However, where the flow is directed upward the streamward flow are much more significant,

preventing the possibility of sediment deposition.

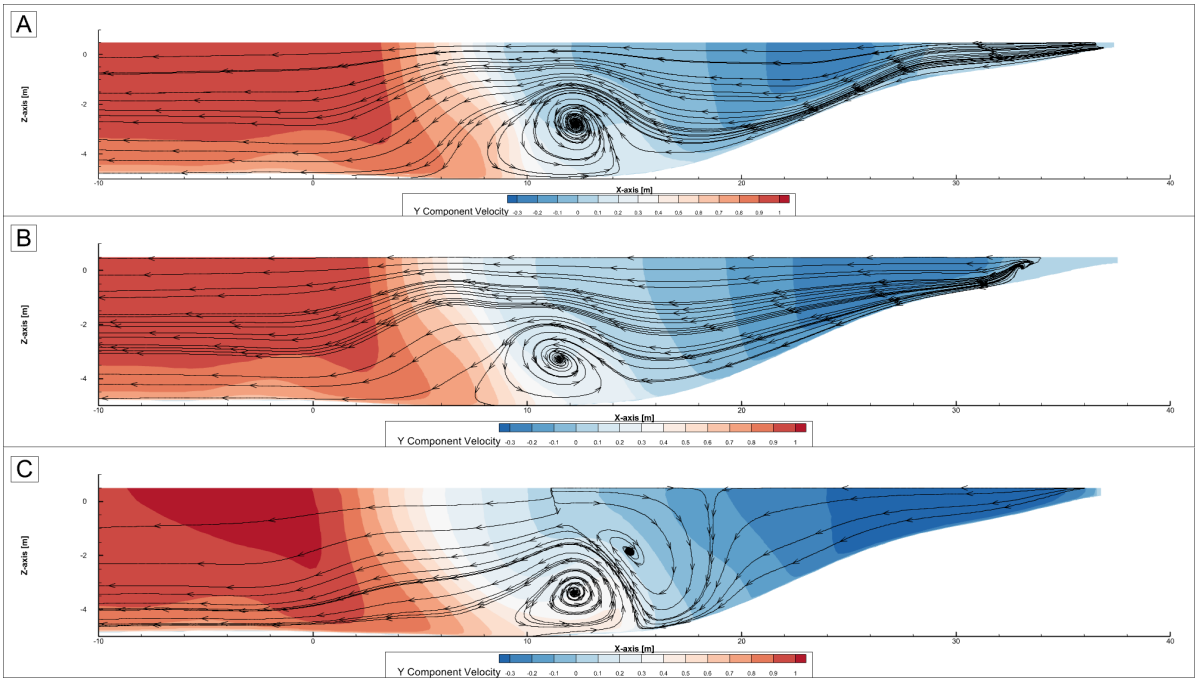

Figure 5.29: Cross-sections at the groyne

Finally, Figure 5.30 illustrates the development of the secondary eddy near the sediment line. This figure is intended primarily to clarify the flow mechanisms that were discussed in this section.

The yellow arrows mark the upstream-directed (recirculating) flow occurring near the riverbank. This flow is deflected back toward the main channel as it approaches the groyne. Further downstream, the flow direction remains only partially oriented toward the channel centre, where it flows toward the outer boundary of the groyne field. There, the flow coincides with the sediment line, where it is redirected vertically upward, as shown by the orange arrows.

This upward motion is a result of a larger counter-clockwise eddy (indicated by red arrows) located just off the main channel. This eddy induces an upward flow near its inner edge, lifting water from the bed region toward the surface. As a consequence, the green-highlighted zone near the bed becomes a low-energy area where sediment can accumulate over time, leading to the gradual formation of a ridge-like feature, namely the sediment line.

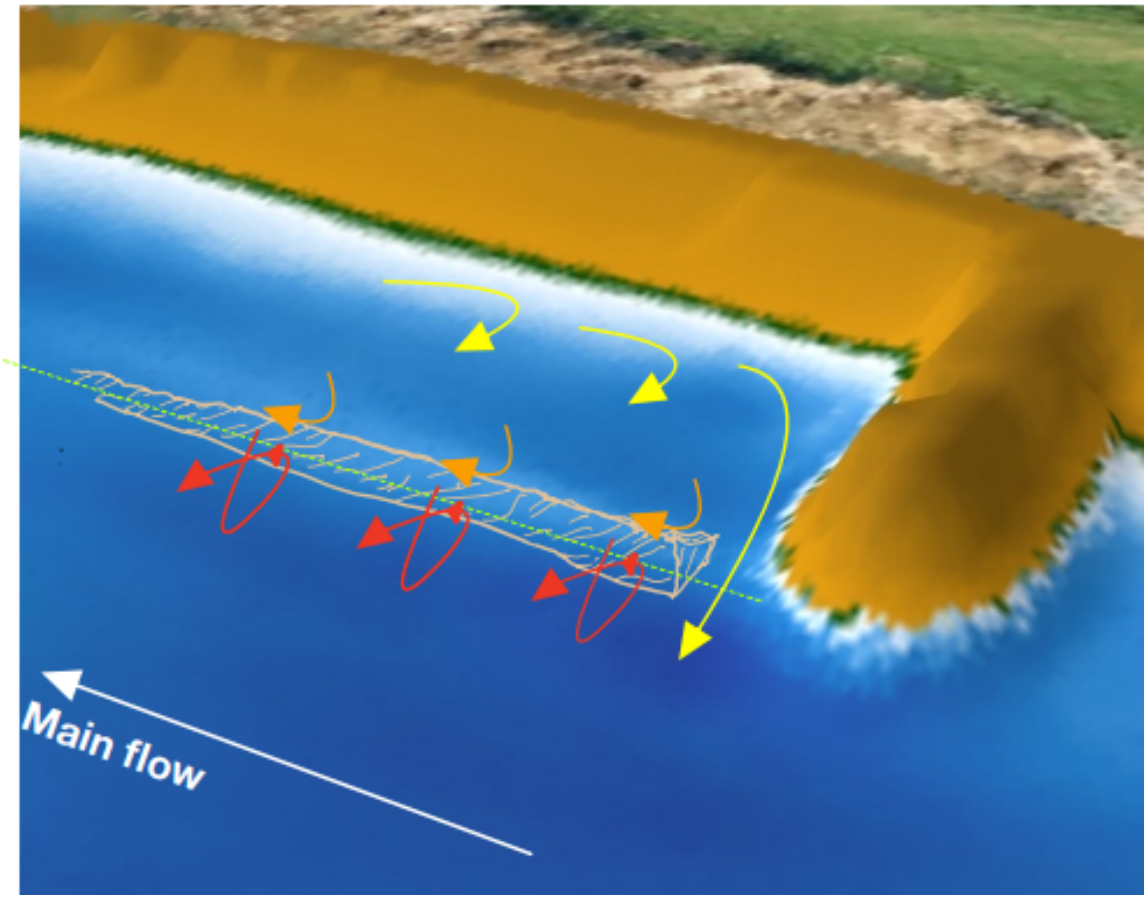

Figure 5.30: Flow principles near the sediment line

6

Discussion

This chapter integrates the findings from the field measurements with the numerical modelling and compares the behaviour at traditional and Xstream groynes. The objective is to critically evaluate the model performance, assess the reliability of the field data, and interpret the observed hydrodynamic and morphodynamic effects in relation to groyne design. This discussion focuses on the limitations and implications that shape the overall understanding of groyne behaviour in a natural river system. Key attention is given to the challenges in validating complex three-dimensional flow structures, the role of groyne geometry in influencing sediment transport and the emergence of unique morphological features such as the sediment line.

Field analysis

The field measurements provided essential insights into the sediment and flow behaviour around the Xstream groyne. However, their interpretation and use in model validation are subject to several important limitations that must be acknowledged and understood.

From a morphodynamic perspective, the key objective was to understand how the groyne influenced sediment transport patterns like erosion and deposition. The multibeam surveys revealed consistent trends, particularly the formation of a sediment line downstream of the groyne. This line appeared shortly after the groyne extension and gradually migrated shoreward under higher discharges, while flattening during low flows. The stability and persistence of this feature suggest an underlying physical mechanism rather than noise or measurement error.

Changes in erosion and deposition patterns appeared to be partially influenced by variations in river discharge during the measurement periods. Higher discharges enhanced sediment mobilisation, while lower discharges promoted deposition and allowed morphological features such as the sediment line to stabilise. However, the effect of groyne submergence was only partially captured, as the period of high discharges was short. Furthermore, by Rijkswaterstaat standards, no genuinely high discharges occurred during the measurements. This leaves a gap in understanding the morphodynamic response of the system under flood-like conditions, where flow depth and energy may fundamentally alter sediment dynamics and scour development.

From a hydrodynamic perspective, ADCP measurements captured a single discharge condition and were collected in a short time frame. As a result, the measured flow field reflects a transient state rather than a steady flow state. This is particularly relevant in regions influenced by recirculation and turbulence, where short-term fluctuations can dominate and misrepresent persistent flow patterns. Furthermore, vertical resolution near the bed and within the groyne field was limited.

Model selection

The model used in this study is based on ANSYS Fluent, which was selected after a multi-criteria analysis of various modelling software. ANSYS Fluent provides robust capabilities for simulating detailed flow separation and turbulence around groyne structures. It solves the full Navier-Stokes equations with a wide range of turbulence models and supports porous media zones essential for modelling the Xstream groyne.

However, certain limitations should be acknowledged. ANSYS Fluent does not allow simultaneous implementation of both permeability and wall roughness in the same domain region. As a result, the Xstream groyne was treated as smooth despite its rough block surface. This simplification likely leads to an underestimation of frictional effects near the structure. Additionally, the complexity of Fluent introduces the challenge of managing numerous solver settings and sub-models, requiring careful configuration to avoid introducing unintended numerical behaviour.

Numerical quality

Sensitivity of the model

A series of sensitivity analyses were conducted to assess the model's robustness. Grid resolution tests showed that finer meshes improved predictions of velocity gradients, turbulent kinetic energy (TKE) and bed shear stress, especially near groyne heads. A fine mesh with 10 million cells was chosen as a compromise between computational cost and accuracy. However, even with this compromise, the model remained computationally expensive, with long simulation times required for a steady solution.

The turbulence model sensitivity analysis compared k-ε and k–ω SST models. Both models produced similar velocity profiles, but k–ω SST more accurately captured turbulence intensities near boundaries. This confirmed its selection for the final simulations. However, the analysis showed only minor differences in accuracy between the models. Given the significantly longer simulation time for the k–ω SST model, the k–ε model could have been an acceptable alternative if computational resources or time were more constrained. Interestingly, the turbulent viscosity showed a large difference of orders of magnitude between the two turbulence models. Although this behaviour could not fully be explained, it introduces a degree of uncertainty in the turbulence representation. Nonetheless, other indicators such as TKE and shear stress distribution remained consistent, suggesting the large-scale flow structure was not significantly affected.

The free-surface boundary was simplified using a rigid-lid assumption. While this neglects surface deformation, pressure gradient analysis showed that the approximation remained valid under a Froude number below 0.5 in the area. Nevertheless, this approach introduces a limitation: it prevents the model from capturing dynamic surface effects such as free-surface fluctuations, which could influence turbulence and momentum exchange near the surface. A more advanced Volume of Fluid (VOF) method would be required to resolve such dynamics accurately.

Validation of the model

Validation of the numerical results was performed using ADCP measurements of velocity profiles and sediment response maps, complemented by qualitative comparisons of flow structures observed in the field. Quantitative validation of the model performance is summarised below using the Root Mean Square Error (RMSE) and the coefficient of determination (R^2). For the traditional groyne, the model showed moderate agreement with the measured profile: RMSE = 0.205 (32.7%), R^2 = 0.108. This indicates that while the velocity magnitudes were (somewhat) reasonably captured, the model struggled to reproduce the vertical shape of the velocity profile. In contrast, for the Xstream groyne, the RMSE was 0.058 (7.1%) and R^2 = –0.232. Despite the low RMSE, the negative R^2 suggests a poor fit in terms of profile shape. This is partly due to the relatively flat measured depth profile, which diminishes the usefulness of R^2 as a measure of agreement.

The validation also examined shear stress gradients and spiral flow behaviour. However, measured values were highly variable and sensitive to the ADCP transect position. While the general patterns showed some similarity, the transient nature of the field data means that comparisons to the steady-state model should be treated cautiously. These inconsistencies highlight the difficulty in using short-term measurements to validate three-dimensional flow structures. Improved field data or validated experimental studies would support a more meaningful model validation.

Bed shear stress distributions from the base case model simulation aligned with observed erosion patterns. High-shear zones corresponded to scour regions seen in multibeam surveys. The model predicted critical shear thresholds consistent with sediment transport theory (τ□ > 0.44 Pa), reinforcing confidence in the morphodynamic representation.

Comparison of traditional and Xstream groyne

Hydrodynamic differences

Field and numerical data both reveal that the Xstream groyne introduces distinct hydrodynamic behaviour compared to traditional groynes. A notable difference is the shape and intensity of the recirculation cell. Float trajectories stayed more aligned with the main channel at the Xstream groyne, while those at the traditional groyne curved visibly into the groyne field, forming a short loop. ADCP profiles confirmed this shape, showing a gradual velocity decline into the groyne field and weaker reverse flow near the bank. Together, these observations indicate a stretched, low-energy recirculation pattern.

Numerical model results supported these field observations. Free-surface contours showed that the traditional groyne generated multiple tight vortices, while the Xstream groyne produced a single, broader recirculation zone that extended further downstream. Near the bed, the Xstream case lacked the distinct recirculation cell observed at the traditional groyne and showed lower turbulent kinetic energy (TKE) around the groyne head. This difference indicates the influence of groyne geometry: the traditional groyne, with its flatter slope, allows for more horizontal flow redirection and vortex formation. In contrast, the steeper slope of the Xstream groyne encourages a more vertical flow path and limits lateral expansion of the recirculation zone.

Streamwise velocity profiles from both ADCP and model data showed consistent trends. Velocities near the bed were higher at the Xstream groyne, suggesting reduced stagnation and weaker return flow. Near-surface velocities were comparable, even though the traditional groyne profile was more uniform and the Xstream profile showed a dampened velocity near the free-surface. In the lower half of the water column, the traditional groyne displayed a sharper velocity drop toward the bed, reflecting

stronger return flow and stagnation. Additionally, the shape of the high-velocity zone in the Xstream configuration was narrower and more focused along the channel axis, influencing the shape of the streamwise velocity profile and further confirming the different flow dynamics. These differences are closely tied to the slope geometry of the groynes: the steeper Xstream design promotes a more uniform velocity profile across the depth, limiting curvature and vertical variability in the flow. In contrast, the flatter slope of the traditional groyne allows flow to distribute more gradually over the depth, also enabling more curvature of flow across the profile.

Although the Xstream groyne is permeable, its permeability is relatively low and therefore has a limited influence on the overall flow dynamics. Both field and numerical results showed that the main flow is still deflected around the groyne head, indicating that the structure acts more like a solid barrier than a transmissive one in hydrodynamic terms.

Morphodynamic differences

Field observations demonstrate that the sediment response differs significantly between the traditional and Xstream groynes. The traditional groyne produced a more localised morphodynamic pattern, with concentrated scour (scour pit) around the groyne head and distinct deposition zones downstream of the groyne field. These observations are consistent with the strong and compact recirculation cell seen in both measurements and simulations. In contrast, the Xstream groyne led to a more distributed sediment response: erosion and deposition were spread over a broader area and no compact erosion zones were detected. This pattern aligns with the weaker, elongated recirculation zone observed around the Xstream structure.

The underlying cause of these morphological differences becomes clearer when considering bed shear stress distributions. In the model, peak shear stresses at the traditional groyne were concentrated just downstream of the groyne head, indicating a high potential for sediment mobilisation and scour. At the Xstream groyne, high shear stress zones were more diffuse and more evenly spread out. This shift in stress distribution indicates a lower risk of concentrated scour and reflects a smoother transition in sediment transport through the groyne field. Instead of trapping or depositing sediment in defined areas, the Xstream groyne promotes a more continuous sediment transport process.

Sediment line formation

A distinctive morphological feature observed at the Xstream groyne was the formation of a sediment line separating the groyne field from the main channel. This feature is not observed at traditional groynes. Field observations showed the first presence of the line four months after extending the Xstream groyne. It was observed that during periods of high discharge, the line shifted toward the riverbank. Also, the line is detached from the groyne by a groove. Additionally, ADCP cross-sections revealed flow patterns around the sediment line: channel-directed flow between the groyne and sediment line. Inside the groyne field, there were uniform low velocities, while a higher magnitude flow directed outward was found on the channel side. A convergence of streamlines was observed at the tail.

Model results provided additional insight into the formation of this feature. The sediment line corresponded with a distinct zone of low bed shear stress that extended along the channel edge, downstream of the Xstream groyne. This region coincided with the presence of a broad, counter-clockwise eddy that formed just outside the groyne field on the main channel side. This eddy was located in an area of low streamwise velocities near the bed, where transverse and vertical velocities play a significant role. The channel-directed flow near the bed from inside the groyne field is redirected upward due to the

eddy. As a result, the lower part of the water column is relatively isolated from the main flow, creating a low-energy area. The combined conditions of limited streamwise velocity and upward-directed flow decrease the bed shear stress and create an ideal environment for sediment to accumulate steadily over time.

Differences in the observations around the sediment line between the field data and numerical results can largely be attributed to the transient nature of the ADCP measurements, which are not well-suited for capturing the full three-dimensional behaviour of the eddy. An explanation for the movement of the sediment line due to higher discharges could be the increase in the volume of flow around the groyne head. This introduces greater curvature in the streamlines and potentially shifts the location of the eddy and the sediment line further toward the riverbank. To validate this, the model should be set up for different discharge values.

7

Conclusion and Recommendations

7.1. Conclusion

How does the flow structure around the Xstream groyne differ from that of traditional groynes based on field measurements?

Field measurements reveal that the flow structure around the Xstream groyne is notably different from that of traditional groynes. The Xstream groyne exhibits a weaker and more elongated recirculation zone, with reduced turbulence intensity and milder velocity gradients across the mixing layer. Float tracking experiments and ADCP measurements confirmed that surface return flows and horizontal entrainment are suppressed at the Xstream groyne, contrasting with the stronger vortices observed around traditional groynes. These differences are mainly attributed to the steeper slope of the Xstream design.

What morphological changes have occurred around the Xstream groyne compared to traditional groynes based on field measurements?

Field measurements indicate that the Xstream groyne induces a broader and more gradual morphological response than traditional groynes. Rather than forming a concentrated scour pit at the groyne head, as seen with traditional groynes, the Xstream groyne led to a more distributed pattern of erosion near the main channel and mild deposition in the groyne field. Additionally, the groyne field around the Xstream structure remained relatively stable over time, with most morphological activity concentrated along the outer edge near the main channel. One notable difference is the emergence of a unique sediment feature called the sediment line downstream of the Xstream groyne, which is not observed near traditional groynes.

To what extent can a numerical model reproduce the flow structures observed around the Xstream groyne?

The numerical model developed in ANSYS Fluent successfully reproduced key flow features such as recirculation zones, velocity distributions, and turbulent structures. The model showed good agreement with field observations near traditional groynes, though performance was more limited at the Xstream groyne. ANSYS Fluent was selected based on a multi-criteria analysis (MCA), which eval-

uated modelling accuracy, flexibility, and practical considerations across several software options. A known limitation is that friction and permeability cannot be combined within the same zone, which may have led to a slight overestimation of flow through the Xstream groyne. Nevertheless, the model effectively captured the broader hydrodynamic differences between groyne types and offered valuable insight into the role of geometry and permeability in shaping local flow separation, mixing, and shear stress.

What insights do the model results provide into the hydrodynamic and morphodynamic mechanisms?

The numerical model offered valuable insight into the mechanisms by which groyne geometry and permeability affect flow structure, turbulence, and bed shear stress. One of the findings was the dominant role of the groyne slope in shaping the local hydrodynamic response. The steep 1:1 slope of the Xstream groyne altered the flow separation process, leading to a narrower and more vertically concentrated mixing layer compared to the broader, more horizontal separation observed at traditional 1:3 groynes. This difference resulted in a reduction in horizontal recirculation strength and vortex formation in the downstream groyne field.

Permeability, though present, appeared to play a secondary role in modifying the flow. While it allowed limited flow through the groyne, its effect was largely overridden by the steep slope. The model results confirmed that even with permeability, the Xstream groyne still acted as a barrier, deflecting water around its head much like a traditional impermeable structure. This finding aligns with field observations showing that the overall flow deflection remained strong despite the groyne's permeability.

Turbulence intensity and bed shear stress patterns provided an explanation for the morphodynamics. The Xstream groyne produced lower levels of turbulent kinetic energy (TKE) near the bed and lacked the concentrated turbulence peaks seen at the heads of traditional groynes. As a result, zones of erosion were more diffuse and spatially distributed. The model's bed shear stress contours supported this, showing a continuous band of moderate bed shear stress extending along the main channel edge, contrasting with the concentrated observed at the traditional groyne.

How do the flow and sediment dynamics contribute to the formation of the sediment line?

The formation of the sediment line is closely linked to a combination of a suppressed streamwise velocity and the emergence of a large counter-clockwise eddy near the main channel. Model results showed that this eddy induces upward vertical velocities at the boundary between the groyne field and main channel, creating a sheltered low-energy zone near the bed. This zone is largely isolated from the high-energy main flow, resulting in reduced bed shear stress and sustained sediment deposition. This makes it an ideal region for the formation of a sediment line.

What is the influence of an Xstream groyne structure on the hydrodynamics and morphodynamics?

The Xstream groyne significantly alters both hydrodynamic and morphodynamic behaviour compared to traditional designs. Hydrodynamically, it modifies the flow separation process, changing the shape of the vortex in the wake zone by making it more elongated over the length of the groyne field. The steep slope of the Xstream groyne creates a narrow, well-defined jet along the main channel, which accelerates flow near the groyne head and enhances flow concentration just outside the groyne field. Morphodynamically, it facilitates broader and more distributed erosion and enables the formation of a sediment line. These changes are primarily driven by the steep slope and partial permeability of

the structure. Overall, the Xstream groyne produces a less concentrated but more spatially extensive morphological impact.

7.2. Recommendations

Future research

Based on the findings of this study, the following recommendations are made for future research and practical applications concerning the Xstream groyne.

1. **Field Measurement Strategies:** Future field campaigns should prioritise the collection of steady-state flow measurements rather than short-term, transient recordings. This includes longer-duration ADCP surveys with improved spatial and vertical resolution. Such data would provide a more reliable basis for model validation and interpretation of three-dimensional flow structures. Additional tracer or dye experiments could be used to complement velocity data and visualise flow separation and mixing layers more effectively.
2. **Separate evaluation of Xstream groyne characteristics:** Mainly, the steeper slope of the Xstream groyne seemed to have an effect on the groyne. However, this effect cannot fully be validated without a study on their individual influences. A structured simulation campaign isolating each parameter is recommended to identify their specific roles in modifying turbulence, velocity gradients and sedimentation patterns.
3. **Free-surface flow:** To improve the resolution of surface-related hydrodynamic features, future numerical studies should consider applying a Volume of Fluid (VOF) method rather than a rigid-lid approach.
4. **Discharge variability:** To better understand how the Xstream groyne behaves across different hydraulic conditions, it is recommended to conduct numerical simulations with varied discharges. This includes low, average and raised discharges, with particular attention to how flow patterns, eddy formation, and sediment deposition zones change with increasing flow intensity. Such analysis would also help to validate the observed shift in sediment line location during higher flow periods.

Practical implementation:

If the Xstream groyne is to be applied in other river systems, when would the groyne implementation be suitable and when not?

When is it suitable?

The Xstream groyne is particularly suitable in river sections where maintaining structural and morphological stability is essential. Field observations and numerical modelling demonstrated that it avoids the formation of deep, localised scour pits commonly seen around traditional groynes. Instead, it induces a broader, more distributed erosion pattern, which reduces the risk of undermining the groyne toe and enhances overall bed stability. At the same time, the design promotes accelerated flow in the main channel, supporting sediment flushing and helping to maintain navigable depths. Additionally, the structure encourages sediment deposition within the groyne field, contributing to riverbank protection by reinforcing bank stability under low to moderate discharge conditions.

When is it not suitable?

The Xstream groyne may be unsuitable in river sections with highly energetic or rapidly changing flow conditions. The groyne can induce sudden flow acceleration along its toe, due to its steep slope. This

local acceleration increases the risk of intensified erosion adjacent to the structure and may pose a hazard to nearby infrastructure, riverbanks or sensitive ecological zones. Moreover, the rapid change in velocity near the groyne could create unexpected hydraulic conditions that are potentially dangerous for recreational use, particularly for swimmers or waders near the groyne field.

References

ANSYS. (2025). ANSYS Fluent Manual. https://ansyshelp.ansys.com/public/account/secured?returnurl=/Views/Secured/corp/v251/en/flu_ug/pt03.html

Arnhem, R. (2022). *Betrekkingslijnen Rijntakken : versie 2022* (tech. rep.). Rijkswaterstaat, Centrale Informatievoorziening. Arnhem.

Buschman, F. (2024, March). *Evaluatie flexibele krib in relatie tot een traditionele krib* (tech. rep.). Deltares. Delft.

Buschman, F., & Kosters, A. (2021, March). *Pilot flexibele kribben in de IJssel* (tech. rep.). Deltares. Delft.

Chanson, H. (2004). 3 - Applications of the Bernoulli equation to open channel flows. In H. Chanson (Ed.), *Hydraulics of open channel flow (second edition)* (Second Edition, pp. 21–49). Butterworth-Heinemann. https://doi.org/https://doi.org/10.1016/B978-075065978-9/50008-8

Chauchat, J., Cheng, Z., Nagel, T., Bonamy, C., & Hsu, T. J. (2017). SedFoam-2.0: a 3-D two-phase flow numerical model for sediment transport. *Geoscientific Model Development*, *10*(12), 4367–4392. https://doi.org/10.5194/gmd-10-4367-2017

Delft High Performance Computing Centre (DHPC). (2024). DelftBlue Supercomputer (Phase 2). https://www.tudelft.nl/dhpc/ark:/44463/DelftBluePhase2

Deltares. (2025). *Delft3D FLOW user manual* (tech. rep.). https://oss.deltares.nl/web/delft3d/manuals

DHI Group. (2025). *MIKE 3 User Guide* (tech. rep.). https://www.dhigroup.com/technologies/mikepoweredbydhi/mike-21-3

Flow Science, I. (2019). FLOW-3D HYDRO. https://www.flow3d.com/products/flow-3d-hydro/

Graf, W., & Blanckaert, K. (2002). Flow around bends in rivers. *New trends in water and environmental engineering for safety and life; eco-compatible solutions for aquatic environments*.

Jansen, P. P., van Bendegom, L., & van den Berg, J. (1994). *Principles of river engineering : the non-tidal alluvial river*. Delftse Uitgevers Maatschappij.

Khosronejad, A., Ghazian, M., Angelidis, D., Bagherizadeh, E., Flora, K., & Farhadzadeh, A. (2019). Comparative Hydrodynamic Study of Rigid-Lid and Level-Set Methods for LES of Open-Channel Flow. *Journal of Hydraulic Engineering*, *145*, 4018077. https://doi.org/10.1061/(ASCE)HY.1943-7900.0001546

Koken, M., & Constantinescu, G. (2008). An investigation of the flow and scour mechanisms around isolated spur dikes in a shallow open channel: 1. Conditions corresponding to the initiation of the erosion and deposition process. *Water Resources Research*, *44*(8), 0. https://doi.org/https://doi.org/10.1029/2007WR006489

Kumar, M., & Malik, A. (2016). 3D Simulation of Flow around Different Types of Groyne Using ANSYS Fluent. *Imperial journal of interdisciplinary research*, *2*. https://api.semanticscholar.org/CorpusID:55381009

MathWorks. (2024). MATLAB.

Nandhini, D., Murali, K., Harish, S., Schüttrumpf, H., Heins, K., & Gries, T. (2024). A state-of-the-art review of normal and extreme flow interaction with spur dikes and its failure mechanism. *Physics of Fluids*, *36*(5), 051301. https://doi.org/10.1063/5.0202439

Pizarro, A., Manfreda, S., & Tubaldi, E. (2020). The Science behind Scour at Bridge Foundations: A Review. *Water*, *12*(2). https://doi.org/10.3390/w12020374

Przedwojski, B., Blazejewski, R., & Pilarczyk, K. (1995). *River training techniques : fundamentals, design and applications : - a literature survey* - (tech. rep.). A.A. Balkema.

Python Software Foundation. (2024). Python.

QGIS Development Team. (2024). QGIS Geographic Information System.

Saberi, O., & Galoie, M. (2017). Numerical Modeling of Flow Around Groynes with Different Shapes Using TELEMAC-3D Software. *American Journal of Water Science and Engineering*, *2*, 43–52. https://doi.org/10.11648/j.ajwse.20160206.11

Schiereck, G. J., & Verhagen, H. J. (2019). *Introduction to bed, bank and shore protection: Revised edition.* Delft Academic Press.

Shampa, Hasegawa, Y., Nakagawa, H., Takebayashi, H., & Kawaike, K. (2020). Three-Dimensional Flow Characteristics in Slit-Type Permeable Spur Dike Fields: Efficacy in Riverbank Protection. *Water*, *12*(4). https://doi.org/10.3390/w12040964

SSRS. (2025). Flexibele kribben opgebouwd uit X-blokken. https://www.ssrs.info/oplossingen/sediment/flexibele-kribben-opgebouwd-uit-x-blokken/

Tecplot, I. (2022). Tecplot 360.

ten Oever, E. (2023). *Hydraulische weerstand kribben Xstream* (tech. rep.). BAM Infraconsult bv. Gouda.

The OpenFOAM Foundation. (2024). *OpenFOAM User Guide Version v2312* (tech. rep.). https://www.openfoam.com/documentation/user-guide

van Alderwegen, E. (2021). *Effects of permeability and head steepness of groynes on local flow characteristics Modelling open channel flow for the features of a flexible groyne* (tech. rep.). http://repository.tudelft.nl/.

van Bendegom, L., Bezuijen, K., & Bouwmeester, J. (1978). Waterloopkunde van rivieren. In *Rivieren en rivierwerken* (pp. 51–64). TU Delft.

van der Heide, G. D., & Hellinga, W. T. (1954). *Het geologisch natuurreservaat 'P. van der Lijn'* (tech. rep.). Grondboor & Hamer.

Wetser, A. (2016). *Flexibele krib Technisch Rapport Stage BAM Infraconsult* (tech. rep.). TU Delft.

Wilbers, A. W. E. (1997). *De bodemsamenstelling van Waal en IJssel in de jaren 1966, 1976, 1984 en 1995: RIZA rapport 97.009* (tech. rep.). Rijswaterstaat. Arnhem.

Xbloc. (2025). Xstream/XstreamPlus. https://www.xbloc.com/our-blocks/xstreamxstreamplus

Yossef, M. (2002). The effect of groynes on rivers: literature review. *Delft University of Technology c/o Delft Cluster, Delft, The Netherlands.*, (Report No. DC 03.03.04).

Zhang, H., & Nakagawa, H. (2008). Scour around Spur Dyke: Recent Advances and Future Researches. *Ann Disaster Prevent Res Inst Kyoto Univ*, *51*.

Zhang, H., Nakagawa, H., Ishigaki, T., & Muto, Y. (2005). Prediction of 3D flow field and local scouring around spur dykes. *Proceedings of hydraulic engineering*, *49*, 1003–1008. https://doi.org/10.2208/prohe.49.1003

A

ADCP figures

(a) Flexible groyne head

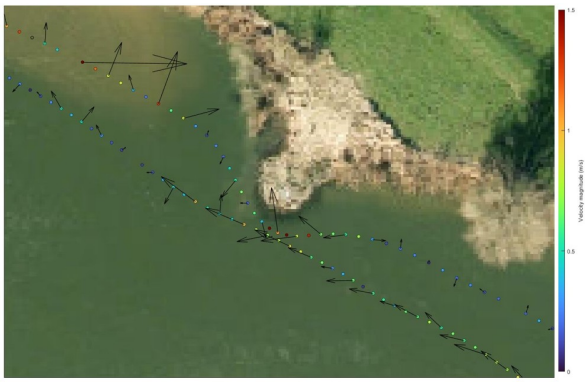

(b) Downstream groyne head

(c) Upstream groyne head

Figure A.1: Depth-averaged velocity plots near the different groyne heads.

B

Model simulation designs

The groyne design determines the difference between the simulations. These were explained in Section 5.1, where three cases were set up. The Xstream groyne geometry and mesh have been shown in Figures 5.7 and 5.9. The geometries and meshes of the other cases are described below:

No groyne case:
For all cases, the groyne was implemented as a separate solid body within the geometry. This modular approach allowed for a straightforward creation of the no-groyne case by simply removing the groyne solid from the existing setup. The resulting geometry is shown in Figure B.1a. To ensure consistency across simulations, the mesh was kept identical to the other cases. However, without the groyne and the associated turbulence it would normally generate, the model is likely over-resolved for this simplified flow. The mesh configuration is presented in Figure B.1b.

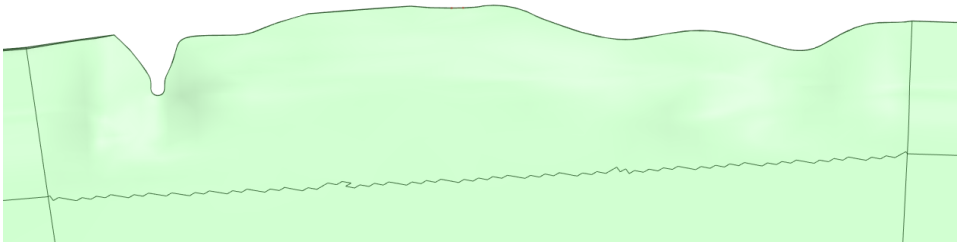

(a) Geometry No groyne case

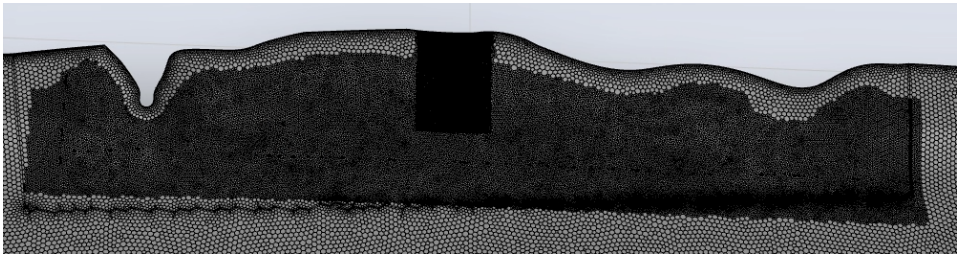

(b) Mesh configuration No groyne case

Figure B.1: Overview of the geometry and mesh for the no groyne case.

Traditional groyne case:
The traditional groyne was also implemented as a separate solid body within the model geometry. It was positioned identically to the Xstream case and shares a similar overall shape. The key difference lies in its fixed 1:3 slope, which results in a more integrated design with the riverbed. The geometry of the traditional groyne case is shown in Figure B.2a.

To enable a fair comparison with the Xstream case, the mesh configuration was made as similar as possible, including local refinements around the groyne structure. The resulting mesh is presented in Figure B.2b.

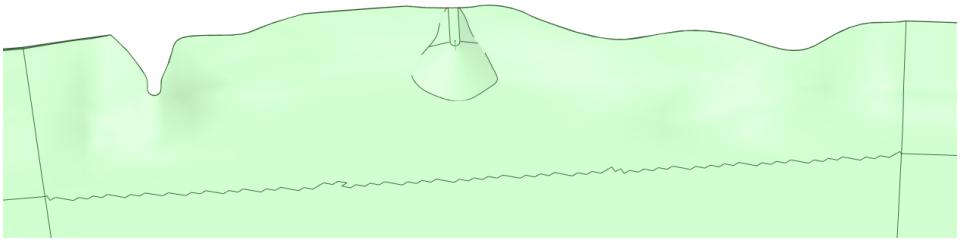

(a) Geometry Traditional groyne case

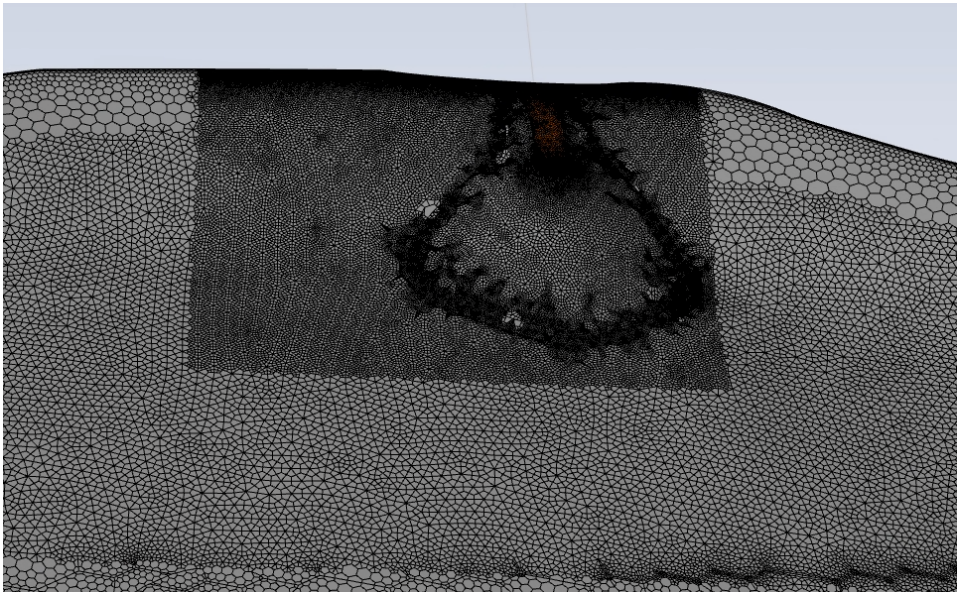

(b) Mesh configuration Traditional groyne case

Figure B.2: Overview of the geometry and mesh for the traditional groyne case.

C

Cross-sections for traditional groyne case

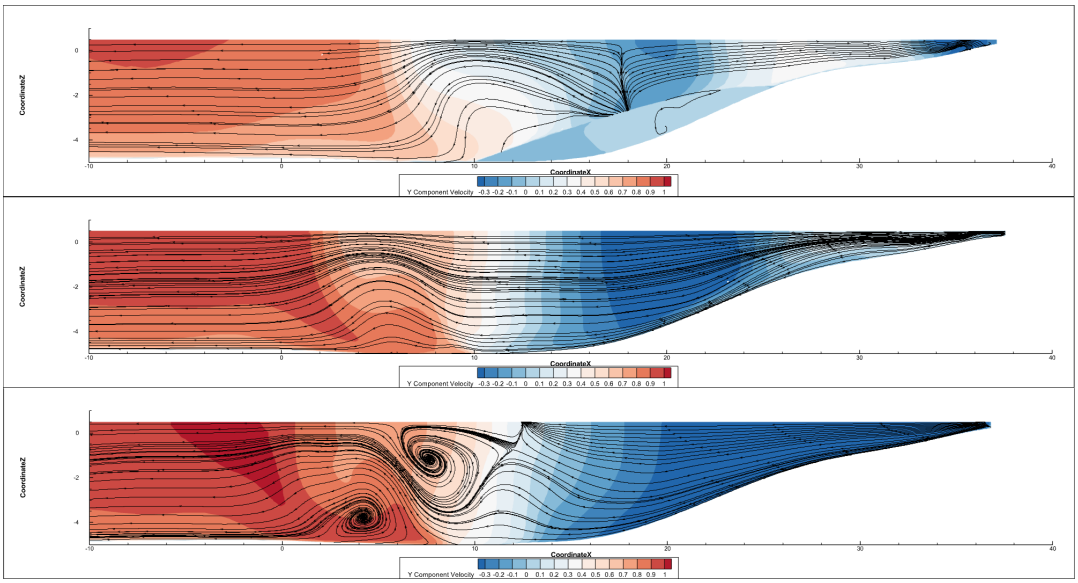

Figure C.1: Cross-section for traditional groyne case. From top to bottom the streamwise coordinate is Y = 600m, Y = 610m and Y=610m